FRACTURE OF HIGH RESTRAINT WELDS IN HIGH STRENGTH QUENCHED AND TEMPERED STEEL

Clair James Schrodt

FRACTURE OF HIGH RESTRAINT WELDS IN HIGH STRENGTH QUENCHED AND TEMPERED STEEL

by

LIEUTENANT CLAIR JAMES SCHRODT, USN
B.S., University of Nebraska
1965

SUBMITTED IN PARTIAL FULFILLMENT
OF THE REQUIREMENTS FOR THE
DEGREE OF OCEAN ENGINEER
AND FOR THE DEGREE OF
MASTER OF SCIENCE IN NAVAL ARCHITECTURE
AND MARINE ENGINEERING

at the
MASSACHUSETTS INSTITUTE OF
TECHNOLOGY

FRACTURE OF HIGH RESTRAINT WELDS IN HIGH STRENGTH QUENCHED AND TEMPERED STEEL

by
Clair J. Schrodt

Submitted to the Department of Ocean Engineering on May 10, 1974, in partial fulfillment of the requirements for the degrees of Ocean Engineer and Master of Science of Naval Architecture and Marine Engineering.

ABSTRACT

The strain response of high restraint slit-type welds during welding is discussed. The mechanical and physical temperature-dependent properties of HY-130, and the estimated results are discussed. The experiments were designed to enable observation of the macroscopic effects, and at the same time, the cracking of quenched and tempered steel of 130 ksi yield strength.

The transient strain response was found to be of equal order of magnitude transversely and longitudinally in the region of the weld arc. There was reasonable correlation of the residual strains between the same weld passes, but a high degree of correlation with the extensiometer data. The time to crack and an empirical stress intensity factor for cracking was developed. The stress intensity factor correlated reasonably well with the values measured by other experimenters.

Recommendations are made concerning continued investigative work aimed at developing better experimental means of measuring strain and at developing the tying together of fracture mechanics, transient response of weld, and computer analysis of welding.

THESIS SUPERVISOR: Koichi Masubuchi

TITLE: Professor of Ocean Engineering & Materials Science

ACKNOWLEDGEMENT

I wish to thank the U. S. Navy for sponsoring my program of studies at MIT. Several organizations and individuals were of particular assistance: Mr. Fred Merlis of MIT's Aerolastics Laboratory, Mr. Anthony Zona of the Materials Joining Laboratory, and Mr. Robert Huston of the Materials Processing Laboratory were especially helpful in the preparation and running of my welding experiments; Mr. Ralph Judy of the Naval Research Laboratory and Mr. Gary Adams of the Portsmouth Naval Shipyard provided the material for the thesis research; and Miss Maureen Gallagher cheerfully assisted in obtaining purchase orders for services for the thesis.

To Professor Koichi Masubuchi, who advised and guided me as a professor and a friend, I am forever grateful.

To my wife, Dorothy, who typed my thesis, and to my children, Debbie, Shane, Jimmy, Darla and Claire, who patiently endured the rigorous schedule involved with studying at MIT, I am forever indebted.

TABLE OF CONTENTS

LIST OF FIGURES

LIST OF TABLES

I. INTRODUCTION

A. General

Welding has become the predominate means of fabrication in the construction of metal structures because of its efficiency over riveting in terms of increased strength of a joint; because of its increased production rate; and because of its many advantages in the design of structures such as ships, bridges, buildings, and pressure vessels. The main disadvantages are distortion and cracking that result from shrinkage during the welding operation.

The analysis of distortion and shrinkage has been studied by many researchers.[1,2,3,4,5,6] An analytical investigation of residual stress and distortions due to welding has been conducted by Masubuchi,[4,7] Satoh,[3] Ueda and Kusachi,[5] Wilson and Corderoy,[8] and Sato, Seo, Nakajima, and Toyosada.[9] To exemplify restraint intensity in a complex structure, Masubuchi and Ich obtained an analytical solution of the restraint intensity in a slit weld in an infinitely large plate.[1] They also made a computer analysis of the restraint intensity for weld cracking slit type test specimens.

The number of factors regarding weld cracking is unlimited; for example, the chemical composition of the base plate and filler metal; the mechanical restraint of

the weld joint; and the welding condition (heat input) which influences the initiation of cracking. However, all factors either affect the mechanical or the metallurgical aspect of the weld which results in crack initiation. From a mechanism of cracking it can be simply stated that a weld crack initiates when the stress and strains induced at a point reach the critical values.

There are two types of cracking experienced in welding--hot cracking and cold cracking. Hot cracking is intergranular and may occur in the weld metal or in the heat-affected base metal during solidification. Cold cracking is transgranular and occurs at much lower temperatures than hot cracking. In steels the temperature is below the austenite martensite transformation temperature.

To determine the mechanical characteristics of cracking it is necessary to know the complete stress-strain history of the welding cycle. This data is limited and very expensive to obtain, however, mainly because it is difficult to estimate both experimentally and theoretically. Nevertheless, the reaction forces induced or the intensity of restraint predicts the weld crack initiation without detailed knowledge of the stress-strain history.[1,10]

The degree of constraint, which characterizes how much a joint is restrained, is an important parameter for studying

weld cracking.[1] Although many tests that predict the tendency of weld cracking have been developed in various configurations and degrees of constraint, they do not predict the weld cracking tendency in an actual structural weld. Masubuchi and Ich attempted to solve this problem by computer analysis, showing that a finite element method solution of a plate with a slit agreed very well with analytical solutions; hence the finite element method could be used to determine the degree of constraint in a complex weld structured joint.[1] The degree of constraint for a given welding condition and a chemical composition of base and filler metals can be determined. For a given degree of constraint, however, it is desirable to develop a method to determine the resistance to cracking, and thus the quality of the weld metal.

B. Technical Background

1. Thermal Stress during Welding and Welding Residual Stresses

Residual stresses--those stresses that would exist in a body if all external loads were removed--are directly related to the phenomena of distortion and cracking in weldments. Cracking, as well as distortion, in a weldment is a function of structural, fabrication, and material parameters.

Structural parameters include configuration and surface condition of the joint, plate thickness, and the geometry of the structure. The welding procedure (heat input, cooling rate, welding sequence, etc.) and the degree of constraint make up the fabrication parameters. The material parameters encompass the composition and condition of the base plate and the filler materials.

To better understand residual stress, it is necessary to understand the mechanism by which thermal stress and strain are developed. The changes of temperature and stress during welding, best described by Masubuchi, is repeated here.[4]

"Figure 1 shows schematically how residual stresses are formed in a weld. Figure 1a shows a bead-on-plate weld in which a weld bead is being laid at a speed v. O-xy is the coordinate axis; the origin, O, is on the surface underneath the welding arc, and the x direction lies in the direction of welding.

Figure 1 shows temperature distribution along several cross sections. Along Section A-A, which is ahead of the welding arc, the temperature change due to welding, ΔT, is almost zero (Fig. 1b-1). Along Section B-B, which crosses the welding arc, the temperature distribution is very steep (Fig. 1b-2).

Along Section C-C, which is some distance behind the welding arc, the distribution of temperature change is as shown in Fig. 1b-3. Along Section D-D, which is very far from the welding arc, the temperature change due to welding again diminishes (Fig. 1b-4).

Figure 1c shows the distribution of stresses along these sections in the x direction, σ_x. Stress in the y direction, σ_y, and shearing stress, τ_{xy}, also exist in a two-dimensional stress field (Fig. 1a).

Along Section A-A, thermal stresses due to welding are almost zero (Fig. 1c-1). The stress distribution along Section B-B is shown in Fig. 1c-2. Stresses in areas underneath the welding arc are close to zero, because molten metal does not support loads. Stresses in areas somewhat away from the arc are compressive, because the expansion of these areas is restrained by surrounding areas that are heated to lower temperatures. Since the temperatures of these areas are quite high and the yield strength of the material is low, stresses in these areas are as high as the yield strength of the material at corresponding temperatures. The amount of compressive stress increases with increasing distance from the weld or with decreasing temperature. However, stresses in areas away from the

weld are tensile and balance with compressive stresses in areas near the weld. In other words,

$$\int \sigma_x \cdot dy = 0$$

across Section B-B. Thus, the stress distribution along Section B-B is as shown in Fig. 1c-2.

Stresses are distributed along Section C-C as shown in Fig. 1c-3. Since the weld-metal and base-metal regions near the weld have cooled, they try to shrink causing tensile stresses in areas close to the weld. As the distance from the weld increases, the stresses first change to compressive and then become tensile.

Figure 1c-4 shows the stress distribution along Section D-D. High tensile stresses are produced in areas near the weld, while compressive stresses are produced in areas away from the weld. The distribution of residual stresses that remain after welding is completed is shown in the figure.

The cross-hatched area, MM', Fig. 1a shows the region where plastic deformation occurs during the welding thermal cycle. The cross-hatched area near the origin O indicates the region where the metal is melted. The region outside the cross-hatched area

remains elastic during the entire welding thermal cycle.

Because of the difficulty in determining the distribution of incompatible strains, no analysis has yet been developed to trace the change of two-dimensional thermal stresses during welding and to determine distributions of three residual-stress components, σ_x, σ_y, and τ_{xy}. In other words, no analysis has been made in which both heat flow and stress fields are treated as two-dimensional problems. In all studies conducted so far, the problem has been simplified in some way."

A weld joint configuration free of external restraint and one with external restraint are shown in Figure 2a and 2b respectively. The typical distribution of residual stress in Figure 2a is illustrated in Figure 3.[4] These residual stresses are the results of welding residual stress in an unrestrained joint. Typical stress distribution curves for a restrained joint, such as the slit joint of Figure 2b, are illustrated in Figure 4. By restraining the weld joint, the transverse residual strain and stress are then of the same order of magnitude as the longitudinal residual strain and stress.

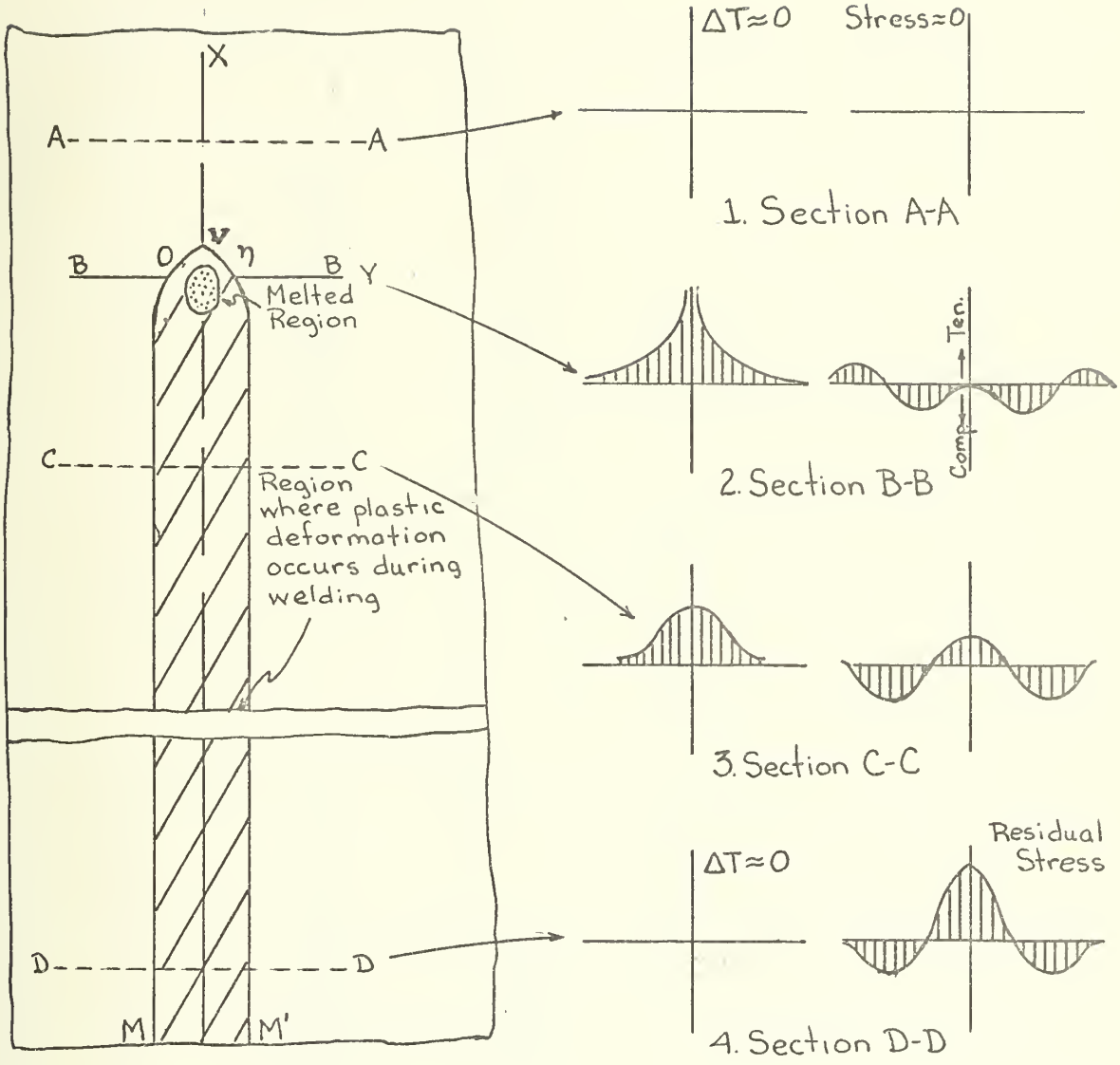

Figure 1. Schematic representation of changes of temperature and stresses during welding

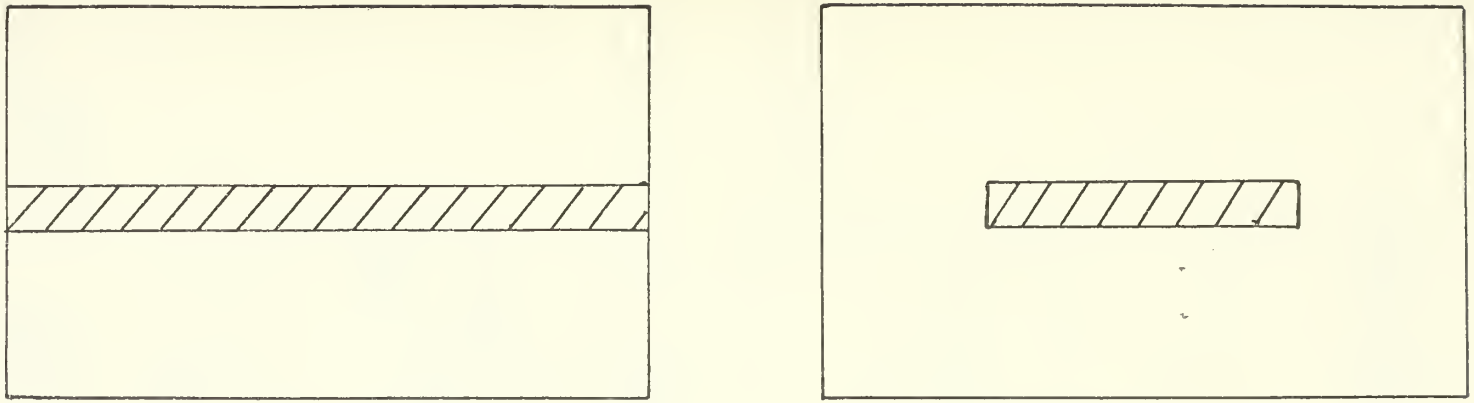

a. Free Joint

b. Restrained Joint

Figure 2. Weld Joints

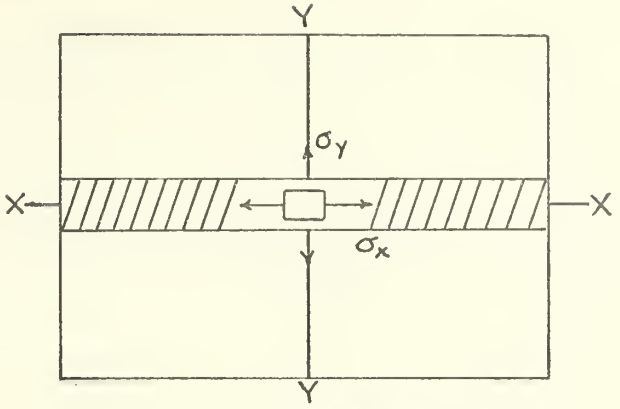

a. Butt Weld

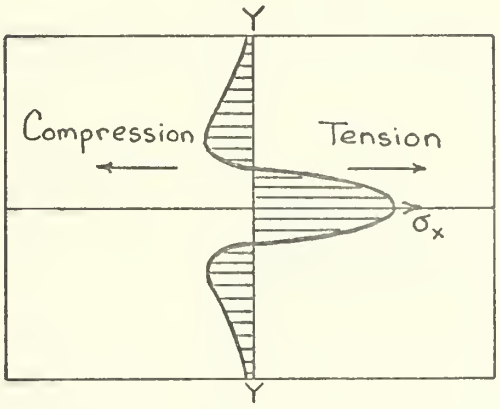

b. Distribution of σ_x Along YY

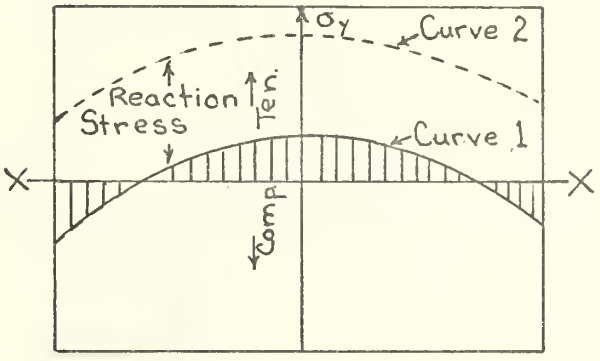

c. Distribution of σ_y Along XX

Figure 3. Typical distributions of residual stresses in butt weld

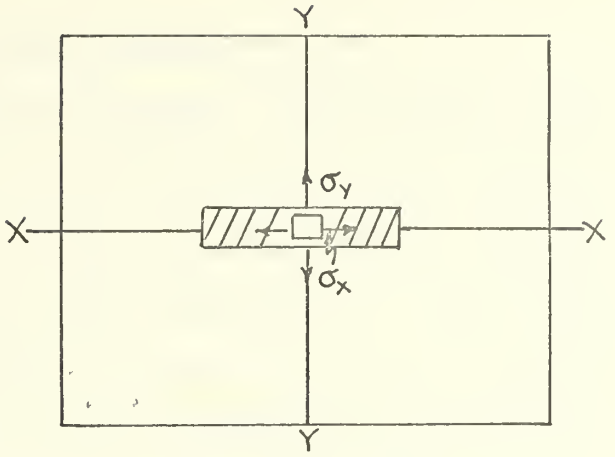

a. Slit Weld

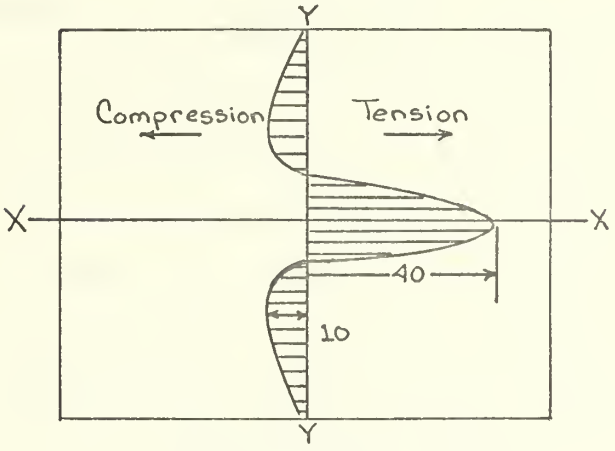

b. Distribution of σ_x

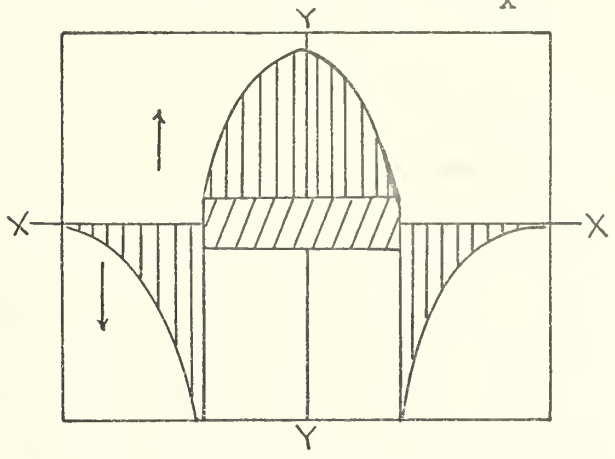

c. Distribution of σ_y Along XX

Figure 4. Typical Distribution of Residual Stress in a Slit-type Weld.

C. Analysis of Weld Cracking

As previously discussed, longitudinal cold cracking which takes place in a weld with a high degree of constraint is transgranular. The magnitude of any plastic strain appears small for crack initiation.[5] This may suggest that the critical values of local stress and strain are the results of metallurgical factors, including small amounts of diffused hydrogen, etc. In any case, the crack appears to be caused by a very complex triaxial stress field resulting from the bulk restraint of the weld metal. It is, therefore, a plane strain condition and fracture without ductile behavior. This is to be expected since the material is physically constrained and the stress system is complex. Although the cracked material does not meet the minimum thickness needed for a valid fracture toughness measurement, that is,

$$B \geq 2.5\left(\frac{K_c}{\sigma_{ys}}\right)^2 \qquad \text{Equation 1}$$

(where B is plate thickness, K_c is fracture toughness, and σ_{ys} is the material yield strength) it does provide a crack which, due to high constraint and complex stresses, appears to be in a plane strain condition. In the context of fracture mechanics, testing is used to gather data on fracture toughness K_c (which is a material constant and

has the dimension of stress $\cdot \sqrt{\text{length}}$. The recommended tests are shown in Table 1.[11] These tests are primarily used to:

1. Determine the probability of catastrophic failure in a material under given conditions,
2. Analyze service failures,
3. Obtain design data such as maximum working stress and minimum operating temperature,
4. Choose among materials for an application.

There is no universal fracture mechanics test used to determine fracture toughness because no one test gives valid data for all materials.

The Charpy V, drop weight tear and dynamic tear tests do not give K_c or K (stress intensity factor) values directly and data from these tests are hard to correlate with values.[11] Despite their limitations these tests can be used within limits, to satisfy fracture mechanics design. In addition, tests designed to measure K factors are very expensive to conduct, and when materials with extremely high toughness are tested, the thickness of the test specimen must be quite large to meet the criteria of Equation 1.

The basis of linear fracture mechanics was the theory proposed by Griffith in 1921. This theory stated that the rupture of brittle material such as glass occurs when the

Table 1. Recommended Uses of Fracture-Mechanics Tests

Principal Use of Test	Material Strength Ranges		
	$\sigma_{ys} < E/300$	$E/300 < \sigma_{ys} < E/150$	$E/150 < \sigma_{ys}$
Determine whether there is a high probability of catastrophic failure under service conditions	Charpy V appearance Notch tensile (very thin sheet)	Charpy V appearance DWT* energy Notch tensile (very thin sheet)	DWT energy value K_{Ic}** K_c (K_{Ic} applied to very thin sheet)
	NDT+	Charpy V appearance and energy	K_{Ic}
Choosing materials on a comparative basis	Charpy V appearance DWT Notch tensile (very thin sheet)	DWT Notch tensile (very thin sheet)	K_c (very thin sheet)
	NDT	DWT	DWT
Quality-control test for materials	Charpy V energy Notch tensile (very thin sheet)	Charpy V energy Notch tensile (very thin sheet)	K_{Ic} K_c (very thin sheet)
	Visual analysis	Visual analysis	Visual analysis
Service-failure analysis	NDT (for steel) Charpy V appearance and energy K_c (at low temperature or in thin sheet)	DWT Charpy V appearance and energy K_c (at low temperature or in thin sheet)	K_{Ic} K_c (very thin sheet)
Establishing design data (a) Safe working stress at given temperature and plate thickness	K_c and K_{Ic}	K_c and K_{Ic}	K_c and K_{Ic}
(b) Safe working temperature at given level of applied stress	NDT (for steel) DWT	DWT and Charpy V appearance K_c and K_{Ic}	Concept not applicable

*Drop-weight test
**From proposed ASTM standard E399-70T
+Nil-ductility temperature test

surface area of the flow increases with an associated increase in surface energy and a decrease in elastic potential energy.[12] Irwin and Orowan subsequently modified the original Griffith theory so that it could be applied to metals; they added a term involving the plastic energy dissipation rate in the plastic region surrounding the crack tip.[13,14] The Griffith-Irwin theory of fracture then, states that when the input energy rate exceeds the dissipation plastic rate, instability occurs and the crack will run.

The input energy rate is the strain-energy release rate G for a unit area increase in the cracked surface of a body. For a plane strain condition in either the opening mode or sliding mode of fracture

$$G = \frac{(1 - \nu^2)}{E} K^2 \qquad \text{Equation 2}^{12}$$

where K is called the stress intensity factor.
For the tearing mode of fracture

$$G = \frac{(1 + \nu)}{E} K^2 \qquad \text{Equation 3}^{12}$$

The values of K for the open, sliding, and tearing modes of fracture (Modes I, II and III respectively) for common configuration have been analytical solved and experimentally confirmed.[11] Since the theory of fracture

mechanics is based on the linear theory of elasticity, the corresponding stress intensity factors for the same mode of crack deformation and identical geometrics can be superimposed; that is,

$$K(\text{Mode I}) = K_1(\text{Mode I}) + K_2(\text{Mode I}) + \ldots + K_m(\text{Mode I}) \qquad \text{Equation 4}$$

$$K(\text{Mode II}) = K_1(\text{Mode II}) + K_2(\text{Mode II}) + \ldots + K_n(\text{Mode II})$$

$$K(\text{Mode III}) = K_1(\text{Mode III}) + K_2(\text{Mode III}) + \ldots + K_p(\text{Mode III})$$

where m, n, and p are integers.[12]

The crack opening force is a scalor term involving the strain-energy release rate. Therefore, crack opening forces for different modes of crack deformation can be superimposed as

$$G = G(\text{Mode I}) + G(\text{Mode II}) + G(\text{Mode III}) \qquad \text{Equation 5}$$

for plane strain.[12] Combining Equations 5, 2, and 3, the stress intensity factor becomes

$$K^2 = K^2(\text{Mode I}) + K^2(\text{Mode II}) + \frac{1}{1-\nu}K^2(\text{Mode III}) \qquad \text{Equation 6}$$

and for a Mode I and a Mode II fracture

$$K = K(\text{Mode I}) + K(\text{Mode II}) \qquad \text{Equation 7}$$

From Reference 11 the stress intensity factor for a finite sheet of width 2b and a crack length 2a is

$$K(\text{Mode I}) = \sigma\sqrt{\pi a}\cdot f(\tfrac{a}{b}) \qquad \text{Equation 8}$$

where $f(\frac{a}{b})$ is an experimentally determined function. For a Mode II crack we find that

$$K(\text{Mode II}) = \tau\sqrt{\pi a} \qquad \text{Equation 9}$$

then

$$K = K(\text{Mode I}) + K(\text{Mode II}) \qquad \text{Equation 10}$$

and

$$K = \sigma\sqrt{\pi a}\, f(\tfrac{a}{b}) + \tau\sqrt{\pi a} \qquad \text{Equation 11}$$

D. Aim and Purpose of This Study

The development and use of high strength steels in monolithic weld structures has added a new dimension to the residual stress and the resulting problem of cracking in weldments. Quenched and tempered steel of 130 ksi strength levels has been found susceptible to cold (delayed) cracking. The purpose of this report is to study cracking in high restraint welds of high strength quenched and tempered

steel weldments. Electric resistance thermocouples, three element strain gage rosettes, and an extensiometer were used to obtain transient and residual strain-temperature data, and transverse shrinkage data of high restraint butt welds. Experiments were performed on specimens of 6x10x1-inch plate with a straight Y slit. These specimens were quenched and tempered steel of 130 ksi nominal yield strength. A manual shield metal arc welding process was used to:

1. See if crack initiation can be determined by examining strain and shrinkage data,
2. Determine if experimental data may be reasonably duplicated using a manual shield metal arc welding process,
3. Verify that cracking of a weld can be easily observed,
4. Determine if a repeatable value of the stress intensity factor to crack initiation can be found using stress-strain and transverse shrinkage data,
5. Observe transient strain magnitudes and direction, and transverse shrinkage magnitudes,
6. Present temperature, longitudinal, and transverse strain data and,
7. Collect and present in useable form, physical

and mechanical temperature dependent data of HY-130.

Because the high temperature strain gages have been proven unreliable, the strain gages used in this experiment will not exceed temperatures of 400°F.[15] All strain measurements will be outside the heat-affected zone. Temperature measurements were taken at the weld line, in the heat affected zone, and at the location of the strain gage.

II. MATERIAL CHARACTERISTICS

A. General

In 1962 the U. S. Navy placed a contract with the United States Steel Company for the development of a steel with a yield strength of 130 to 150 ksi; the contract was to include associated welding procedures and consumables. The result of this steel development program was a quenched and tempered steel designated HY-130. The chemical composition of HY-130 is shown in Table 2.

The mechanical properties of the steel in the "as received" quenched and tempered condition are as follows:

Yield Strength - 130 to 145 ksi

Elongation in 2 inches - 15%

Reduction of area - 50% minimum transverse
70% through thickness

Impact requirements - 60 ft-lbs at $0^{\circ}F$ and room temperature

The physical and mechanical characteristics of a material as a function of temperature must be known to study residual stresses and metal movement during the welding process. Developments of new finite element programs require the knowledge of these characteristics.[16] The importance of these parameters and their temperature

Table 2. Composition Ranges of HY-130 Steel

Element	Percent Chemical Composition
C	0.08 - 0.12
Mn	0.60 - 0.90
P	0.010 maximum
S	0.015 maximum
Si	0.20 - 0.35
Ni	4.75 - 5.25
Cr	0.40 - 0.70
Mo	0.30 - 0.65
Ti	0.02 maximum
V	0.05 - 0.10
Cu	0.25 maximum
Fe	Remainder

dependency, including mathematical formulation, is extensively discussed by Bryan.[16] Since steel has phase changes, the problem becomes very complex and has been solved by other researchers by breaking the mechanical and physical property curves into several straight line approximations to allow for computer simulation.[17]

B. Mechanical Properties

The data of the mechanical properties as a function of temperature is not readily available for metals, and is difficult to obtain for the range from room temperature to melting temperature. Figures 5 through 10 provide the typical mechanical properties for HY-130 at room temperature and at elevated temperatures.

Figure 5, an estimated stress-strain curve for HY-130 one-inch plate, was developed from References 18, 19, and 20.

Figure 6, which shows the approximate effect of temperature on the 0.2% offset yield stress, was developed from data of T-1 steel (a quenched and tempered, high strength steel), and a low alloy nickel steel.[6,21] The change in slope at approximately 800°F and 1400°F compares favorably with the slope change of the straight line approximations assumed by Hibbitt.[17]

Figure 7 demonstrates the effect of temperature on Young's modulus.[21,22]

Figure 8 shows the room temperature tangent modulus at various stress levels. Its straight line approximation in the stress range of 120 to 158 ksi is

$$H \times 10^{-3}(psi) = -.77\sigma + 122.4 \qquad \text{Equation 12}$$

The highest stress level shown on this figure is 169 ksi, which equates to a tangent modulus of 740 ksi. Assuming that[16]

$$H(T^{o}F) \propto E(T^{o}F)$$

then

$$H(T^{o}F) = \frac{H(RT) \times E(T^{o}F)}{E(RT)} \qquad \text{Equation 13}$$

Equation 13 is used to develop an approximate curve of tangent modulus as a function of temperature and is illustrated in Figure 9.

Figure 10 shows the variation of Poisson's ratio as a function of temperature. Poisson's ratio will probably change with temperature, but should not exceed a maximum value of .500 in the weld puddle because of volume consideration when melted (at .50, there will not be a volume change.) Hibbitt estimated that Poisson's ratio varied linearly with temperature from .30 to .46 as temperature varied from room temperature to 2600°F.[17]

Table 3 is a tabulation of the mechanical properties of HY-130 as a function of temperature.

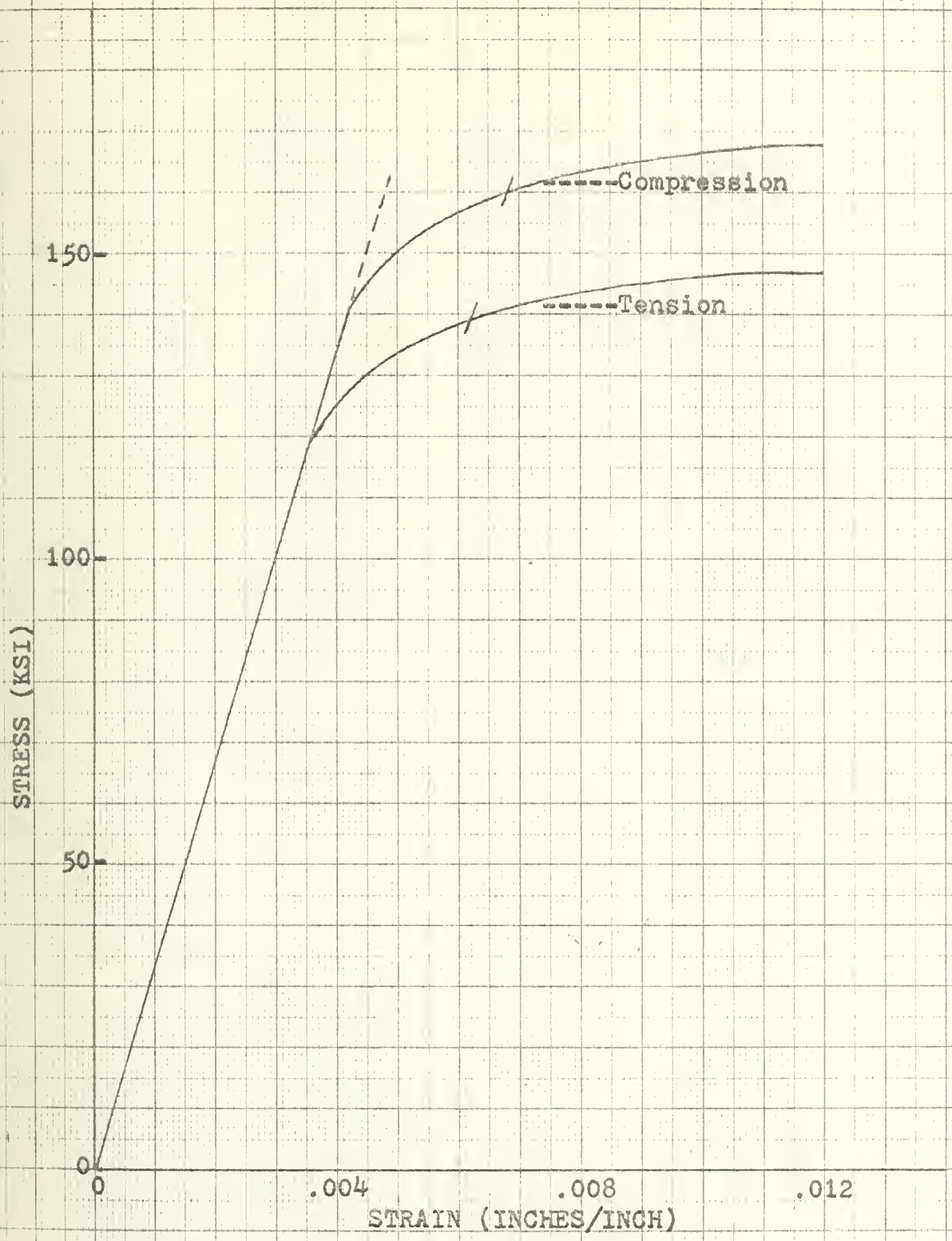

Figure 5. TYPICAL STRESS STRAIN DIAGRAM FOR HY-130 AT ROOM TEMPERATURE

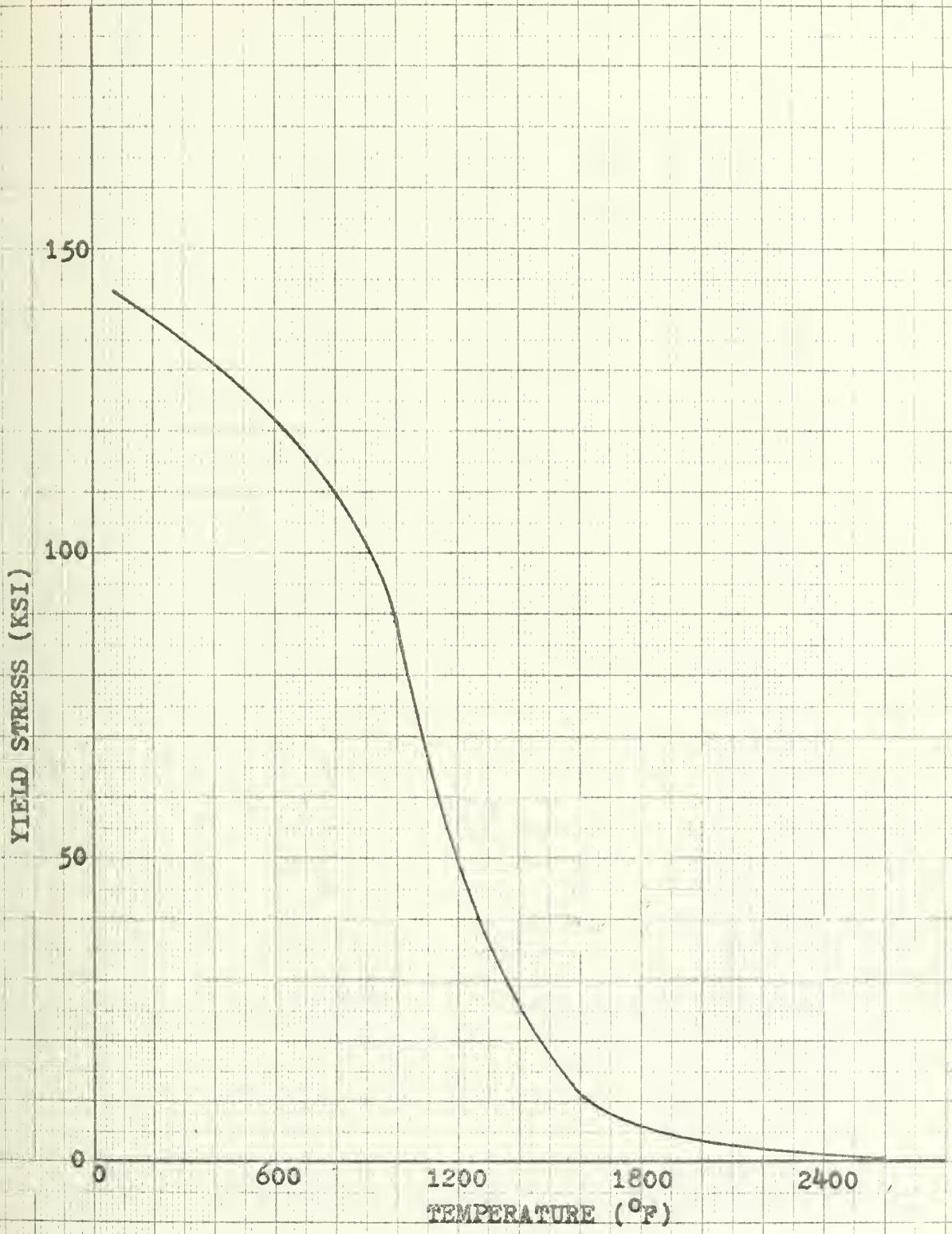

Figure 6. ESTIMATED EFFECT OF TEMPERATURE ON 0.2% OFFSET YIELD STRESS FOR HY-130.

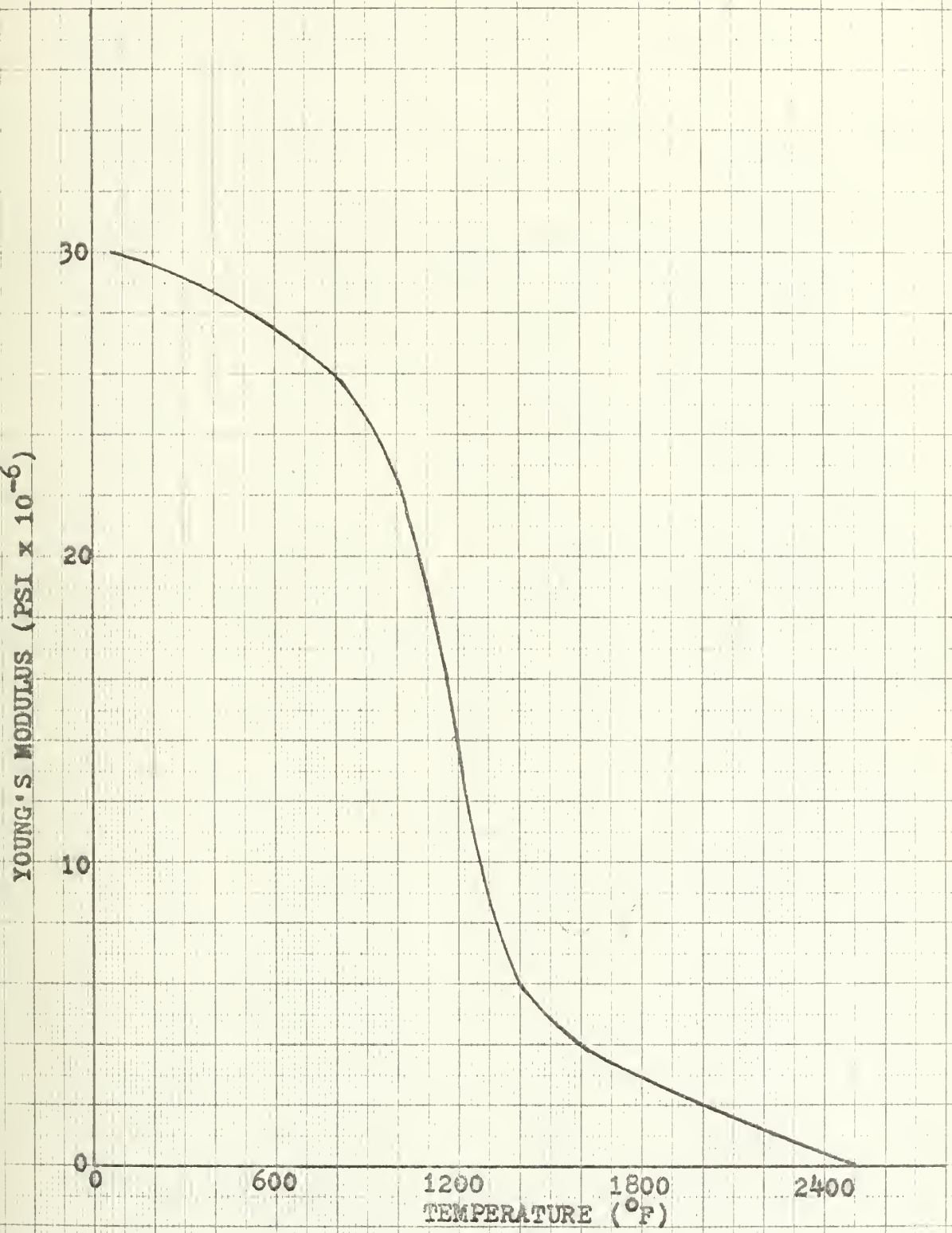

Figure 7. ESTIMATED EFFECT OF TEMPERATURE ON YOUNG'S MODULUS FOR HY-130.

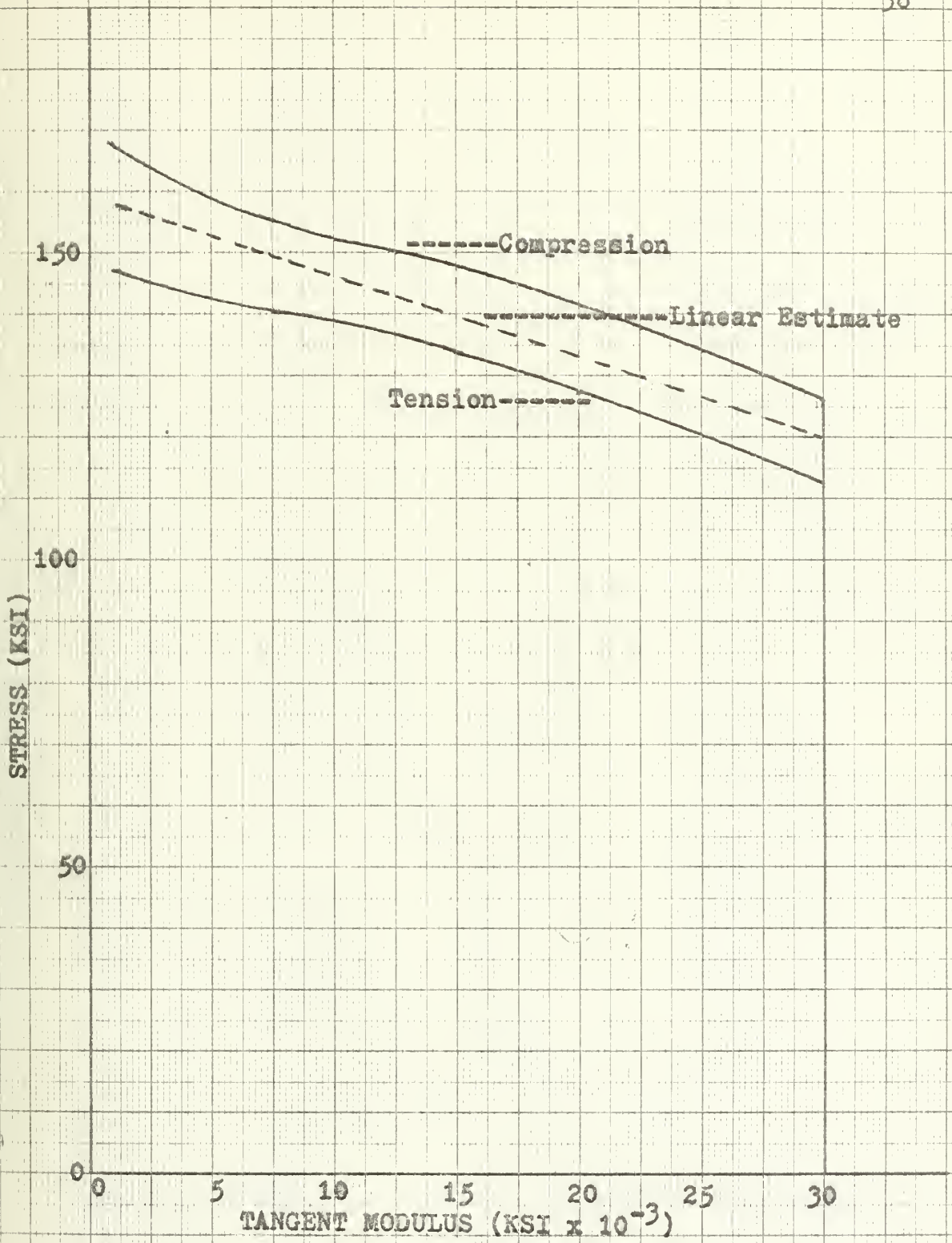

Figure 8. TANGENT MODULUS CURVES FOR HY-130.

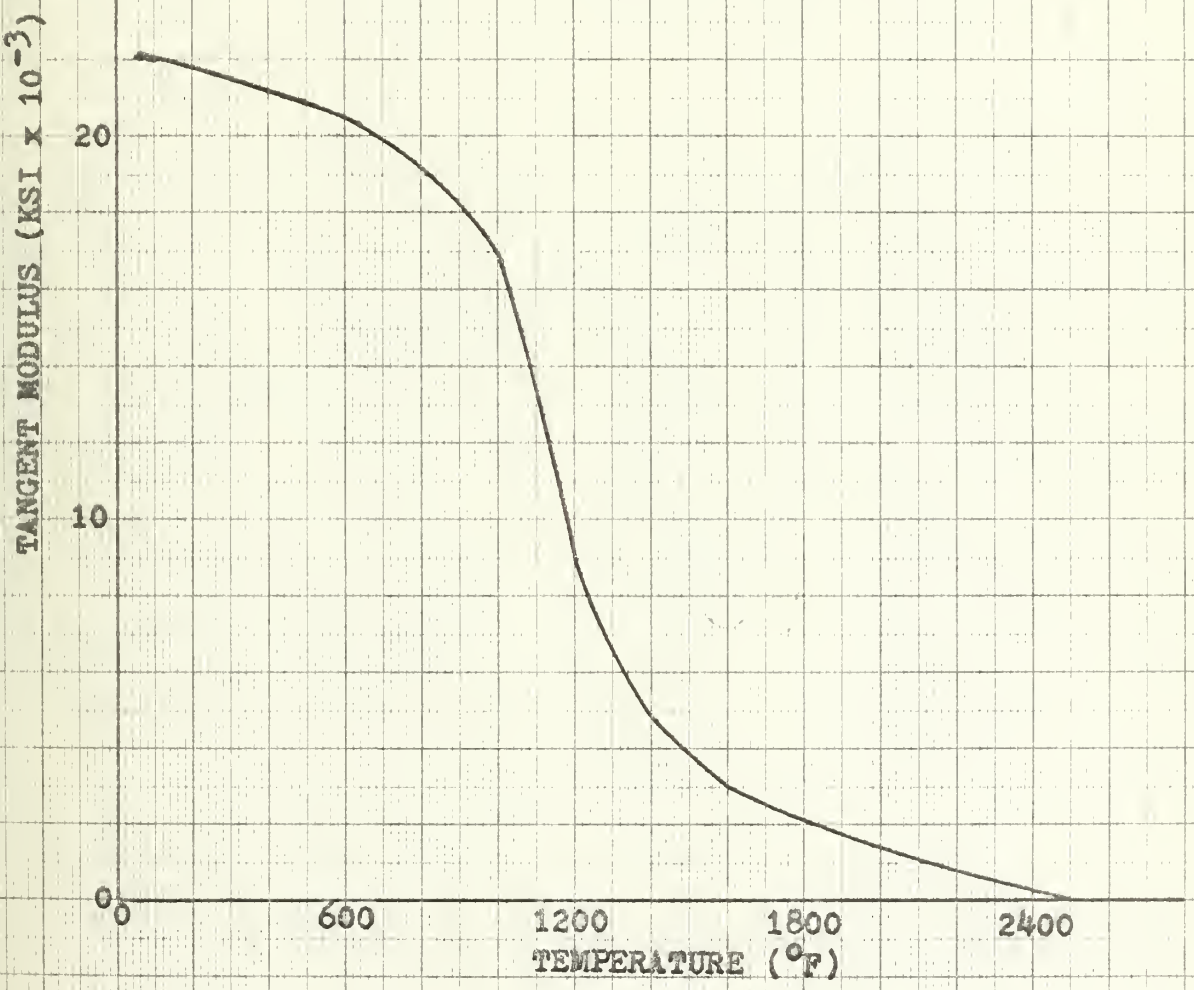

Figure 9. ESTIMATED EFFECT OF TEMPERATURE ON TANGENT MODULUS FOR HY-130.

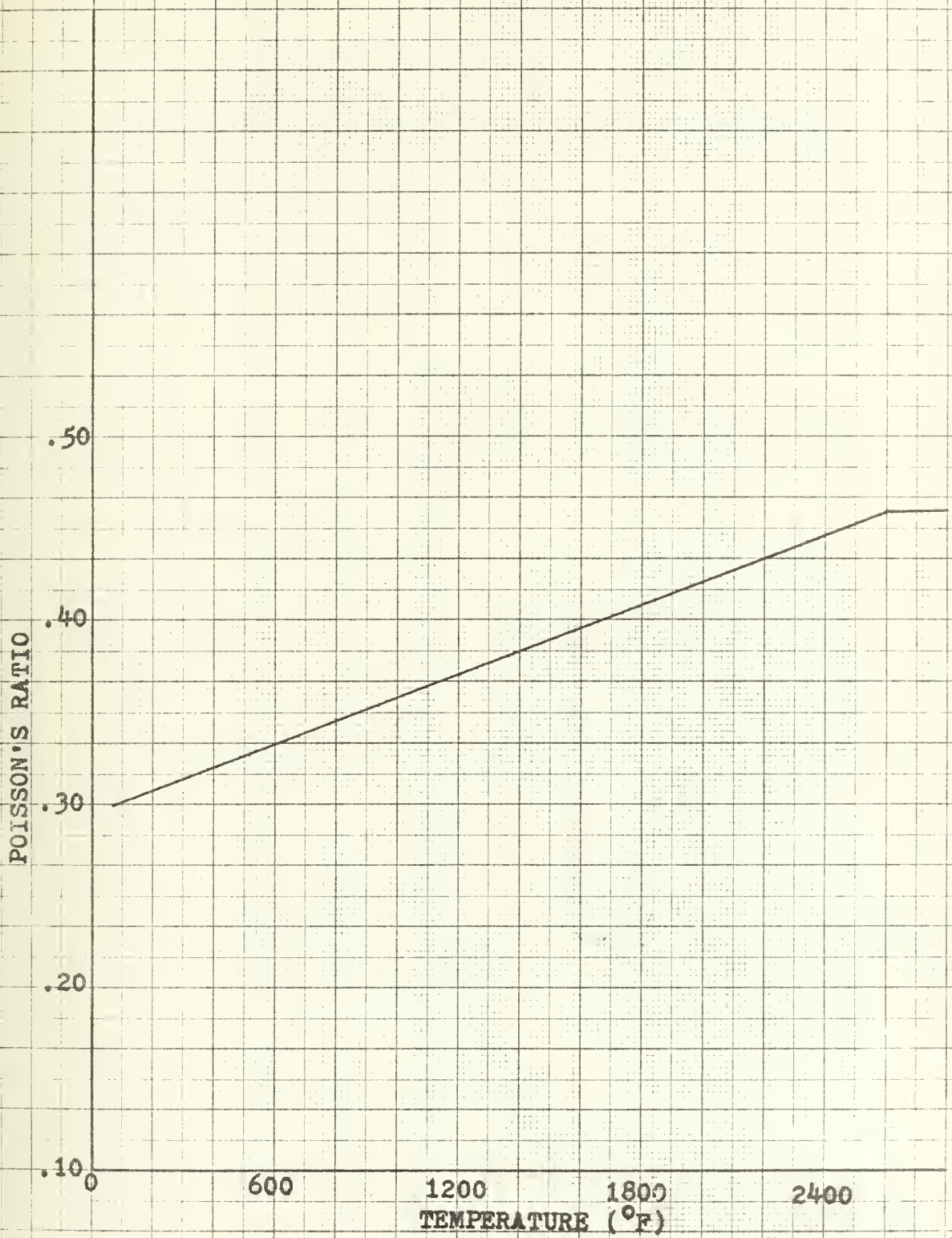

Figure 10. ESTIMATED EFFECT OF TEMPERATURE ON POISSON'S RATIO FOR HY-130

Table 3. Summary of Mechanical Properties for HY-130 Steel

T	68	200	400	600	800	1000	1200	1400	1600	1800	2000	2200	2400	2500
σ	143	138	131.5	122	110	88	50	25.5	11.2	6.0	4.0	2.0	1.0	0
E	30	29.6	28.8	27.7	26	22.7	14.0	5.0	4.0	3.0	2.0	1.2	.4	0
H	22.2	21.8	21.2	20.5	19.2	17.0	9.2	4.9	3.1	2.2	1.5	.8	.4	0
ν	.30	.308	.321	.334	.346	.359	.372	.384	.397	.410	.422	.435	.447	.454

NOMENCLATURE

T = Temperature (^{o}F)

σ = Yield Stress 2% Offset (KSI)

E = Elastic Modulus (PSI x 10^{-6})

H = Tangent Modulus (KSI x 10^{-3})

ν = Poisson's Ratio

C. Physical Properties

Figures 11 through 14 show the effect of temperature on the average coefficient of thermal expansion α, density ρ, thermal conductivity k, and specific heat C. The average coefficient of thermal expansion shown in Figure 11 is based on data for low alloy steel containing .10 percent carbon and 3.5 percent nickel.[23]

The variation of density as a function of temperature shown in Figure 12 is based on a low carbon steel with a carbon content of .10 percent. The density was calculated from thermal expansion data and a measured density of 0.2840 lb/in^3 at 32^oF.

Figure 13 shows thermal conductivity as a function of temperature, and is based on data from the same steel as Figure 11.

Figure 14, which shows specific heat as a function of temperature, is based on the data from low carbon steel used for Figure 12 data. A high degree of accuracy cannot be expected in the properties, but as Tall concludes, the range of variation for carbon steel is not great.[24] Since the carbon and nickel, as well as the other constituents of the steels used to develop the curves in Figures 5 through 14, approach the composition of HY-130, it is a valid assumption that these curves are good approximations

for HY-130, with no more than a 5 percent error. Table 4 is a tabulation of the physical properties of HY-130 as a function of temperature.

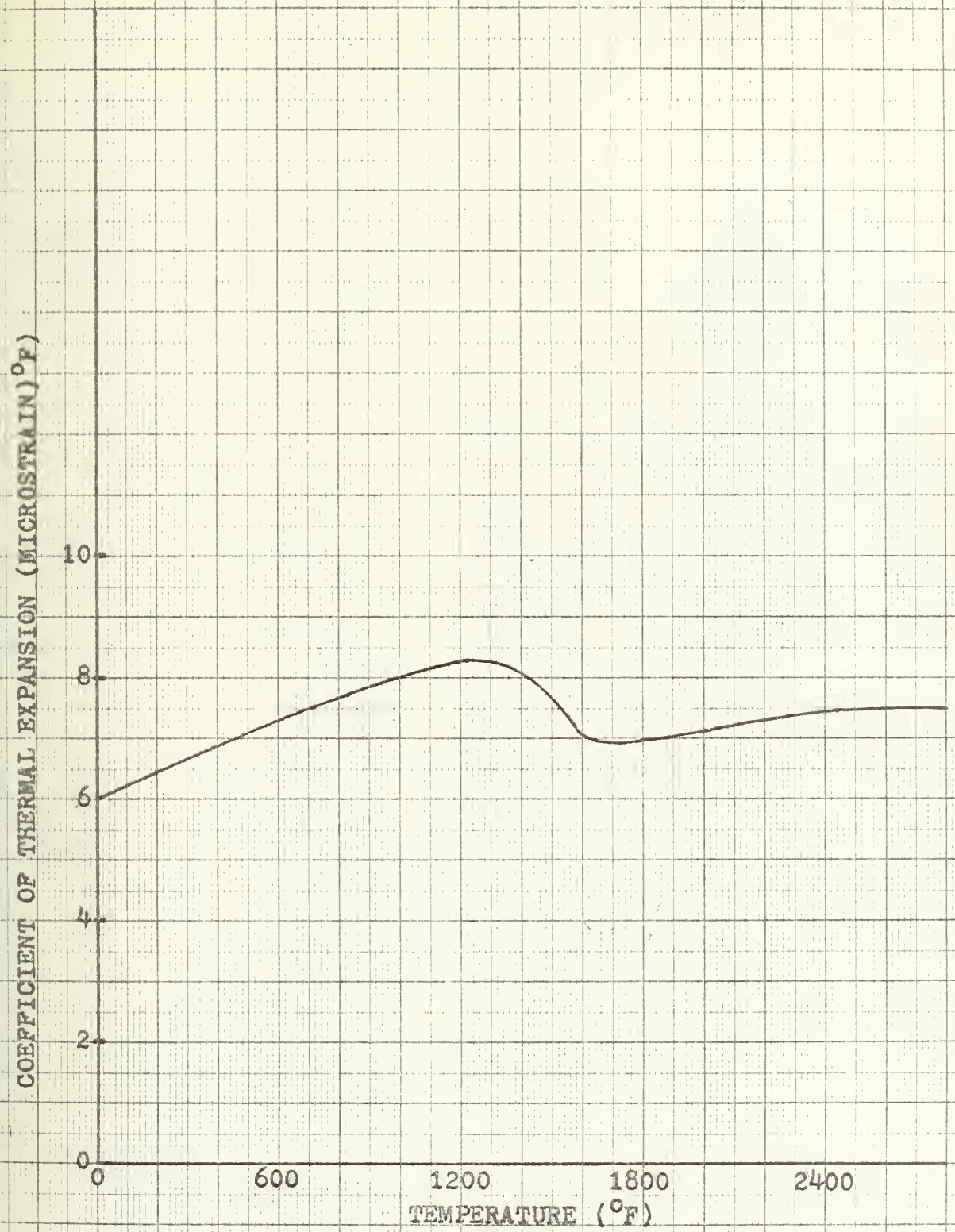

Figure 11. ESTIMATED COEFFICIENT OF THERMAL EXPANSION FOR HY-130.

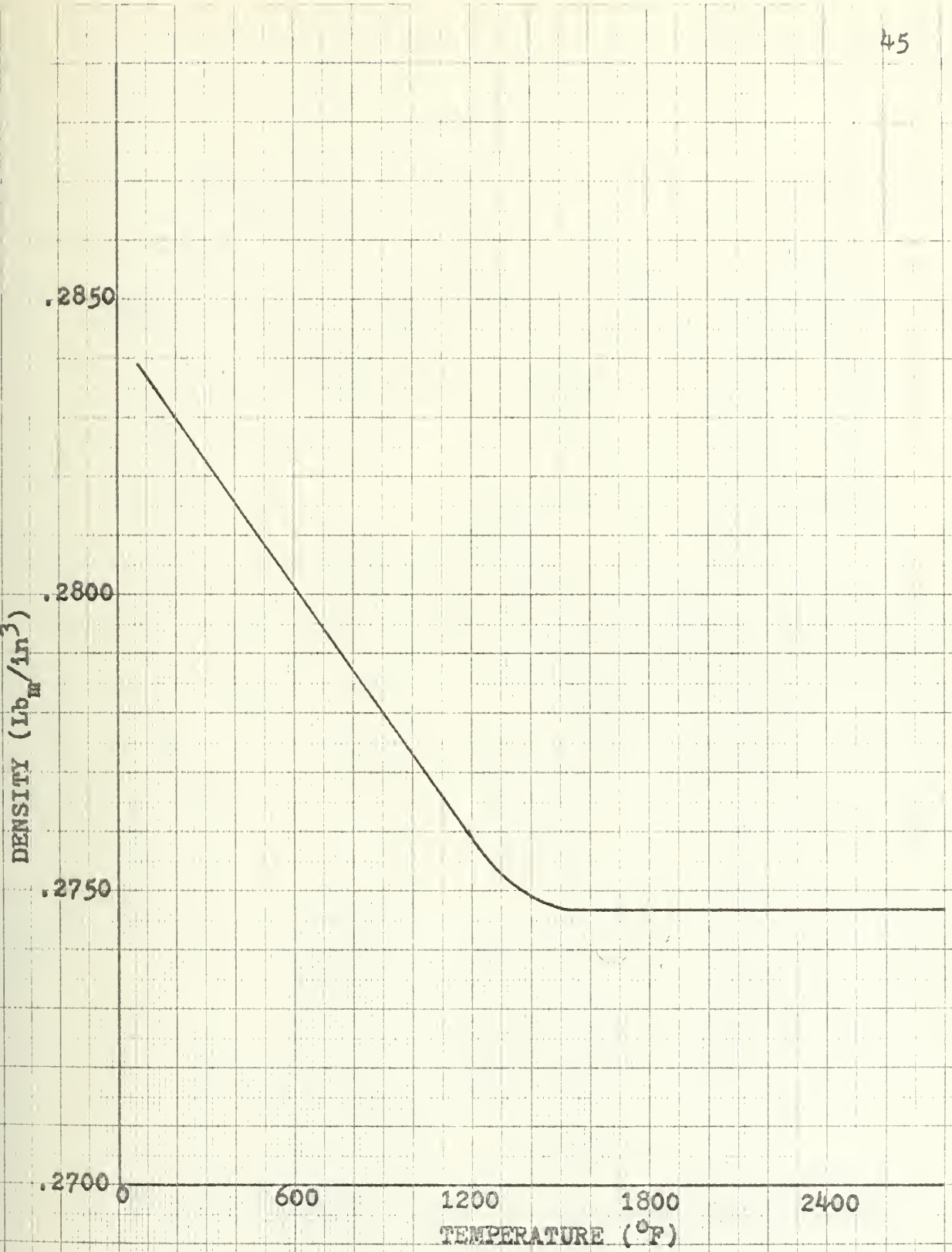

Figure 12. EFFECT OF TEMPERATURE ON DENSITY FOR HY-130.

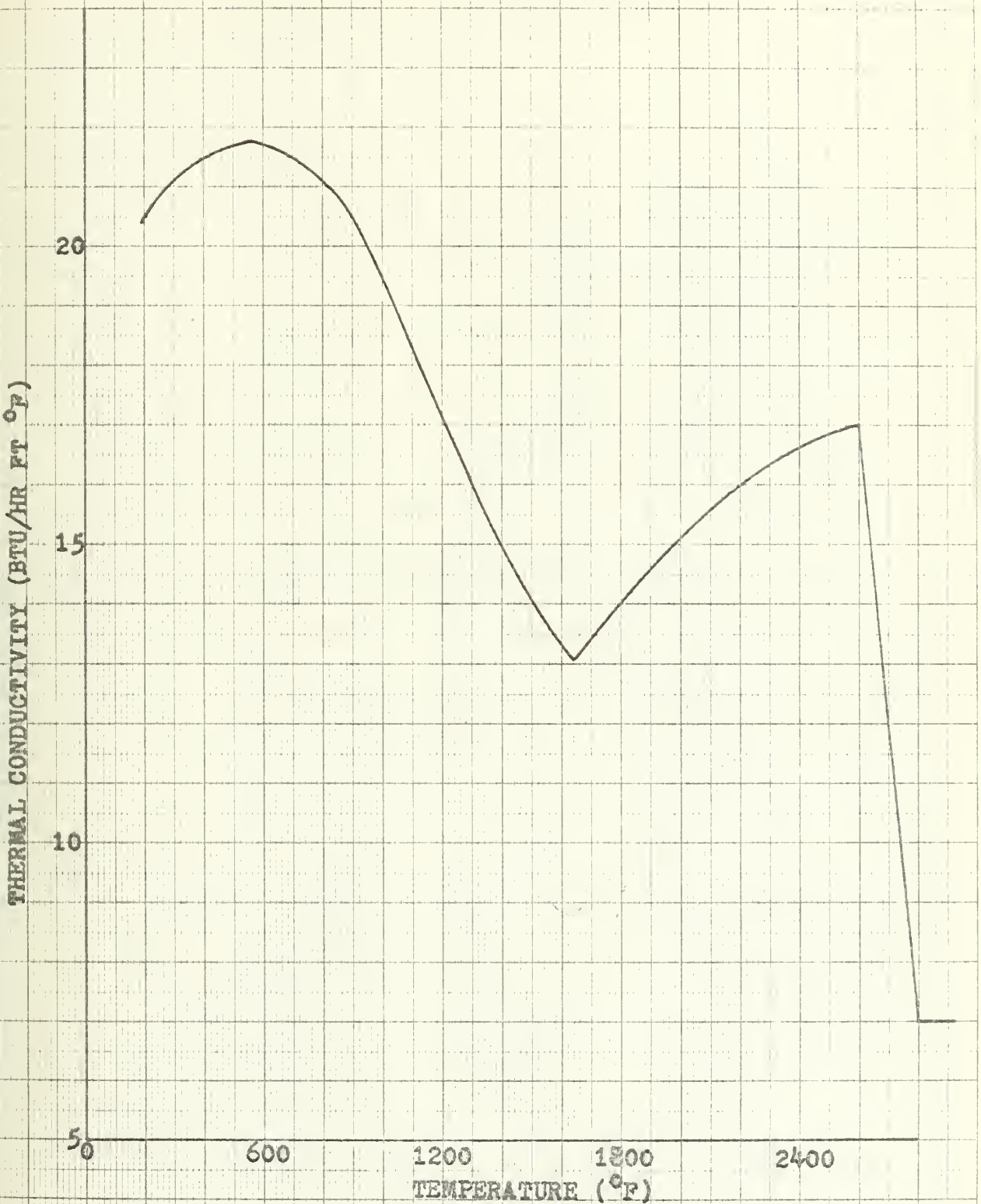

Figure 13. ESTIMATED EFFECT OF TEMPERATURE ON THERMAL CONDUCTIVITY FOR HY-130.

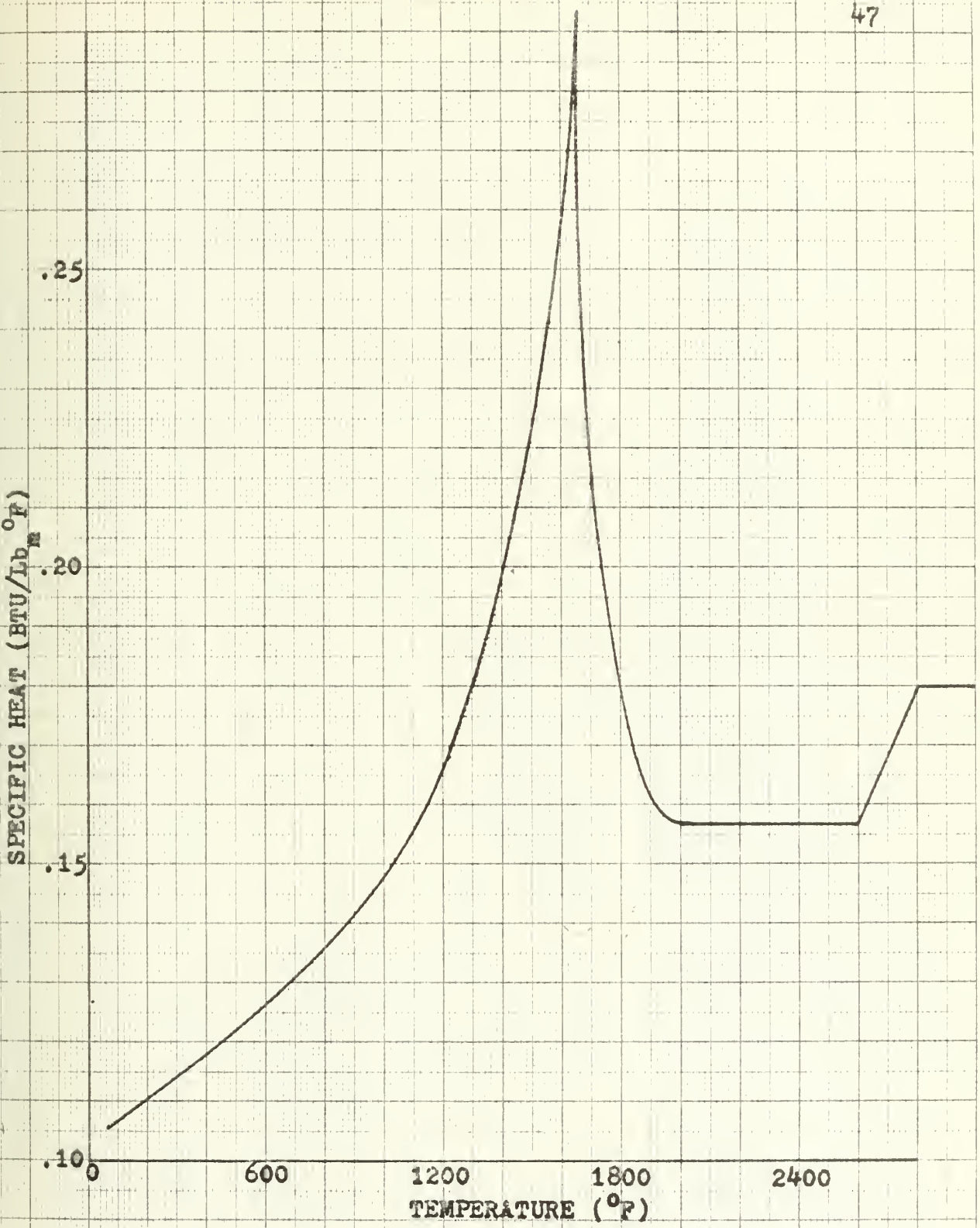

Figure 14. ESTIMATED EFFECT OF TEMPERATURE ON SPECIFIC HEAT FOR HY-130.

Table 4. Summary of Physical Properties for HY-130 Steel

T	68	200	400	600	800	1000	1200	1400	1600	1660	1800	2000	2200	2400	2600	2800
ρ	.284	.283	.282	.280	.279	.278	.276	.275	.275	.275	.275	.275	.275	.275	.275	.275
α_T	6.1	6.5	6.95	7.3	7.7	8.0	8.3	8.18	7.05	6.92	7.0	7.2	7.3	7.4	7.5	7.5
C	19.4	20.4	21.5	21.8	21.2	19.5	17.1	15.0	13.4	13.1	14.0	15.0	16.0	16.7	17.0	7.0
K	.107	.11	.118	.126	.136	.148	.168	.197	.255	.293	.18	.158	.158	.158	.158	.18

NOMENCLATURE

T = Temperature (^{o}F)

ρ = Density (Lb_m/in^3)

α_T = Coefficient of Thermal Expansion (Microstrain/^{o}F)

C = Thermal Conductivity (BTU/HR FT ^{o}F)

K = Specific Heat (BTU/Lb_m ^{o}F)

III. PROCEDURES

A. General

Twelve experiments were performed measuring temperature, strain, and transverse shrinkage changes during welding. The model used was a constraint butt weld in a Y-slit specimen constructed from quenched and tempered HY-130 steel. The welding procedures, which provide low heat input with full penetration, were developed by Portsmouth Naval Shipyard. Strain gages were placed as close to the weld line as possible without exceeding their temperature limit of 400°F.

B. Material, Specimen Design, and Welding Process Selection

Selection for the material for this study was based on its probable use in future construction of submersibles and submarines. The one-inch plate thickness was selected because of availability, and because of the use of one-inch plates in previous Y-slit experimental work. The test plate size of 6x10 inches was governed by availability of material and by the size of specimens used in high constraint welding experiments in the past. The manual shield metal arc weld process (SMA) was used to determine whether or not repeatable results can be obtained with this process. The length of the weld slit, and therefore the size of the

test plate, was determined by the 14-inch length of the manual metal electrodes available.

C. Measurement of Strain

In most cases the experimental stress is determined by actually measuring the strain and calculating the stress from the strain measurement. The three most widely used methods of measuring strain are photoelasticity, brittle coatings, and wire or foil strain gages. Wire or foil strain gages are by far the most convenient, and are used extensively for measuring the normal strains on the surface of a body.

The principle of this gage is based on the physical property that a metal strained in tension or in compression will change its resistance a fractional amount somewhat greater than the strain. The gages can be attached to a surface with relative ease and the resistance change of the gage can be measured. Resistance change of the gage occurs by a change on the body being measured, or by mechanical and thermal strain in the body. The mechanical strain may consist of both elastic and plastic strain.

In strain measurements being made during welding, the resistance change R is made up of the following:

$$\Delta R = \Delta R(\varepsilon_e) + \Delta R(\varepsilon_p) + \Delta R(\alpha_T) + \Delta R(T) \qquad \text{Equation 14}$$

where

ΔR = total resistance change

$\Delta R(\varepsilon_e)$ = resistance change due to elastic mechanical strain in body

$\Delta R(\varepsilon_p)$ = resistance change due to plastic mechanical strain in body

$\Delta R(\alpha_T)$ = resistance change due to temperature-induced thermal strains in body

ΔR (T) = resistance change due to thermal resistance characteristics of gages

In order to determine the mechanical strain it is necessary to separate the resistance change $\Delta R(\alpha_T)$ and $\Delta R(T)$ from the total resistance ΔR. The strain gages used in this experiment had an α_T of 13.0 microstrain/$^{\circ}$F. The $\Delta R(T)$ and the difference between the base plate α_T and the gage α_T will generate an error.

To determine this error a test gage of the same type and lot used in the experiment was mounted on a sample of HY-130. This sample with the strain gage attached was heated and the strain vs temperature data was recorded. Table 5 shows the tabulated results of this strain gage calibration data. At each temperature point the temperature equilibrium of the sample plate was ensured prior to recording strain data. The data from Table 5 was plotted

to give a curve of "apparent strain" vs temperature (illustrated by Figure 15). The gage measurements recorded in the welding experiment were corrected by subtracting out the apparent strain to give the mechanical strain. The strain gages used in this experiment are manufactured in the form of rosettes which provide three independent strain readings in three directions at one location.

D. Test Apparatus

The test specimen and location of instrumentation is illustrated in Figure 16 and 17. The output of all test devices was recorded continuously during the welding process, providing dynamic measurements of temperatures, strain, and transverse shrinkage data.

T-1, T-2, and T-3 are thermocouples.

A, B, and C are strain gages.

E. Sensors and Instrumentation

1. Strain Gages

One type of strain gage (SR-4 foil 45° rosette) was used in this investigation. The gage properties were as follows:

Gage	SR-4 Rosette
Designation	FAER-18RB-12S13L
Manufacturer	BLH Electronics
Grid Length	3/16 inches

Grid Width	0.90 inches
Overall Length	0.230 inches
Overall Width	0.540 inches
Temperature Range	-50 to +400°F
Resistance	120 Ohms
Gage Factor	2.03
Cement	EPY-550
Protective Covering	BLH Barrier C

2. Temperature Sensors

All temperature sensors used were Chromel/Alumel thermocouples made from Leads and Northrup No. 28 wires. Three thermocouples were spot-welded onto each test specimen and protected by No. 33 Sauereisen sealing cement. The temperature sensors for the rosette strain gage was located .375 inches (approximately 5 seconds) behind the rosette strain gage, mid-axis. One temperature sensor was located .125 inches directly below the weld at the mid-axis of the strain gage. The third temperature sensor was located .45 inches from the weld centerline.

F. Instrumentation

The strain gages were connected into a potentiometer circuit used to balance and calibrate the gages (indicated schematically in Figure 18). The thermocouples were referenced to a 32°F ice bath and calibrated (Figure 19).

Table 5. Strain Gage Calibration Data

Test Plate - HY-130 - Thickness, one inch	
Temperature (°F)	Microinches/inch (all compression)
78	REF
90	25
110	150
130	285
160	500
180	665
200	810
225	980
240	1100
260	1240
280	1400
300	1530
320	1625
340	1740
360	1825
380	1925
400	2000

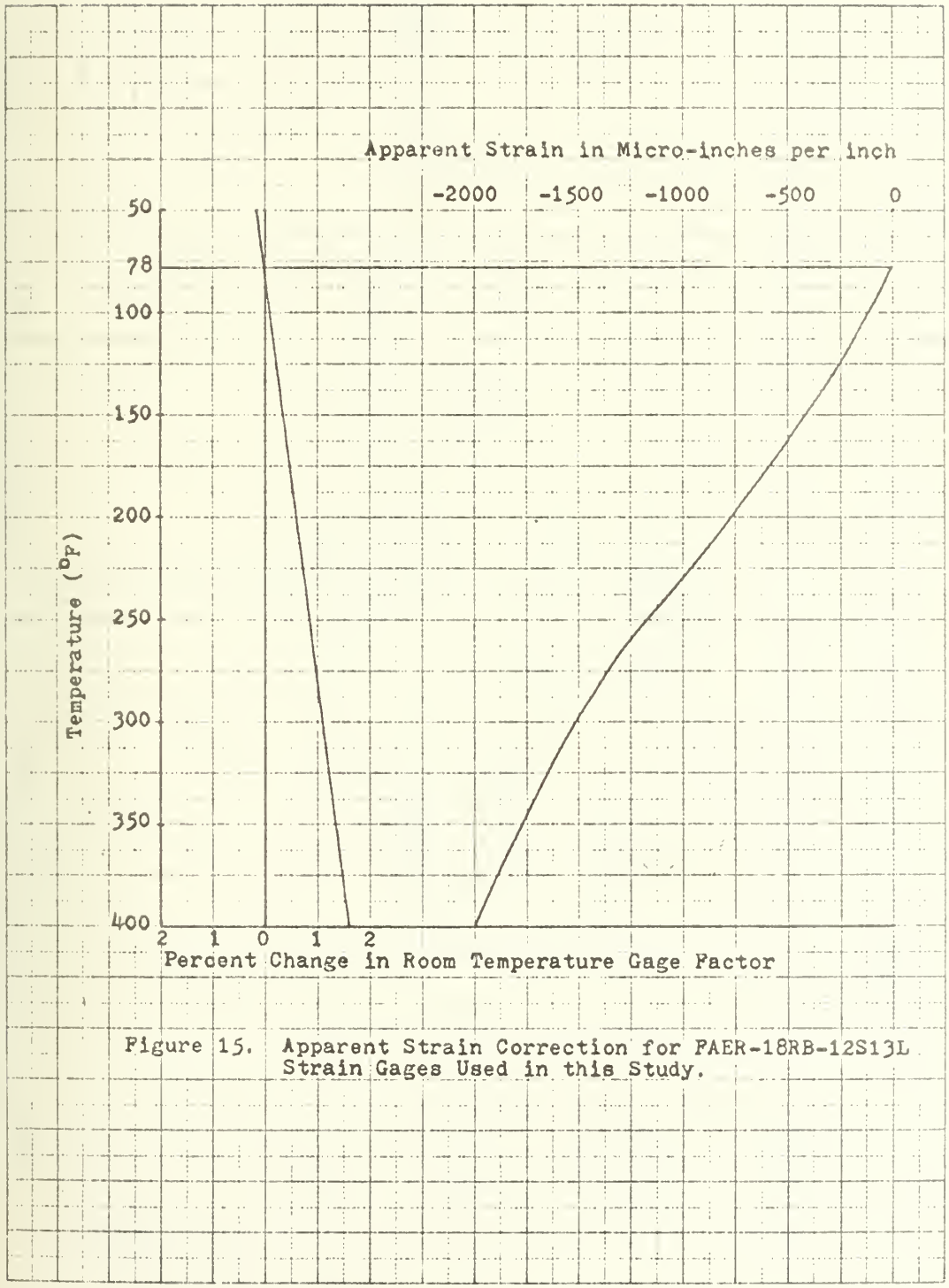

Figure 15. Apparent Strain Correction for FAER-18RB-12S13L Strain Gages Used in this Study.

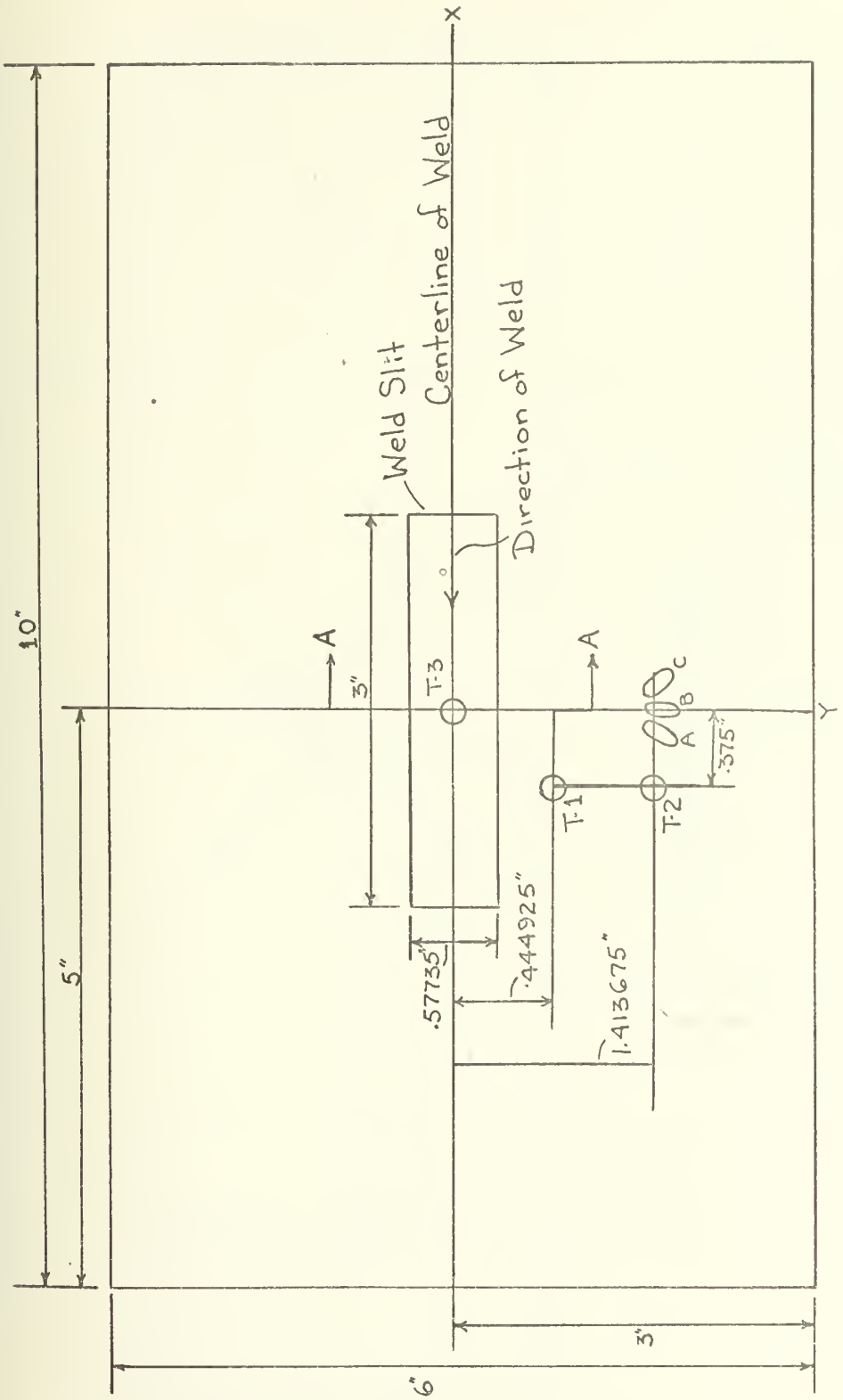

Figure 16. Test Specimen

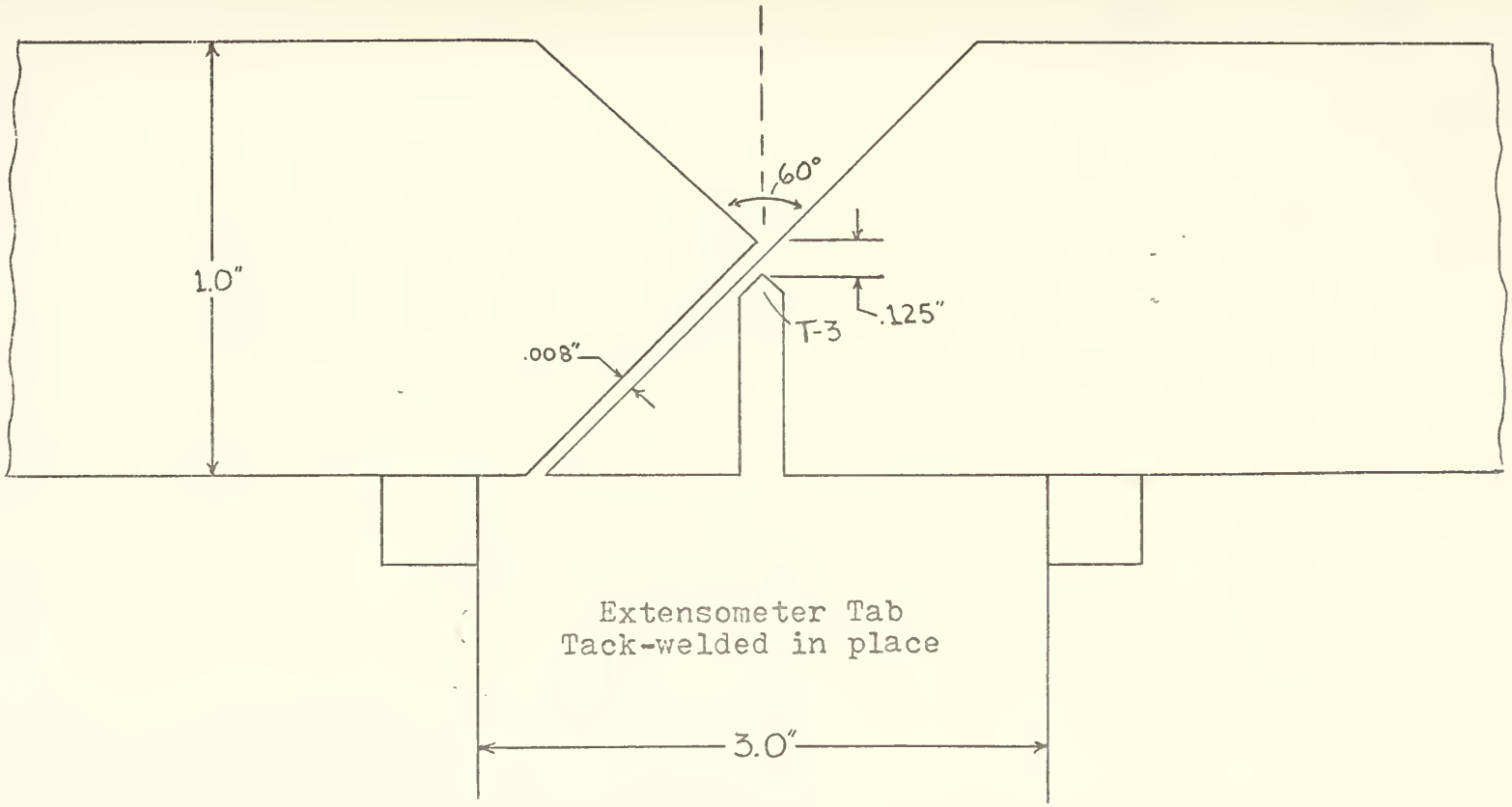

Figure 17. Section View A-A of Figure 16

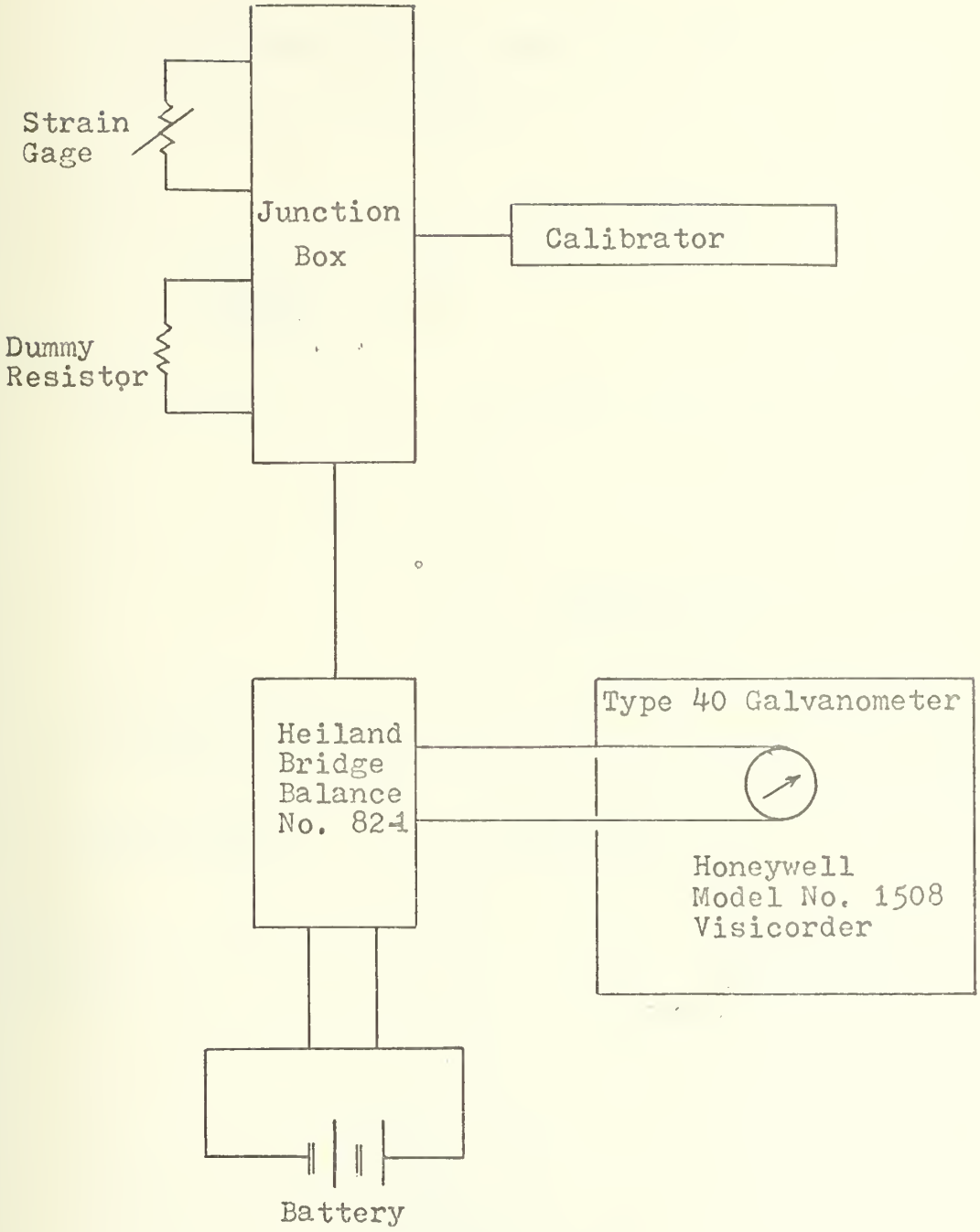

Figure 18. Strain Gage Instrumentation Circuit (1)

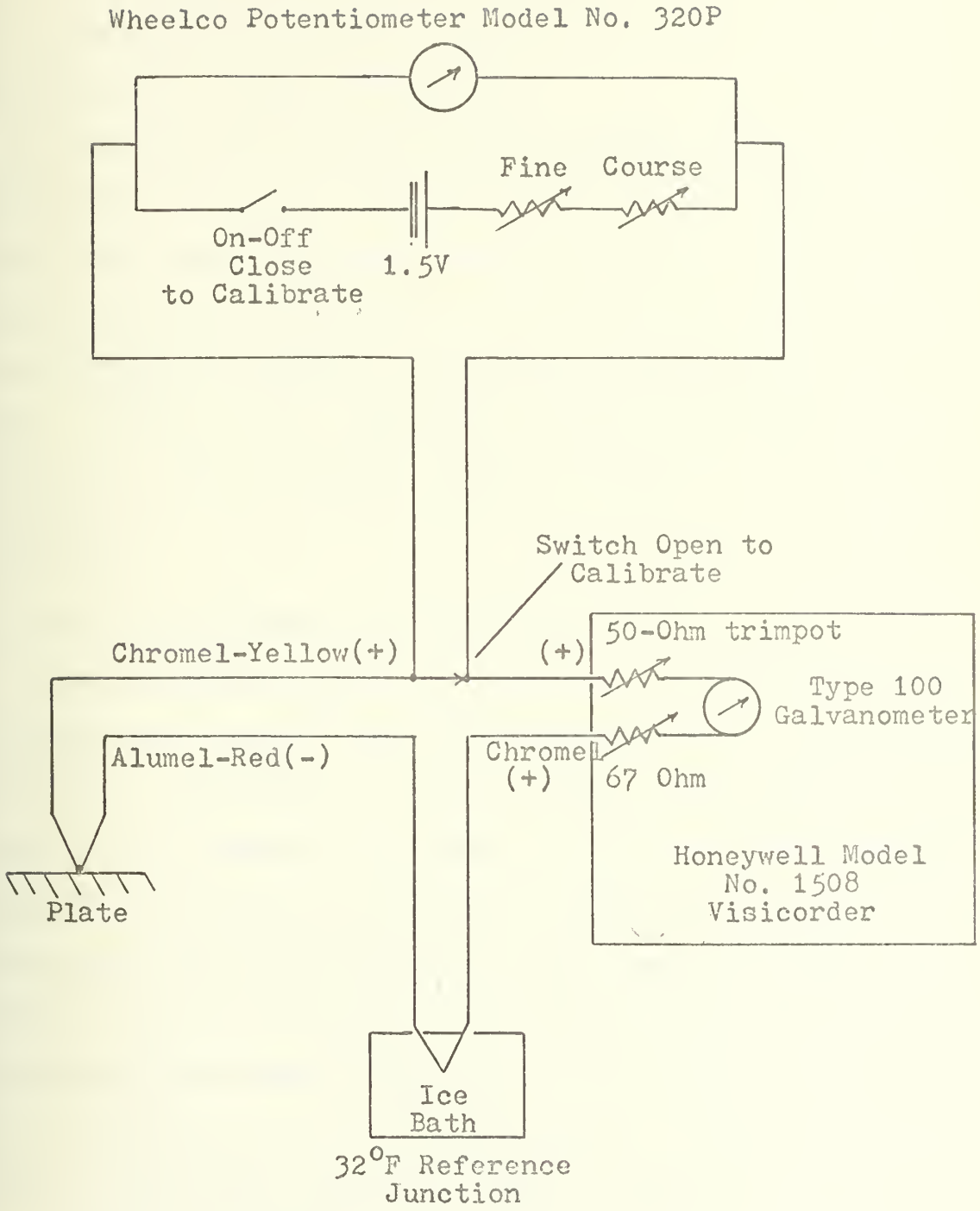

Figure 19. Thermocouple Instrumentation Circuit (1)

The extensiometer with strain gages located on both sides of a spring steel was also balanced and calibrated with a potentiometer circuit (Figure 20).

All circuits were fed into a Honeywell continuous-recording, 12-channel viscorder. Because the thermocouple and strain gages were not located at the same position along the weld line, the raw data from the recorder tape was delayed or advanced as necessary when the data was read. Timing of the experiment was done simultaneously by an electric stop watch and a timer integrated into the viscorder.

G. Welding Equipment and Conditions

The welding machine that was used was manufactured by Air Reduction (trade name--AC/DC Heli Welder). The welding conditions, including the travel speed, arc voltage, amperage, and arc length, are shown in Table 6. The amperage, which was monitored continuously during the welding, fluctuated about ±10 percent of the recorded values. The voltage was also monitored continuously during the welding and fluctuated about ±5 percent of the recorded values. The electrodes used were 14-inch long, 5/32-inch diameter, E14018 electrodes produced by McKay Company of York, Pa.

Figure 21 shows one of the six test specimens prior to welding with all instrumentation installed.

Figure 22 shows the test specimen with the extensiometer mounted in place.

Figure 23 is an overall view of the experimental equipment showing the instrumentation and recorder.

Figure 24 is a test specimen with both the first and second weld passes completed.

H. Experimental Procedures

The experimental operation is shown schematically in Figure 25. The test plate was oriented as shown, and the extensiometer was located below the plate. The viscorder was actuated; as the arc was struck, the timer was started. The viscorder was marked when the arc passed the mid-axis of the strain gage location. When the weld bead was completed, the plate was allowed to cool to between 100° and 150°F, or until a weld crack was visible, while the recorder continued monitoring the temperature sensors and strain gages. Then the second weld arc was performed following the same procedures as the first weld pass. After each weld pass, the length of weld rod consumed was recorded so the weight of weld metal deposited per pass would be known.

I. Data and Calculation Procedures

The experimental data (Appendix A) was corrected for temperature, and strain and stress calculations were

performed with the aid of the computer program from Reference 16. The basic program was used with some modifications for rosette location, material parameters, and welding conditions.

The coordinate system and the mathematical formulation used to reduce the data with the computer program is presented in Appendix B. The reduced data is presented in Appendix C. The material parameters--coefficient of thermal expansion, Young's modulus, and yield stress as a function of temperature (see Chapter II)--were used in the program to determine whether plastic condition as defined by Masubuchi had resulted at the point of measurement.[7,16]

The time to crack was determined by first observing the time that a crack was visible; then observing the time of the slope change of transverse shrinkage; and then the time of the slope change of transverse strain due to dynamic change of the test plate cooling. From the time to crack a value of K fracture toughness was determined by using the empirical fracture mechanics models discussed in Chapter I. The empirical equation used was

$$K = 1.06\sigma_{YY}\sqrt{\pi a} + \sigma_{XX}\sqrt{\pi a} \qquad \text{Equation 15}$$

where σ_{YY} and σ_{XX} are as defined in Appendix B and a is one-half the slit length, or 1.5 inches.

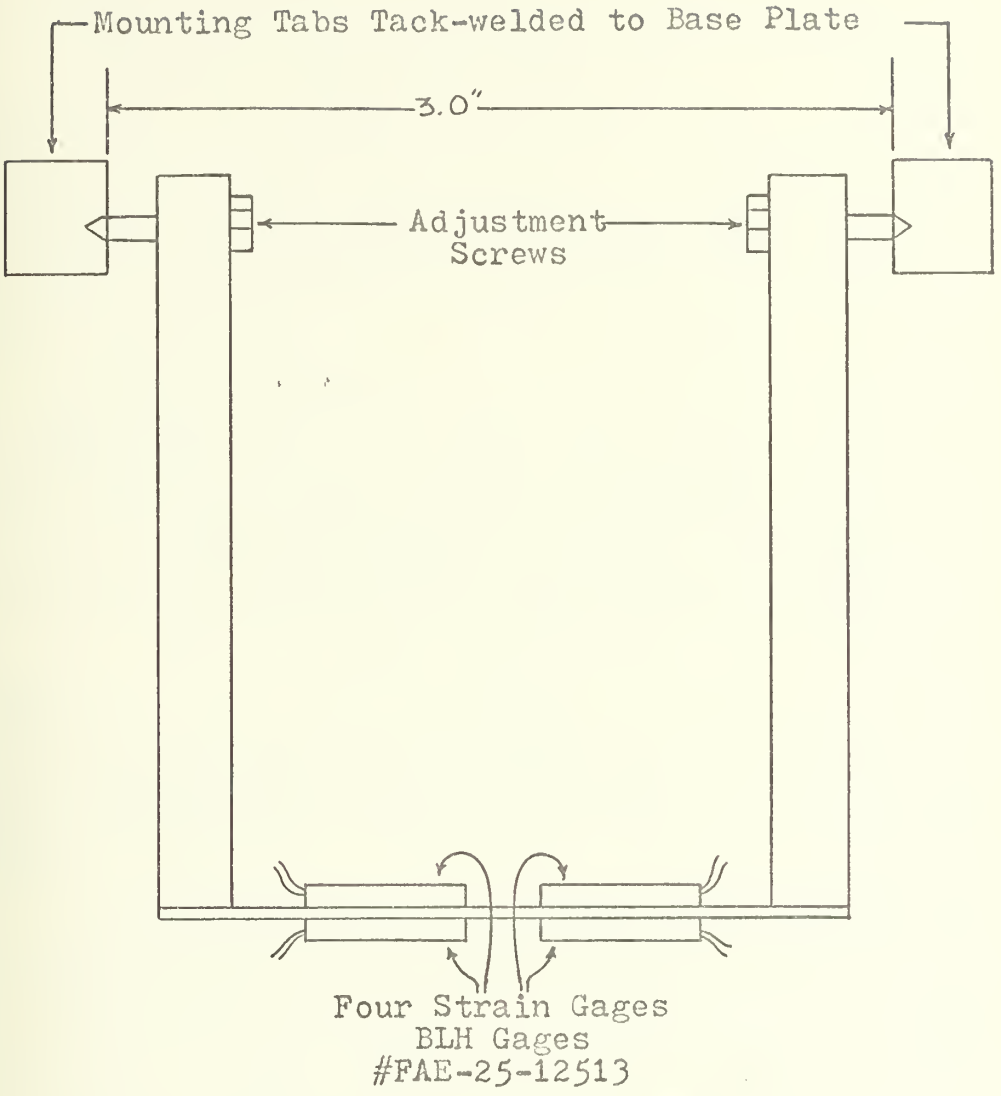

Figure 20. Extensiometer

Table 6. Summary of welding conditions for each test

Test Number	Pass Number	I* Amperes	V** Volts	v In/sec	Weld Metal Deposited Wt = Lb_m	Heat Input Joules/inch	Heat Intensity BTU/sec
1	1	260	25	4.719	.2658	82,644.6	6.16
	2	260	25	4.468	.2636	87,287.4	6.16
2	1	220	25.5	3.821	.2832	88,092.1	5.32
	2	220	26	3.818	.2701	89,889.9	5.42
3	1	200	26	3.560	.2745	87,640.5	4.92
	2	200	26	3.818	.2701	81,718.2	4.93
4	1	200	26	3.725	.2658	83,758.4	4.93
	2	200	26	3.852	.2701	80,996.9	4.93
5	1	200	26	3.717	.2745	83,938.6	4.93
	2	200	26	3.762	.2636	82,934.6	4.93
6	1	200	26	3.621	.2658	86,164.1	4.93
	2	200	26	3.889	.2679	80,226.3	4.93

*Amps varied ± 10% from recorder value.

**Volts varied ± 5% from recorder value.

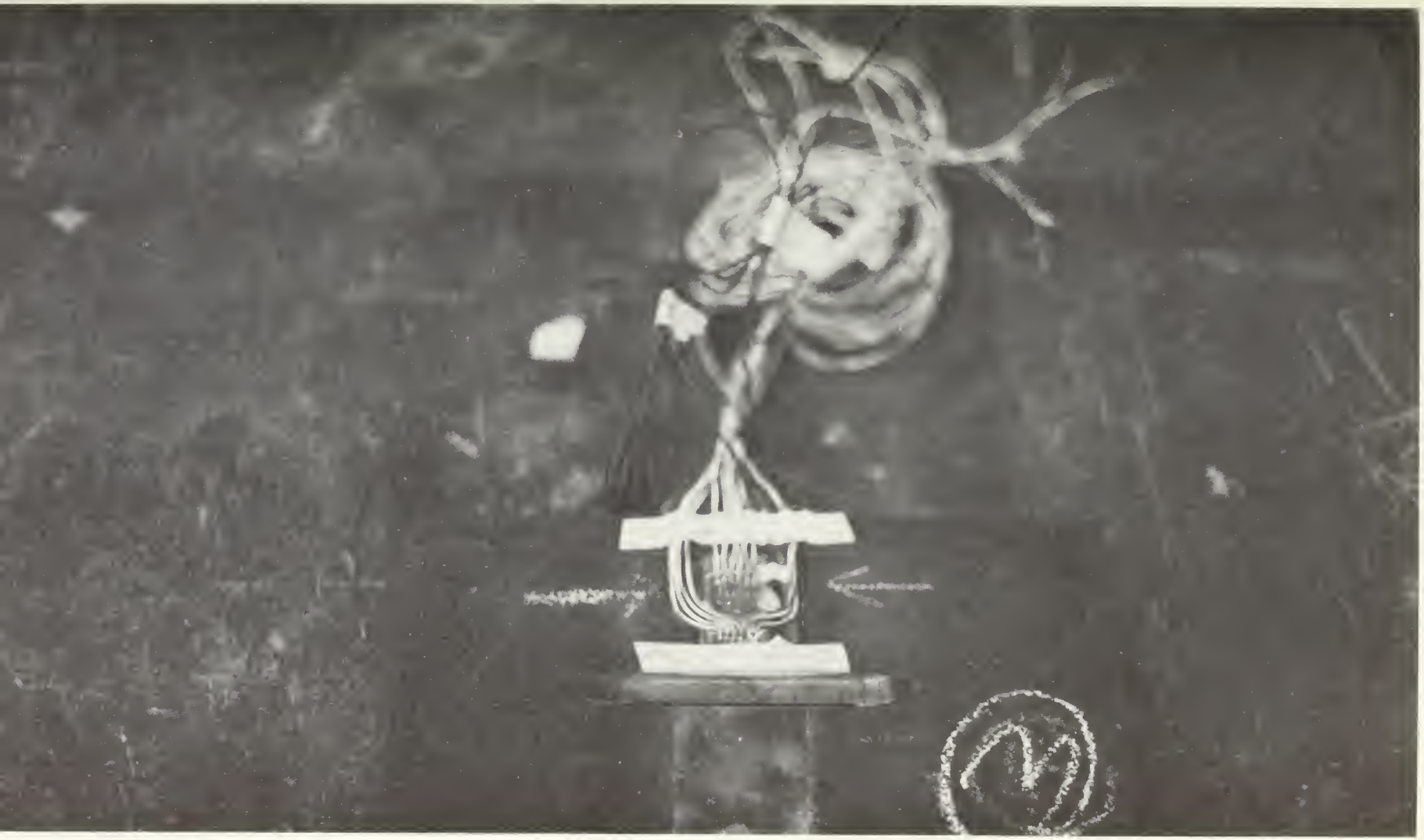

Figure 21. Test Specimen with instrumentation attached

Figure 22. Test specimen with extensiometer below the weld

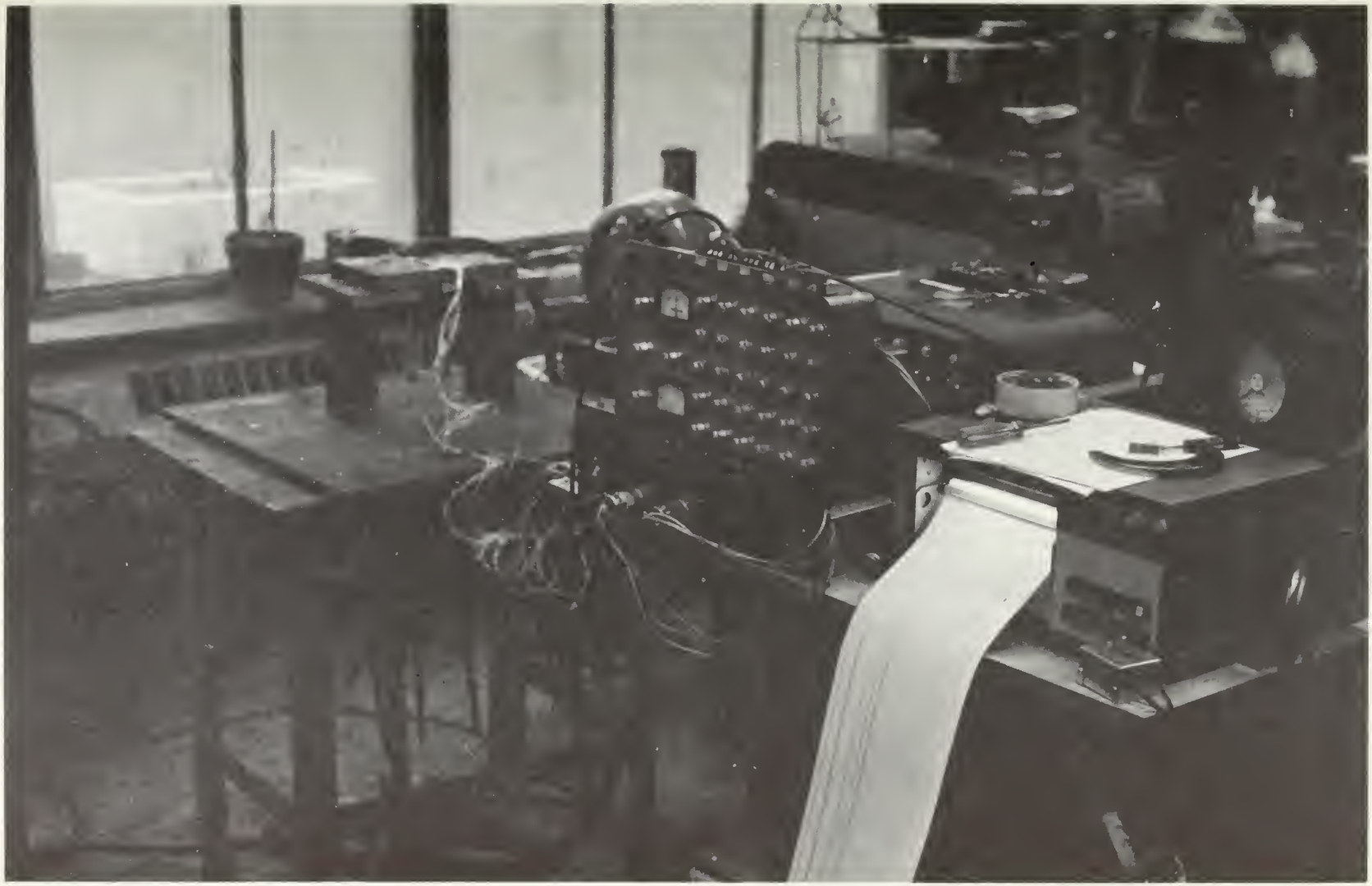

Figure 23. Experimental equipment showing instrumentation and recorder

Figure 24. Test specimen with weld completed

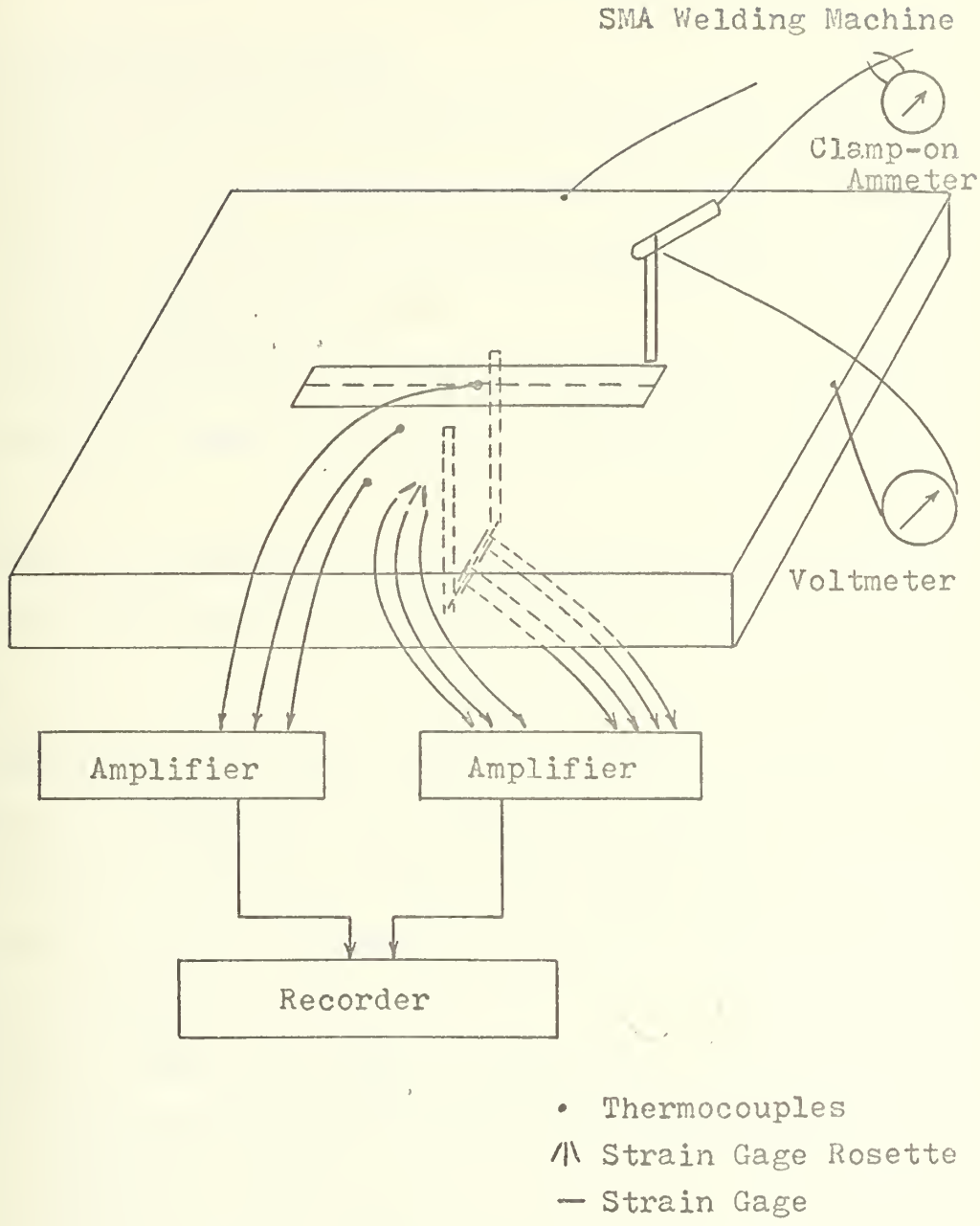

Figure 25. Schematic of Apparatus and Procedure (1)

IV. RESULTS AND CONCLUSIONS

A. Presentation of Results

Figures 26 through 37 are the temperature profiles of T-1, T-2 and T-3 as a function of time for Passes 1 and 2.

Figures 38 through 41 are the extensiometer outputs plotted as a function of time.

Figures 42 through 45 are the strains in the X direction calculated from the measured output of the rosette gages.

Figures 46 through 49 are the strains in the Y direction calculated from the measured output of the rosette gages.

Figures 50 through 57 are the stresses in the X and Y directions calculated from the above strains.

Figures 58 through 60 show the temperature distribution for T-1 and T-2 compared to the one-dimension computer analysis solution.

Table 7 shows the times to crack and the calculated stress intensity factors for the crack initiation for Tests 1 through 6, Pass 1.

Appendix A is the tabulated experimental results of temperature, strain, and transverse shrinkage.

Appendix C is the results calculated from the experimental data using the mathematical model of Appendix B.

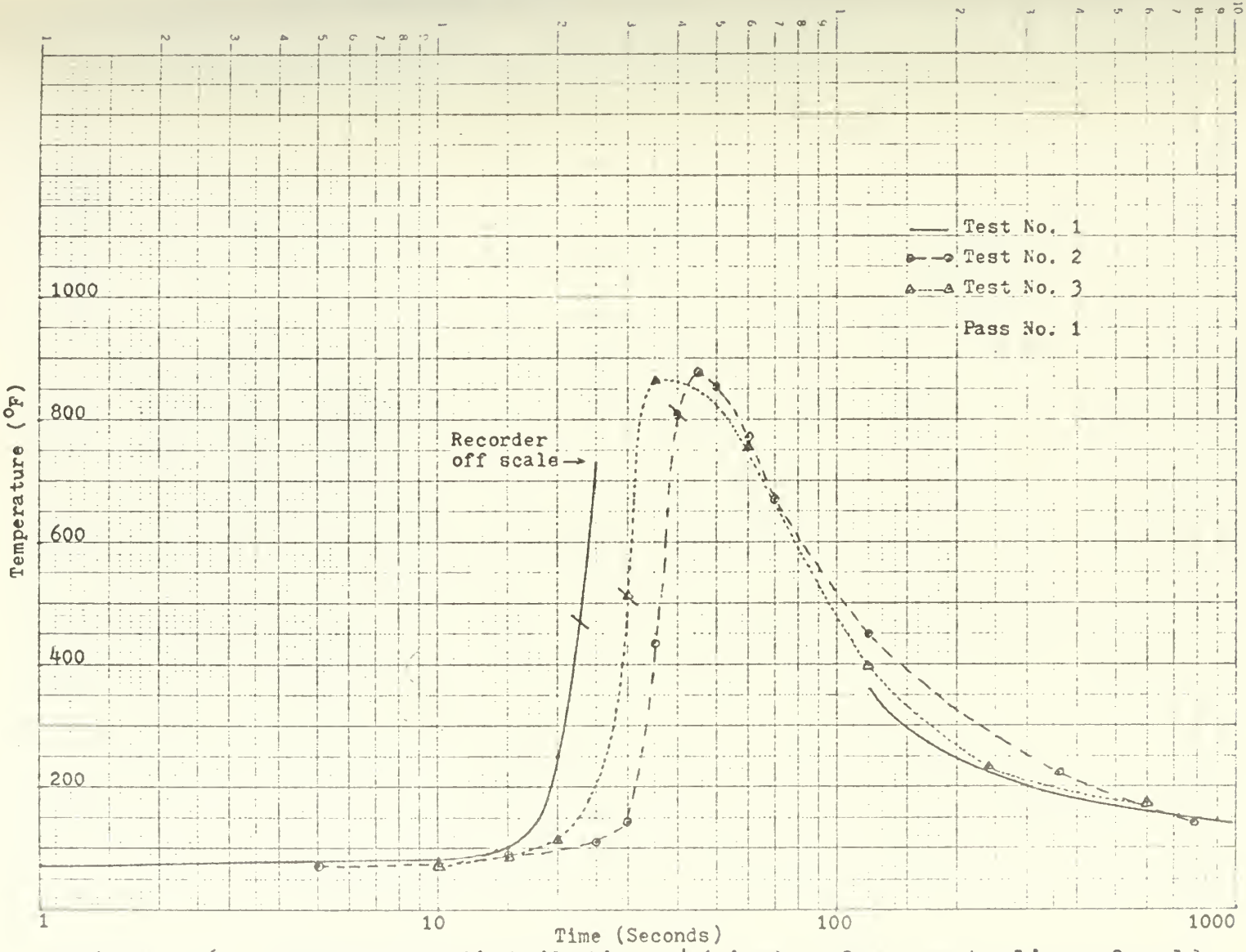

Figure 26. Temperature distribution .45 inches from centerline of weld

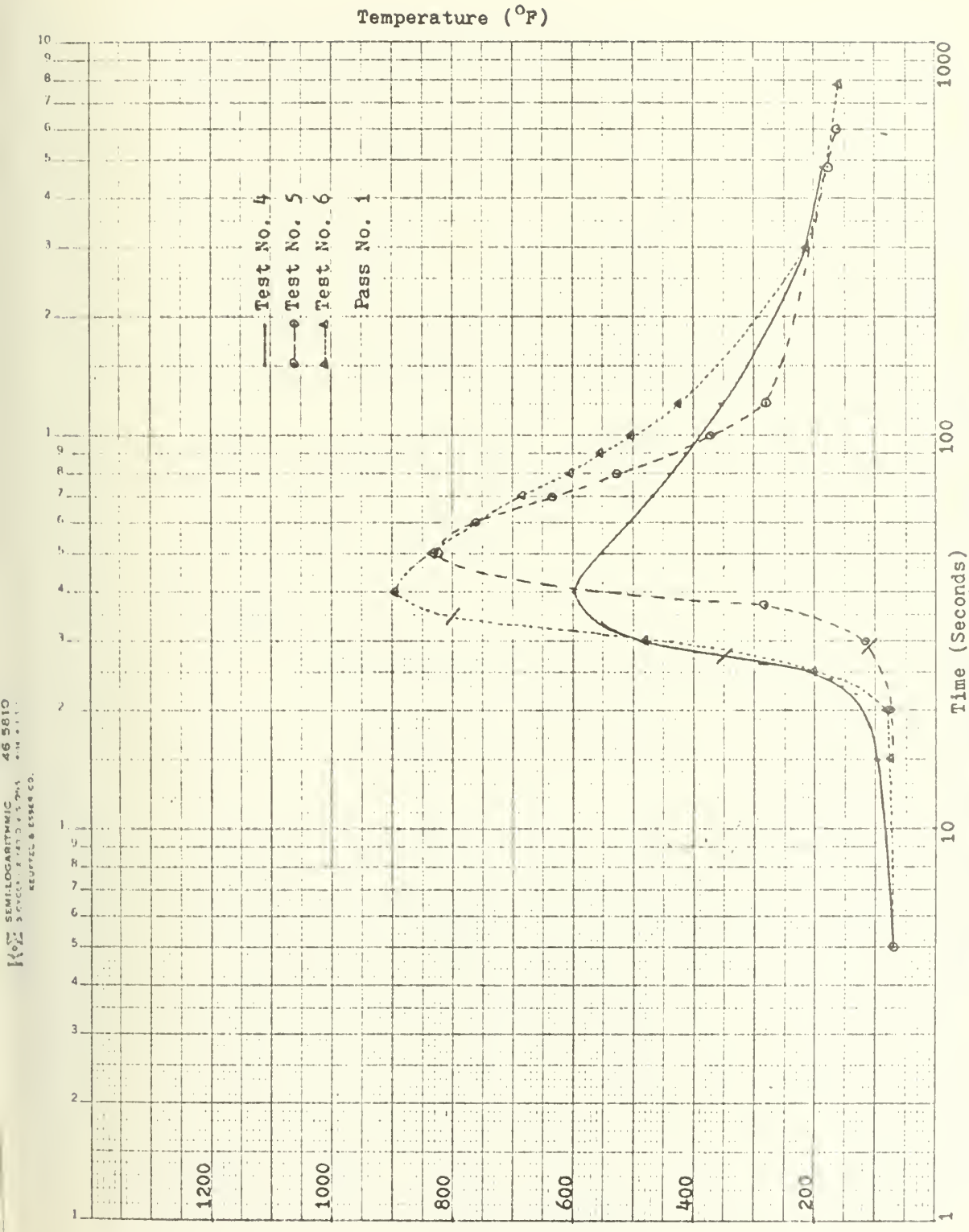

Figure 27. Temperature distribution .45 inches from centerline of weld

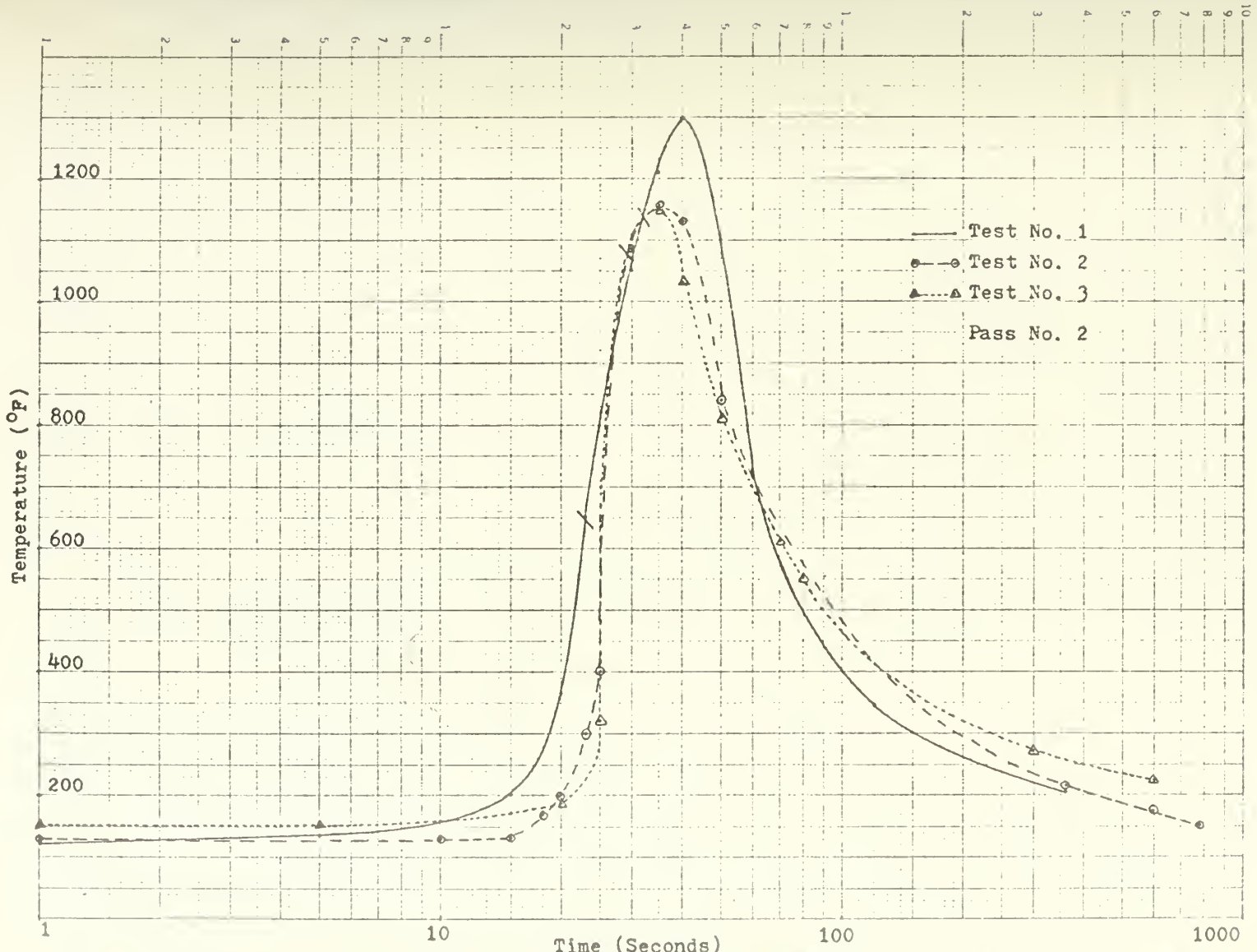

Figure 28. Temperature distribution .45 inches from centerline of weld

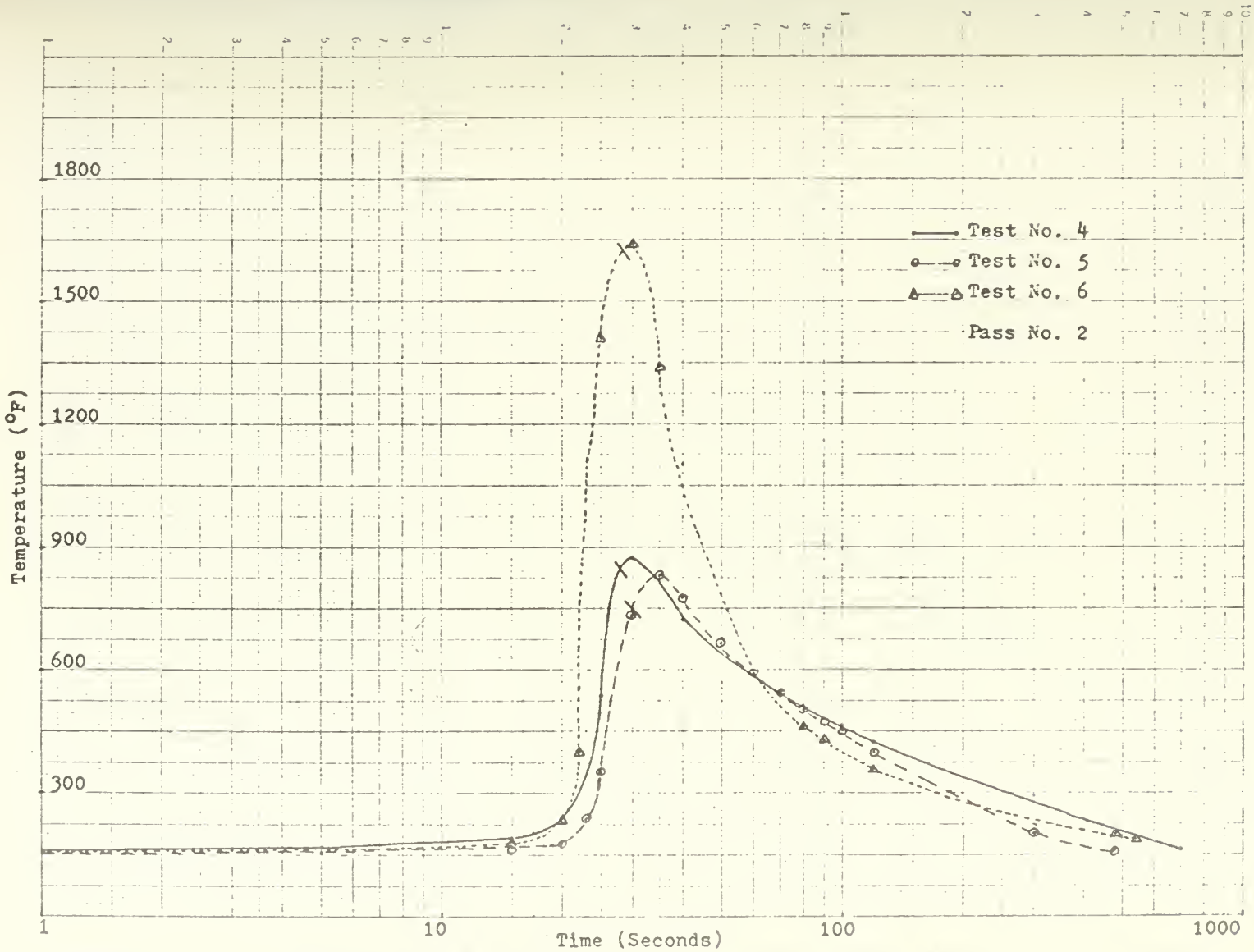

Figure 29. Temperature distribution .45 inches from centerline of weld

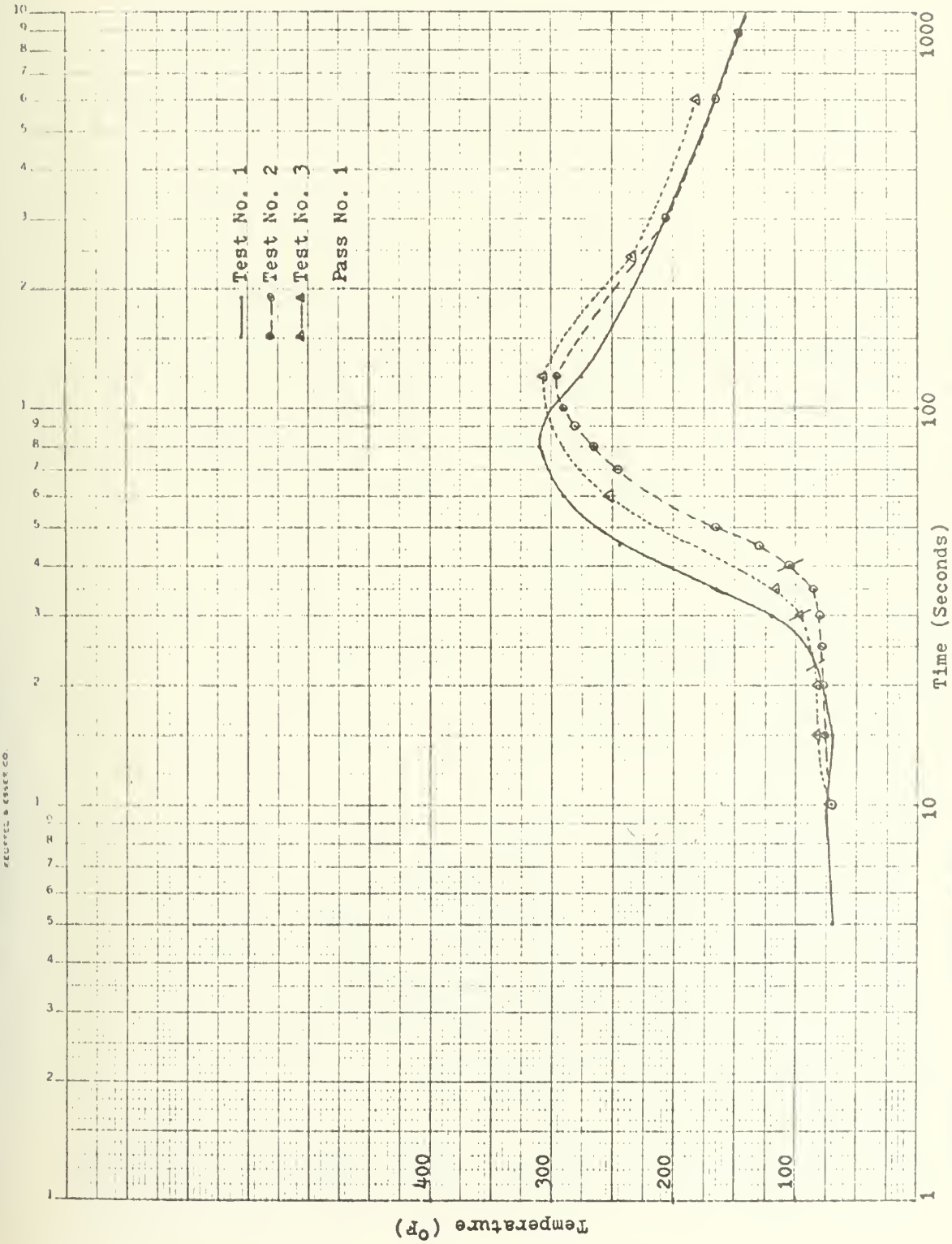

Figure 30. Temperature distribution 1.4 inches from centerline of weld

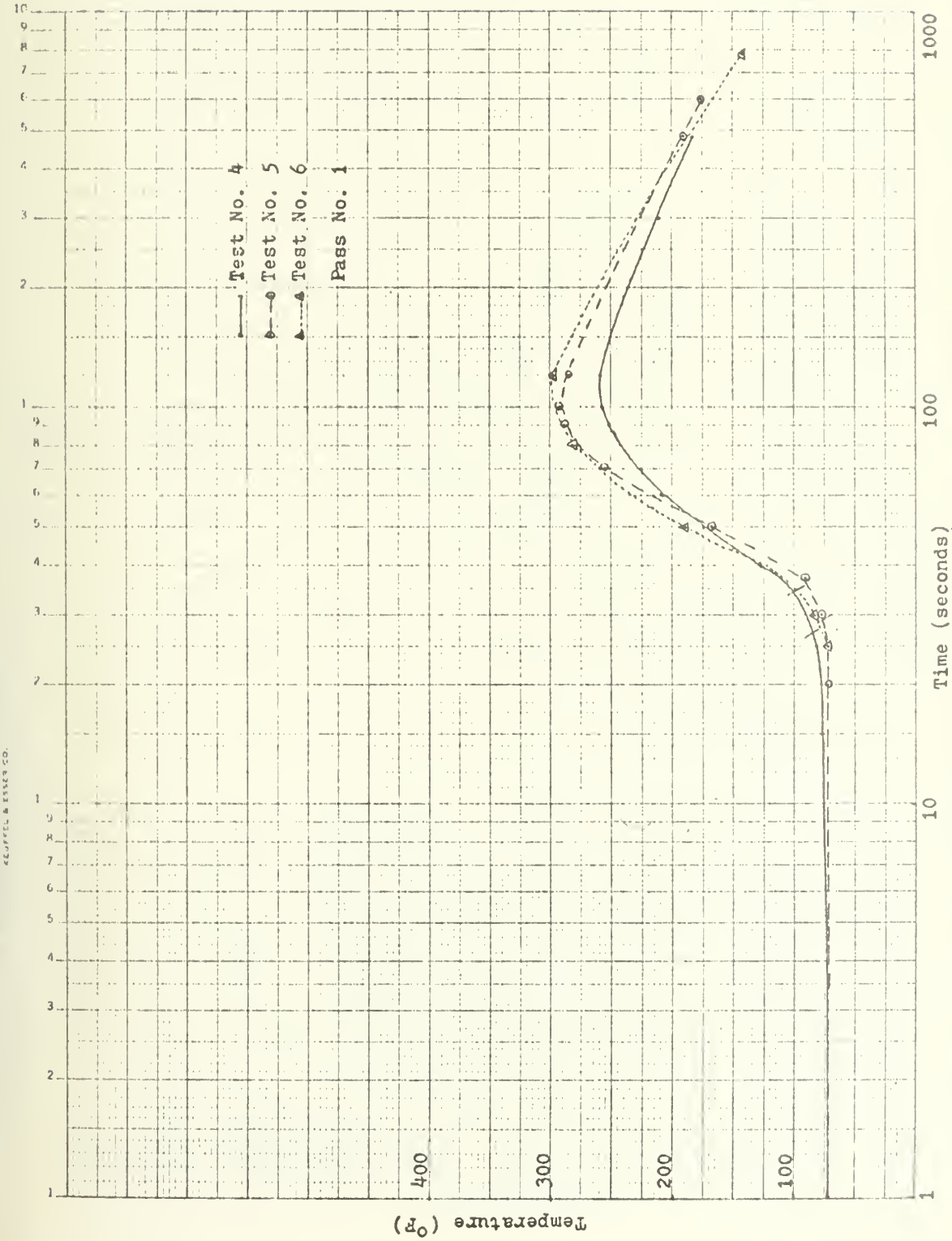

Figure 31. Temperature distribution 1.4 inches from centerline of weld

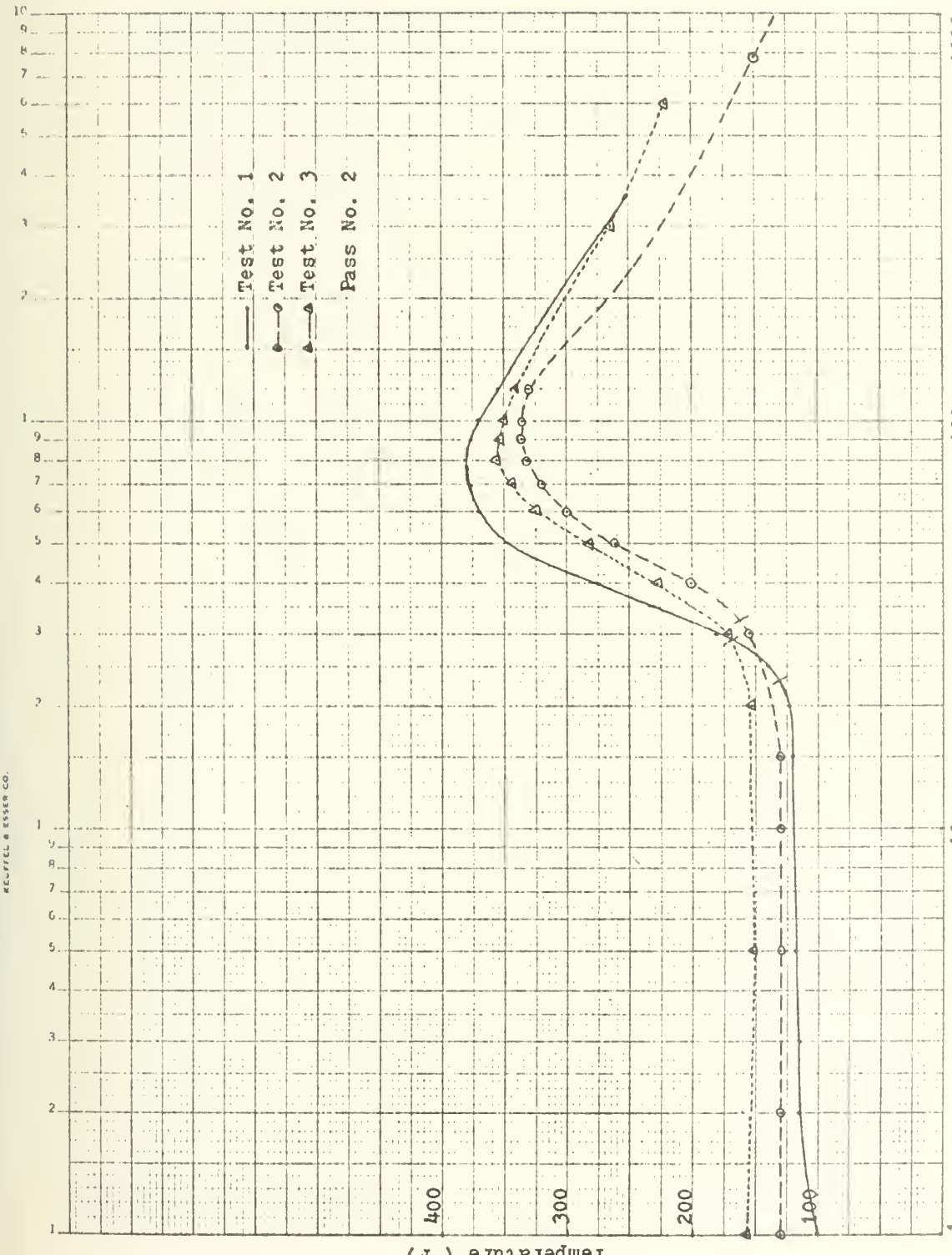

Figure 32. Temperature distribution 1.4 inches from centerline of weld

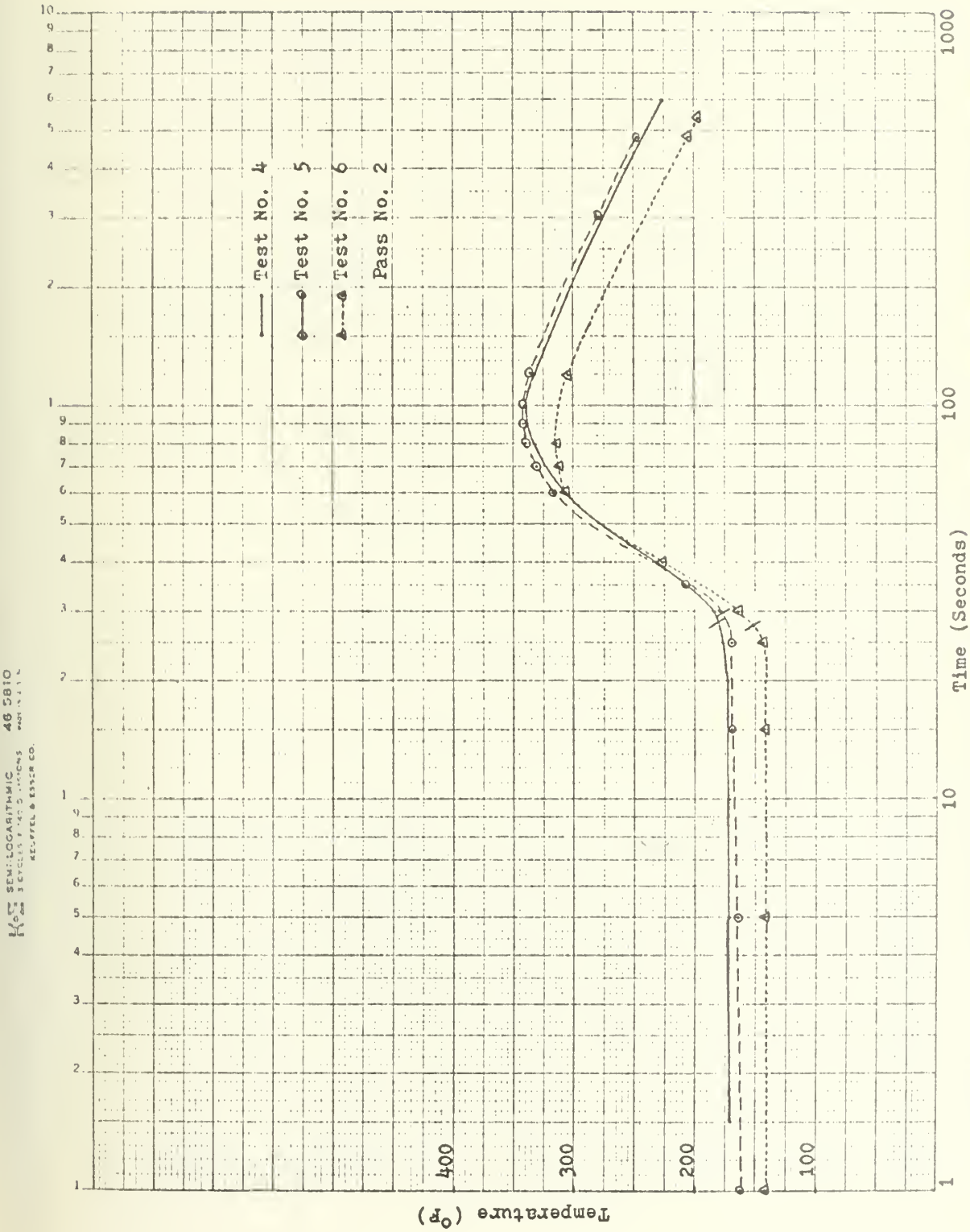

Figure 33. Temperature distribution 1.4 inches from centerline of weld

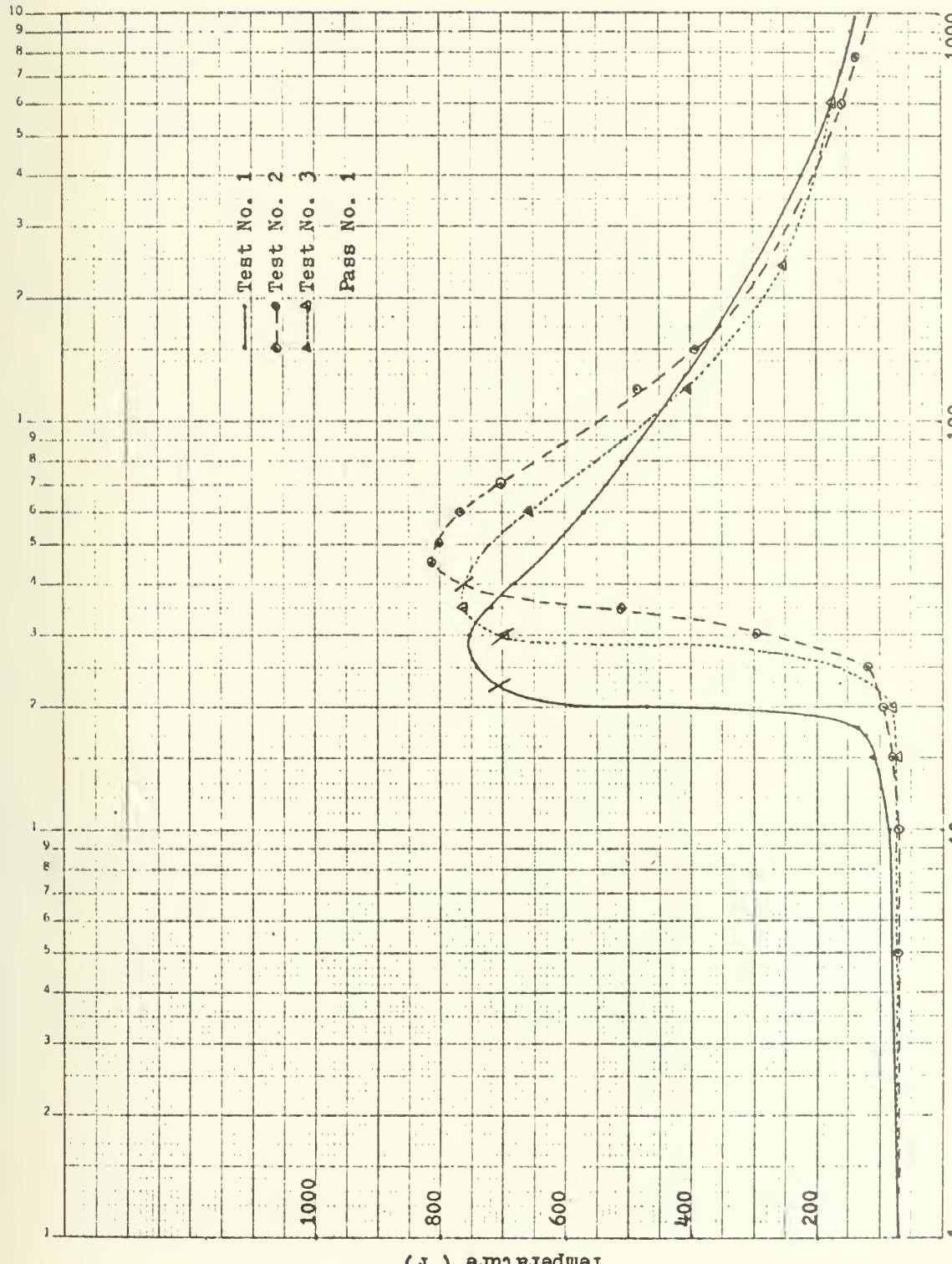

Figure 34. Temperature distribution .125 in. below weld on centerline of weld

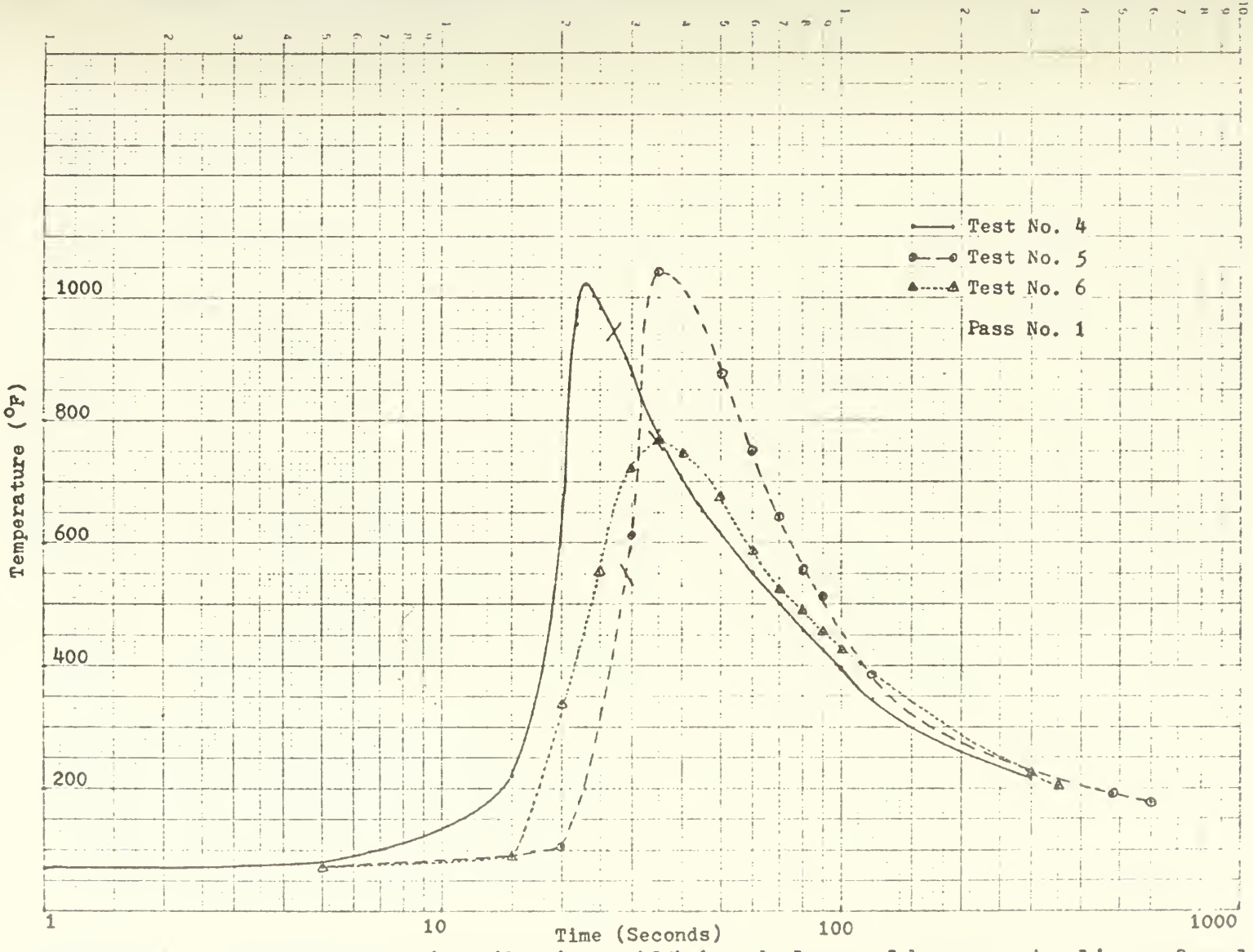

Figure 35. Temperature distribution .125 in. below weld on centerline of weld

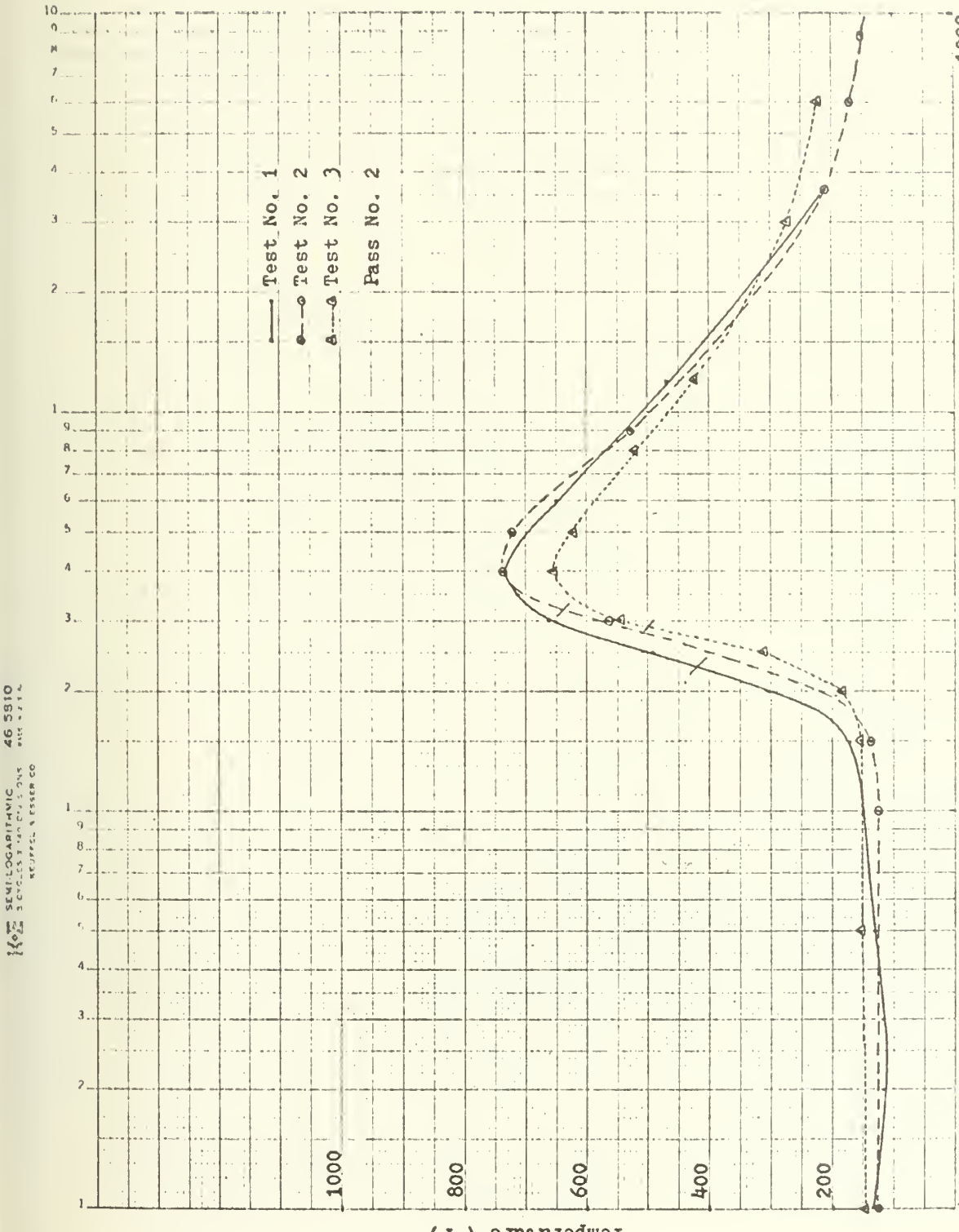

Figure 36. Temperature distribution .125 in. below weld on centerline of weld

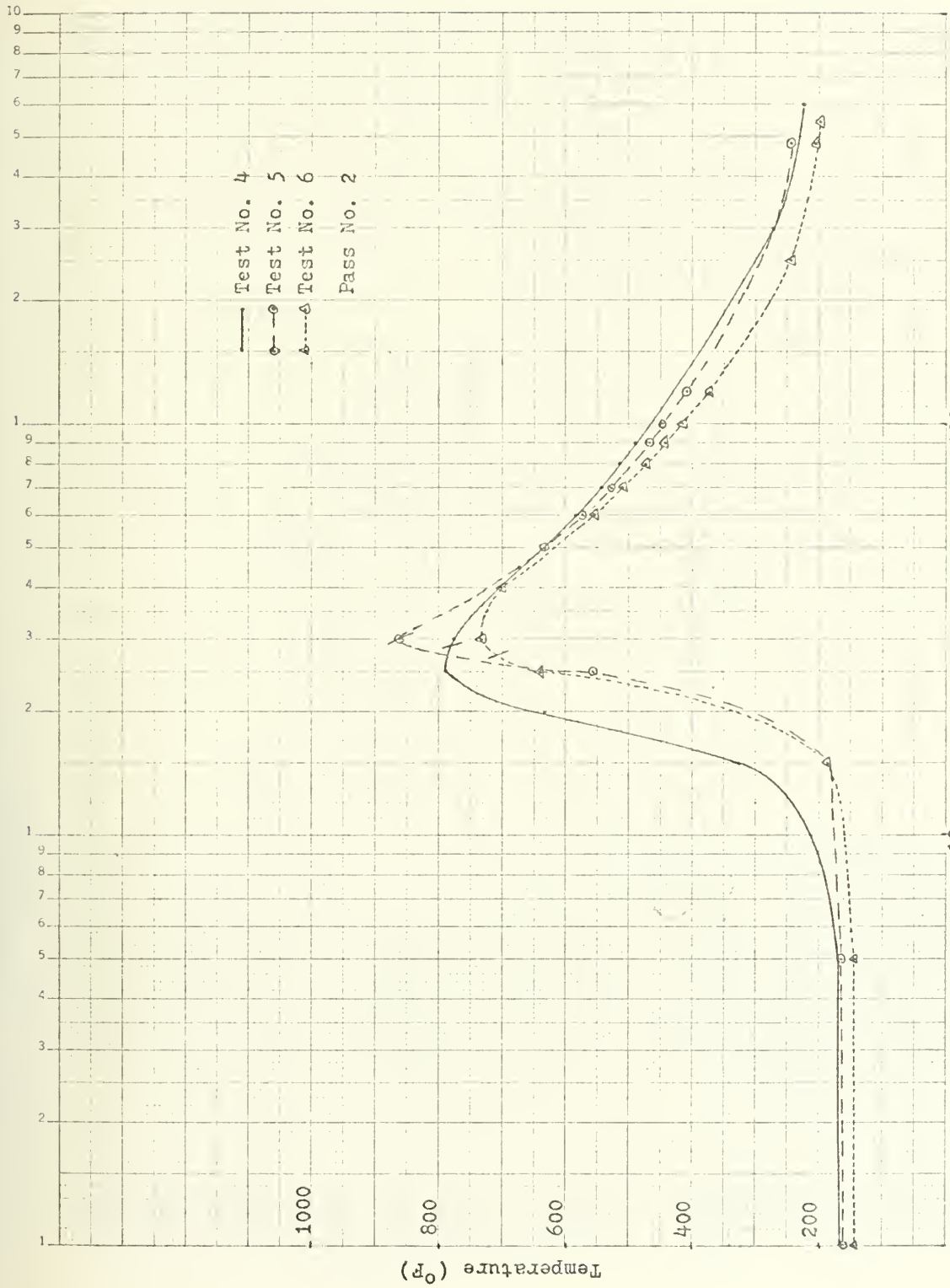

Figure 37. Temperature distribution .125 in. below weld on centerline of weld

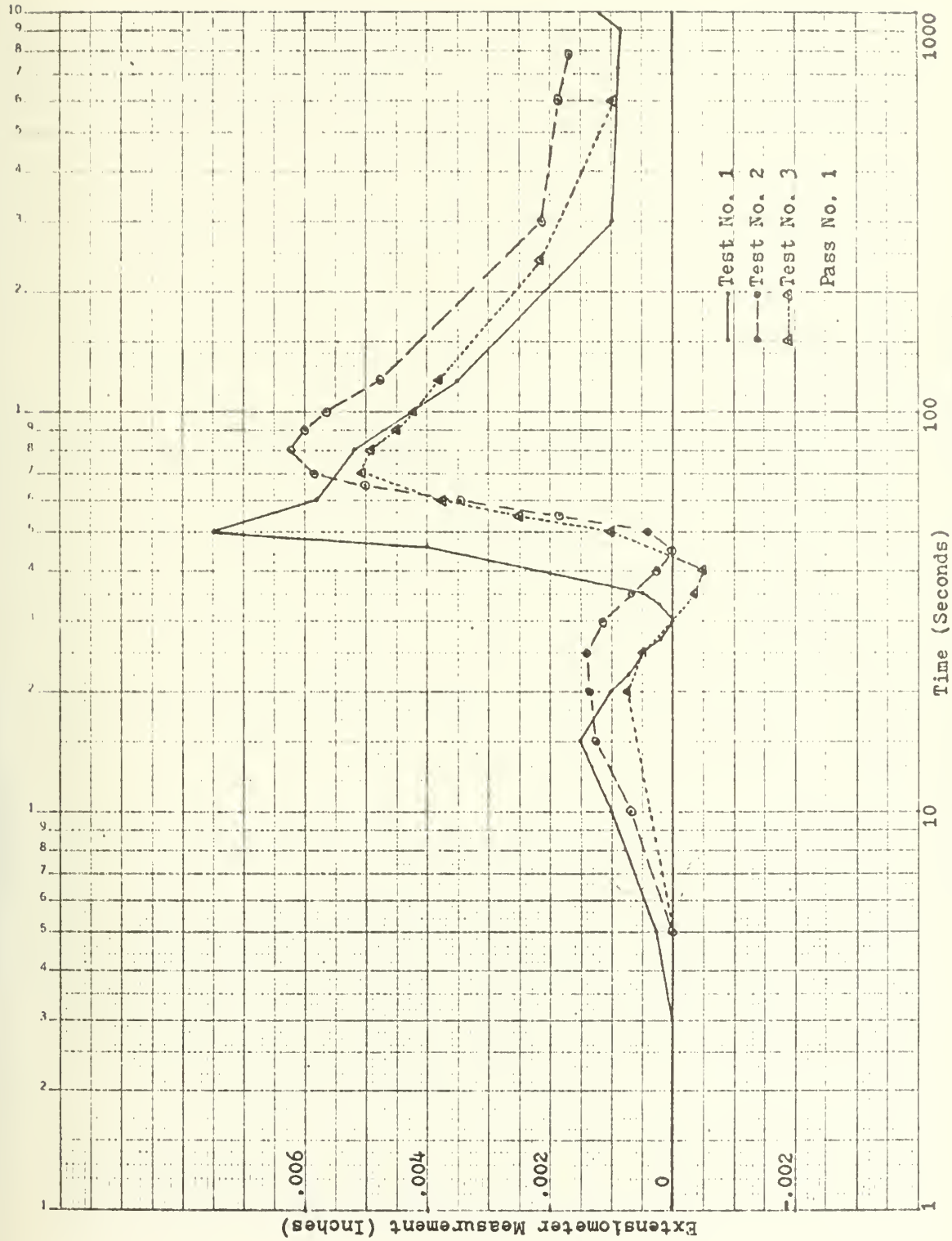

Figure 38. Extensiometer measurements

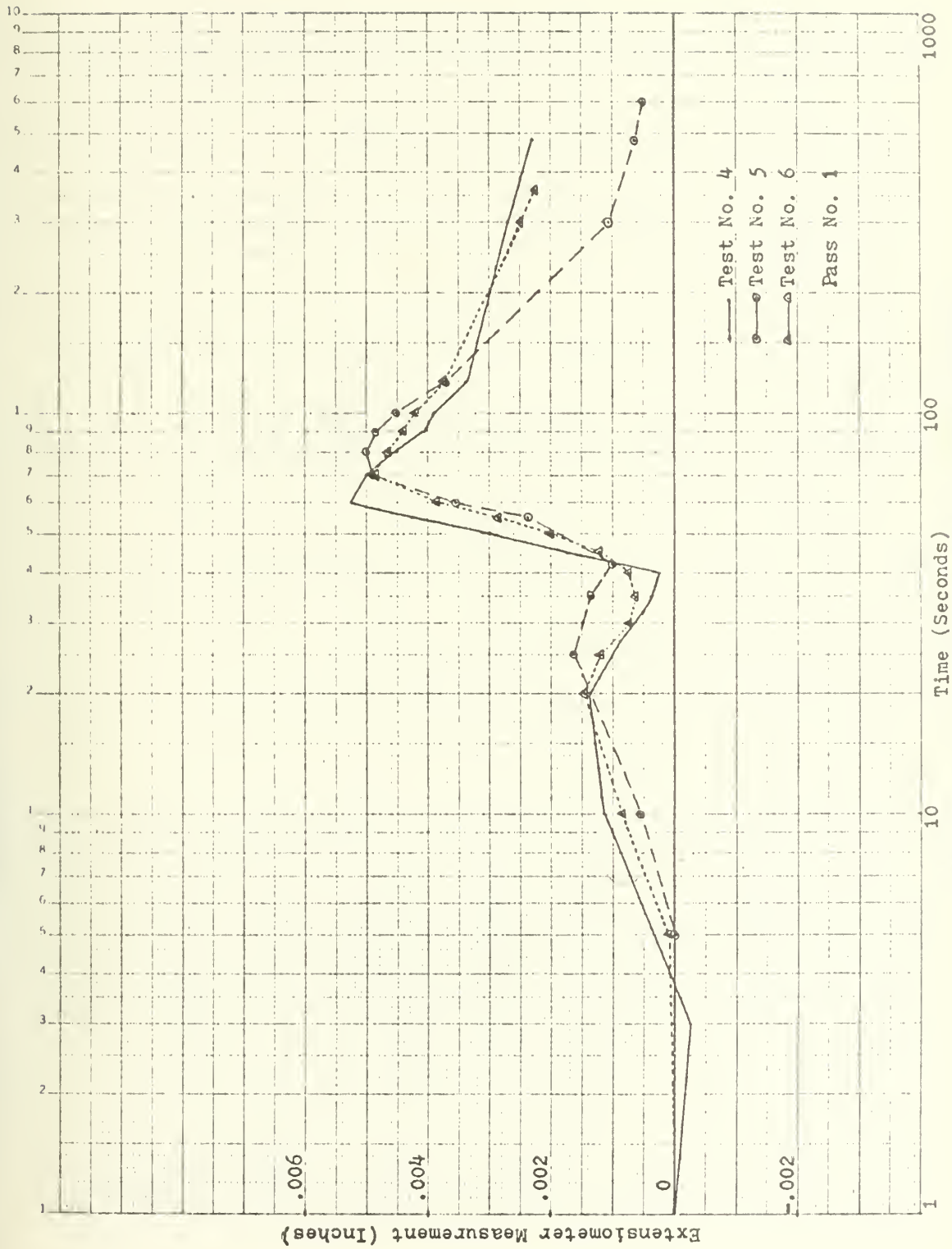

Figure 39. Extensiometer measurements

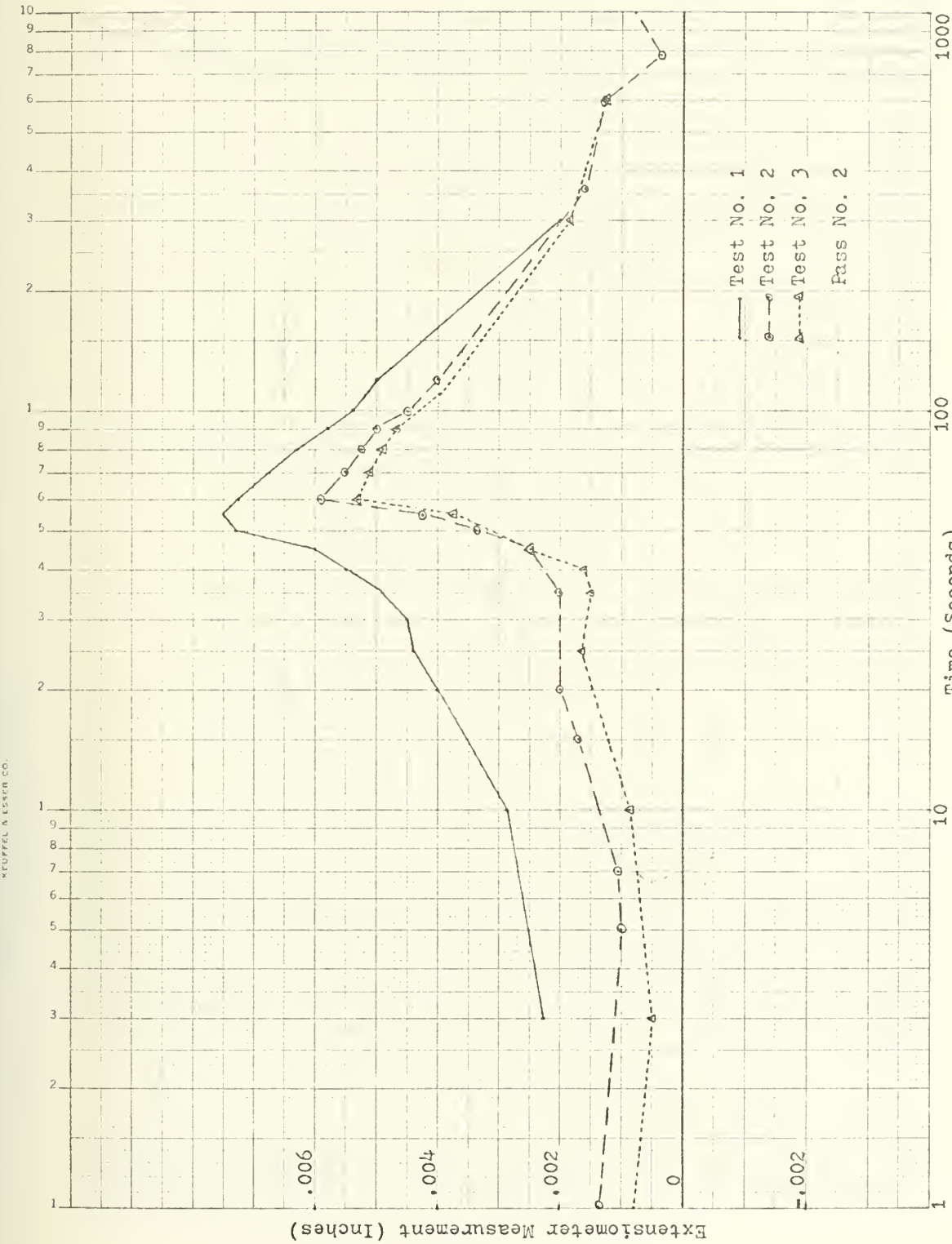

Figure 40. Extensiometer measurements

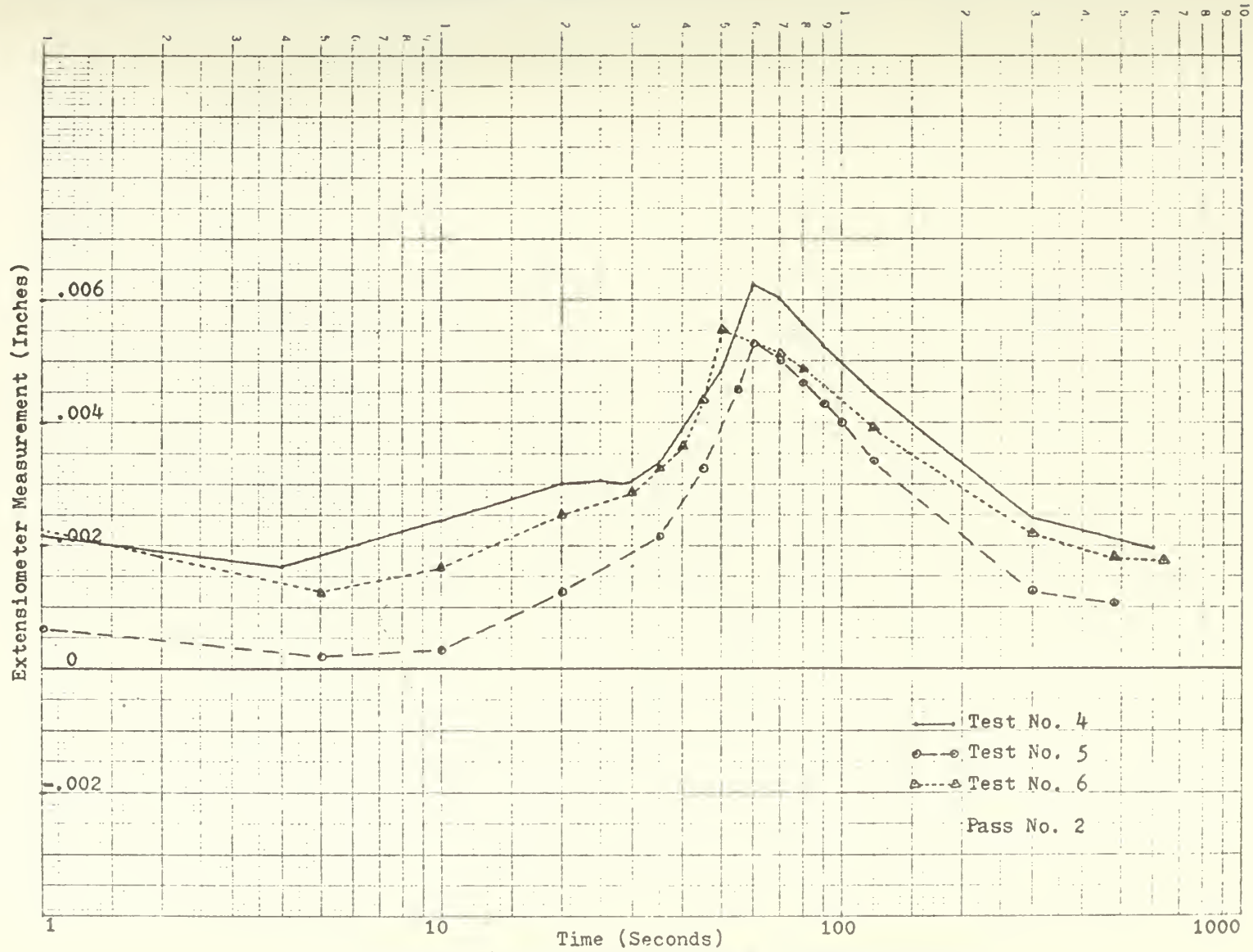

Figure 41. Extensiometer measurements

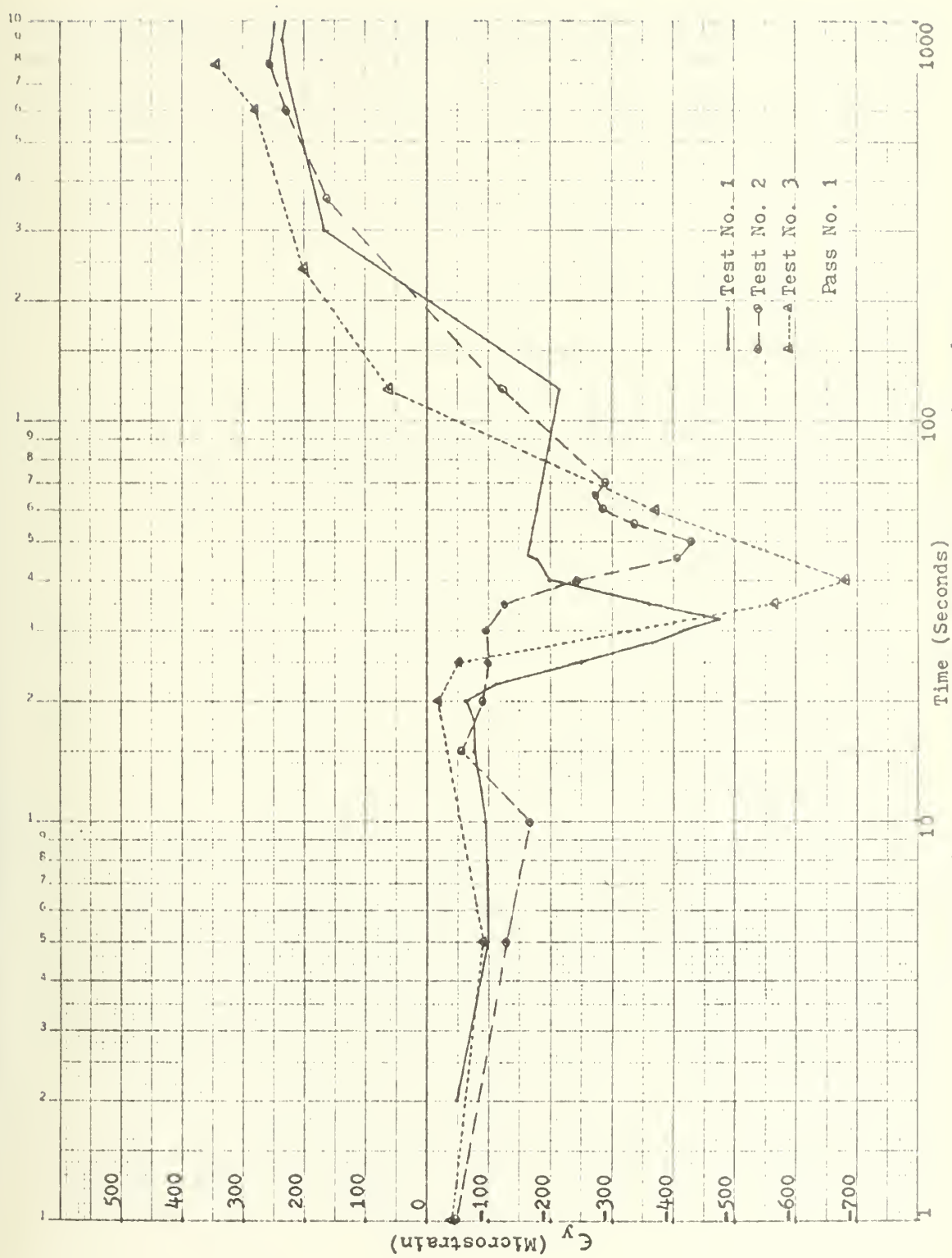

Figure 42. Transverse strain distribution

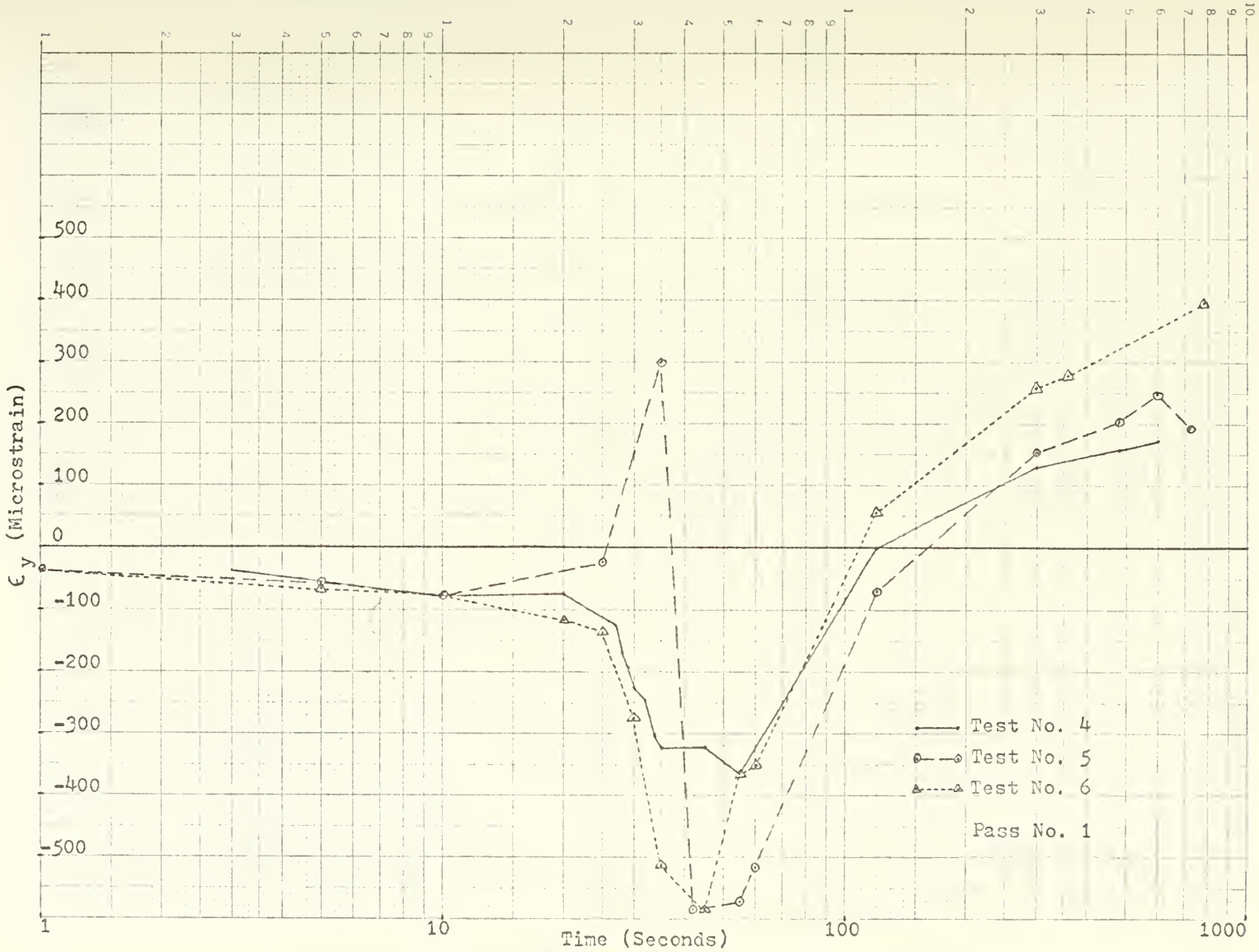

Figure 43. Transverse strain distribution

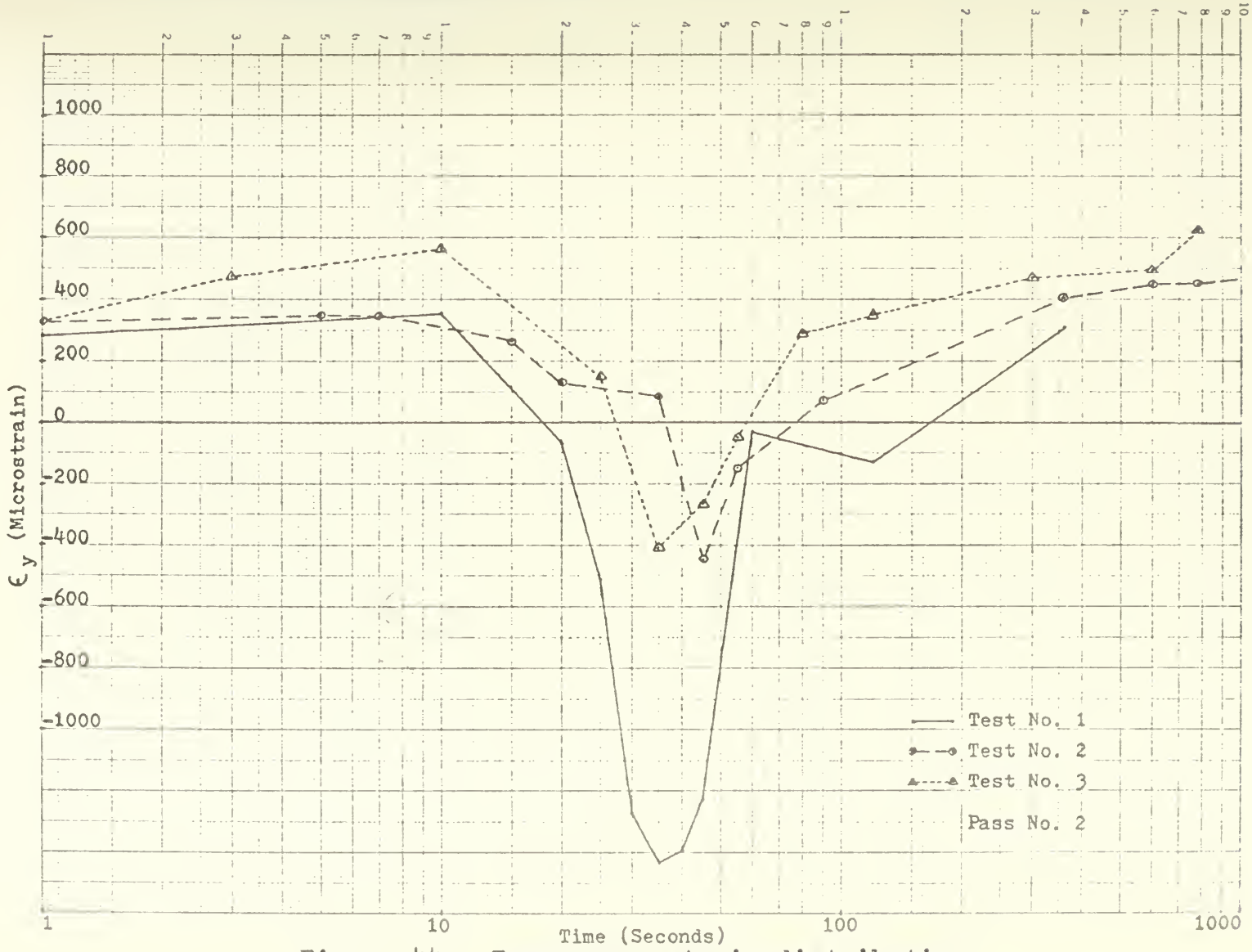

Figure 44. Transverse strain distribution

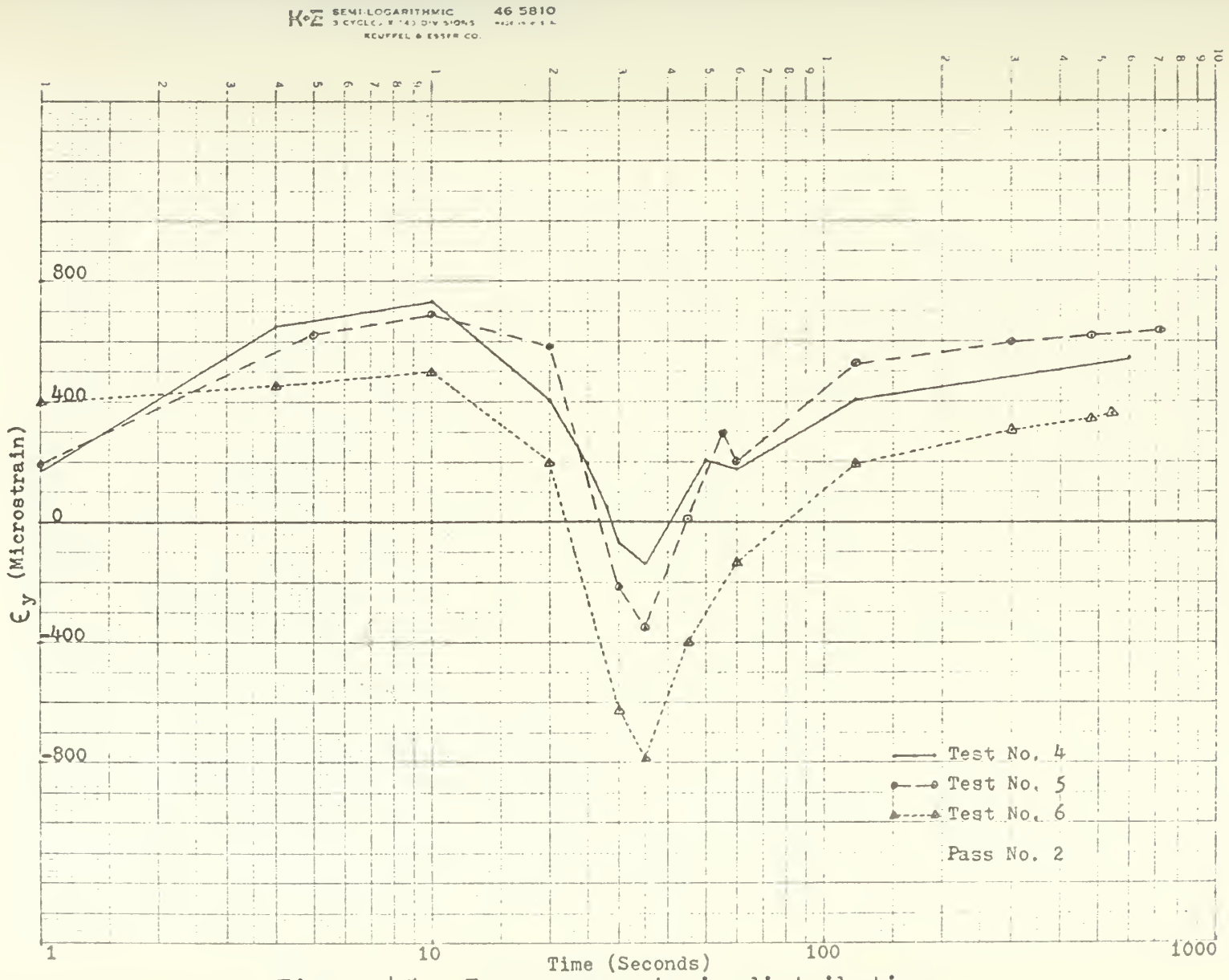

Figure 45. Transverse strain distribution

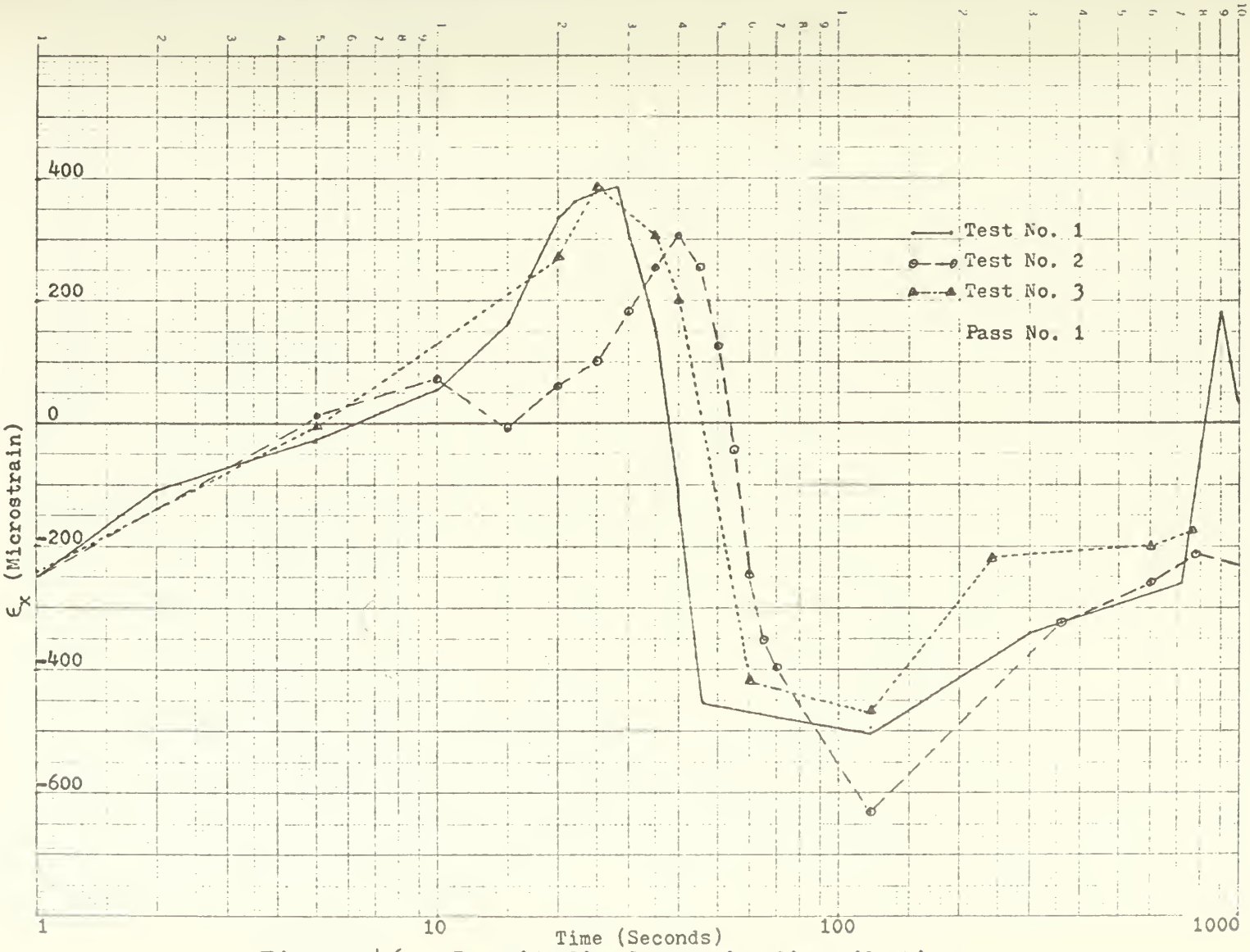

Figure 46. Longitudinal strain distribution

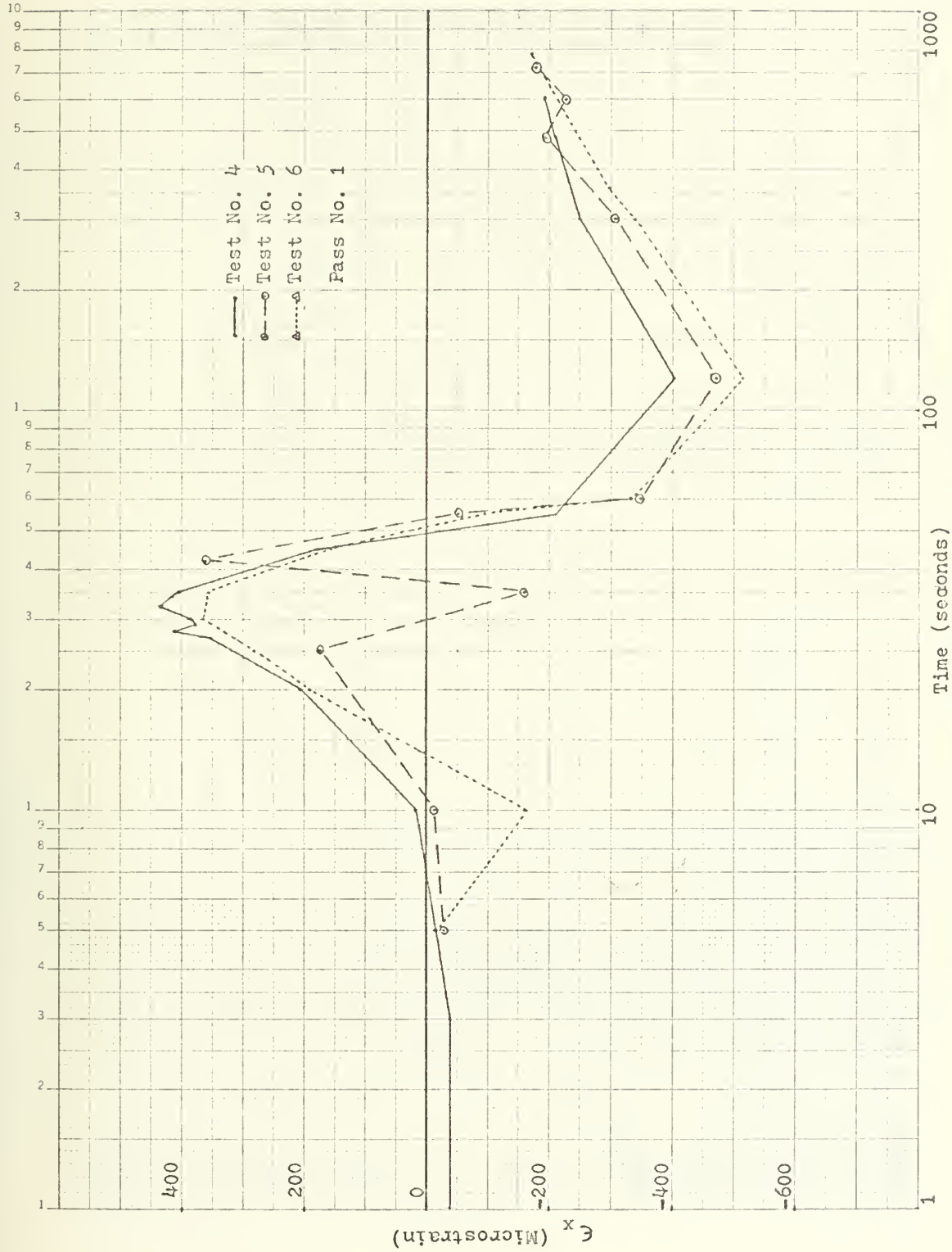

Figure 47. Longitudinal strain distribution

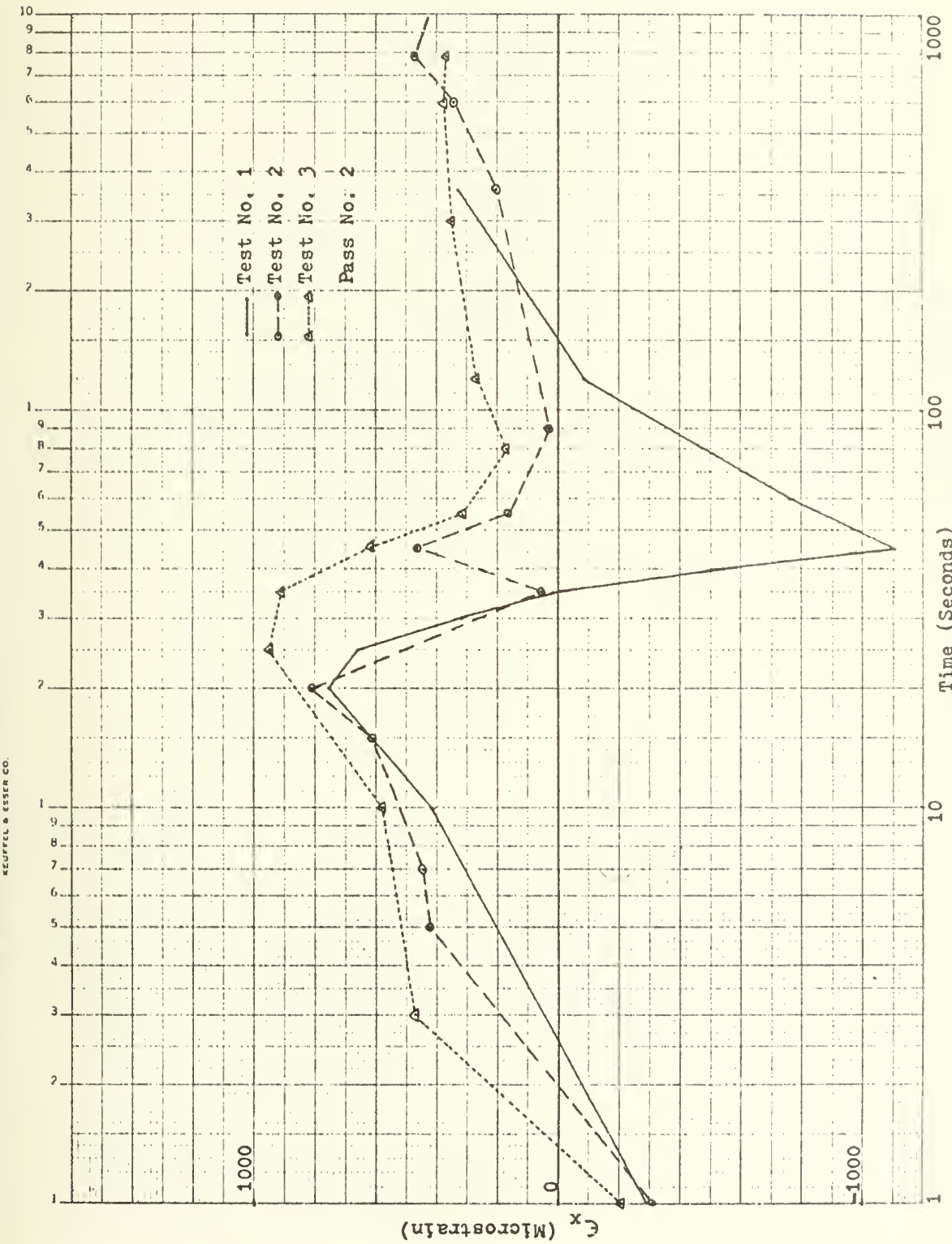

Figure 48. Longitudinal strain distribution

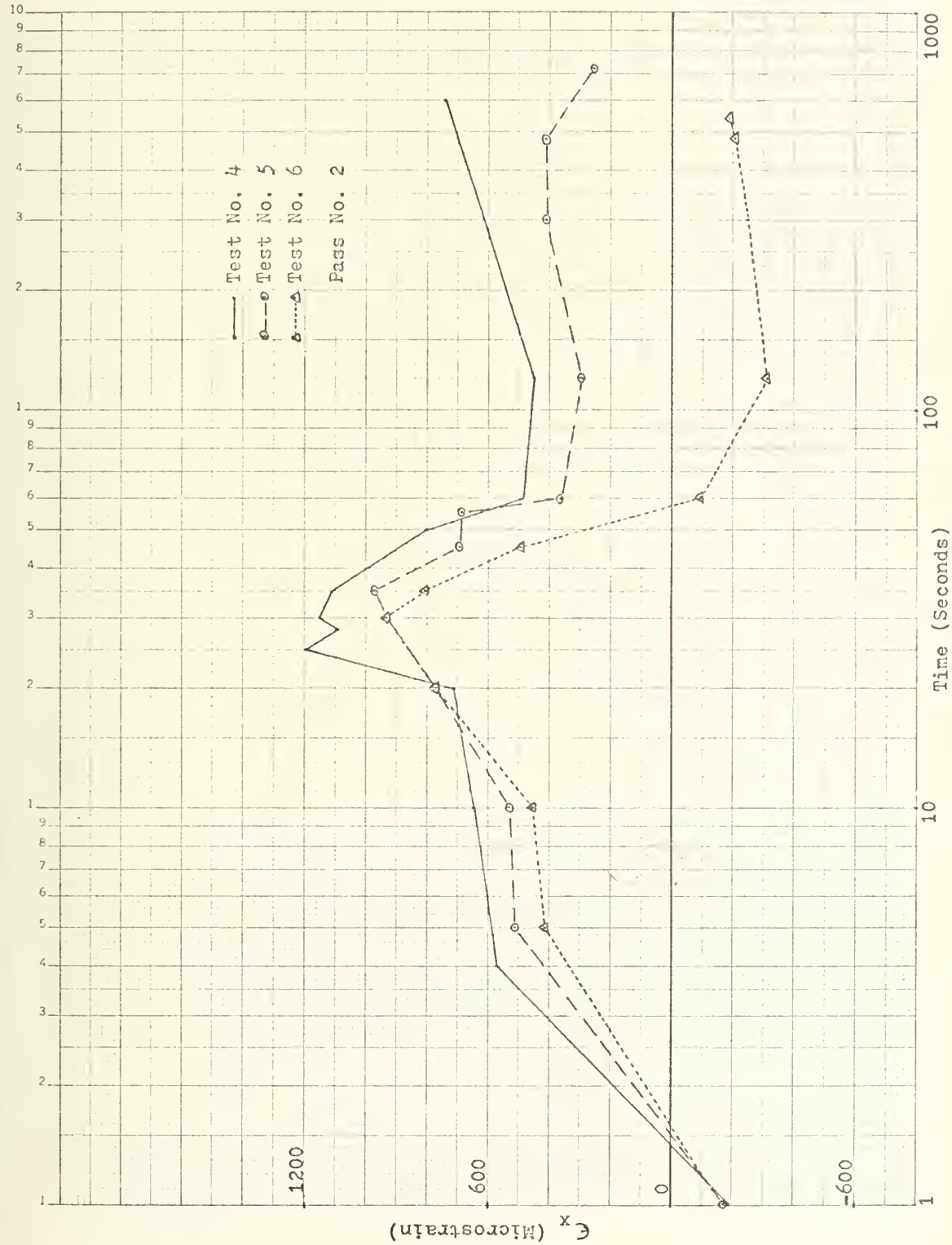

Figure 49. Longitudinal strain distribution

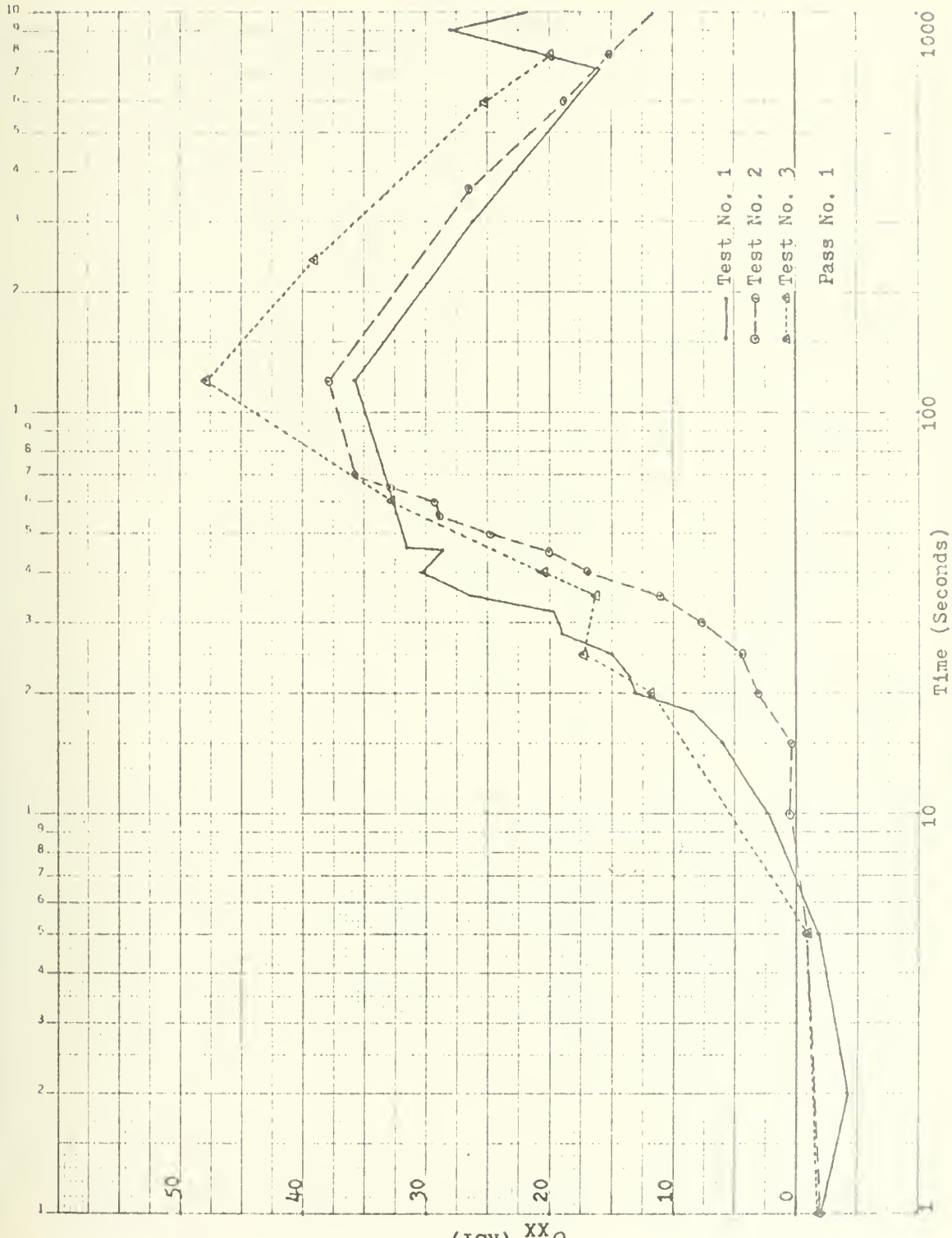

Figure 50. σ_{XX} Distribution

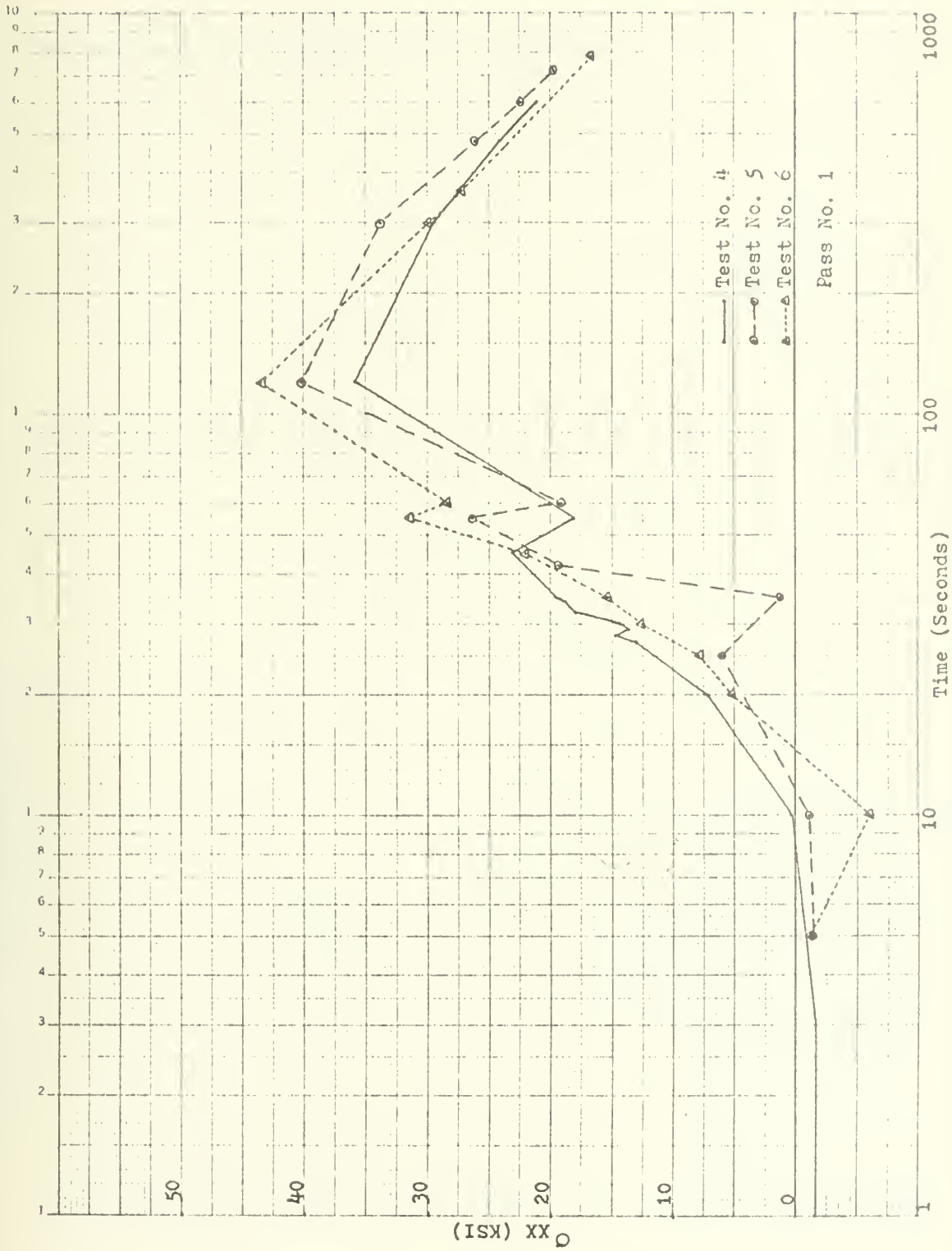

Figure 51. σ_{XX} Distribution

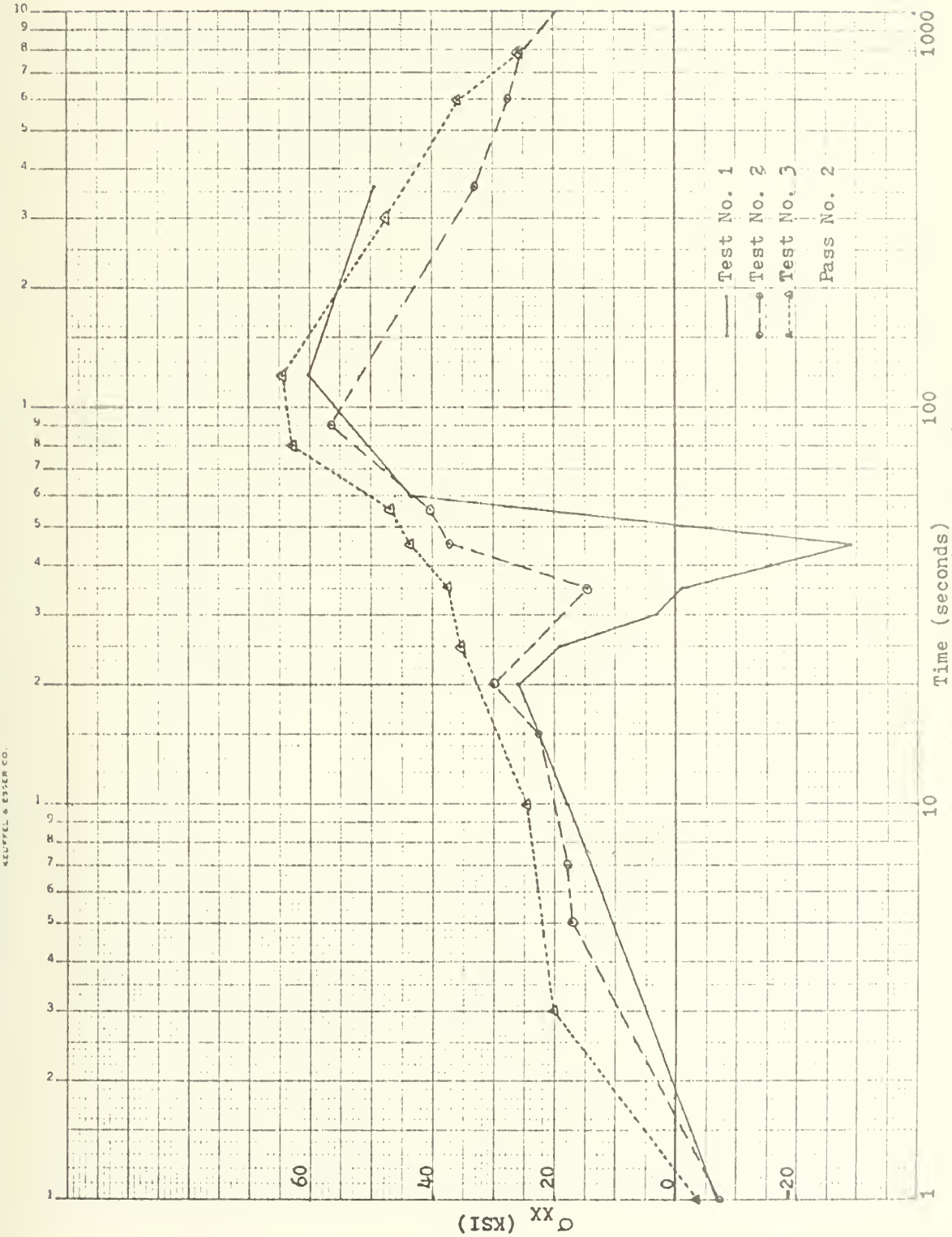

Figure 52. σ_{xx} Distribution

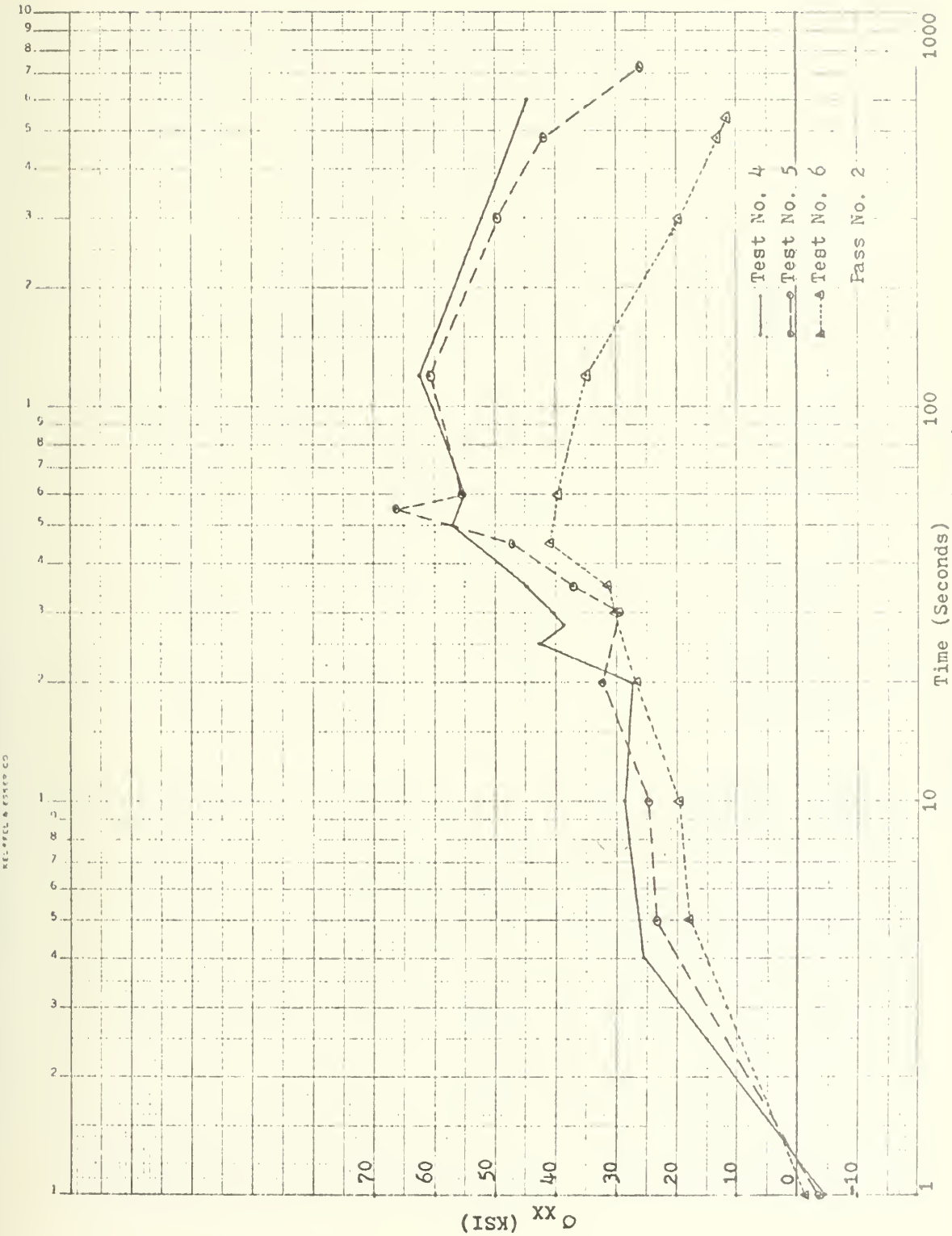

Figure 53. σ_{xx} Distribution

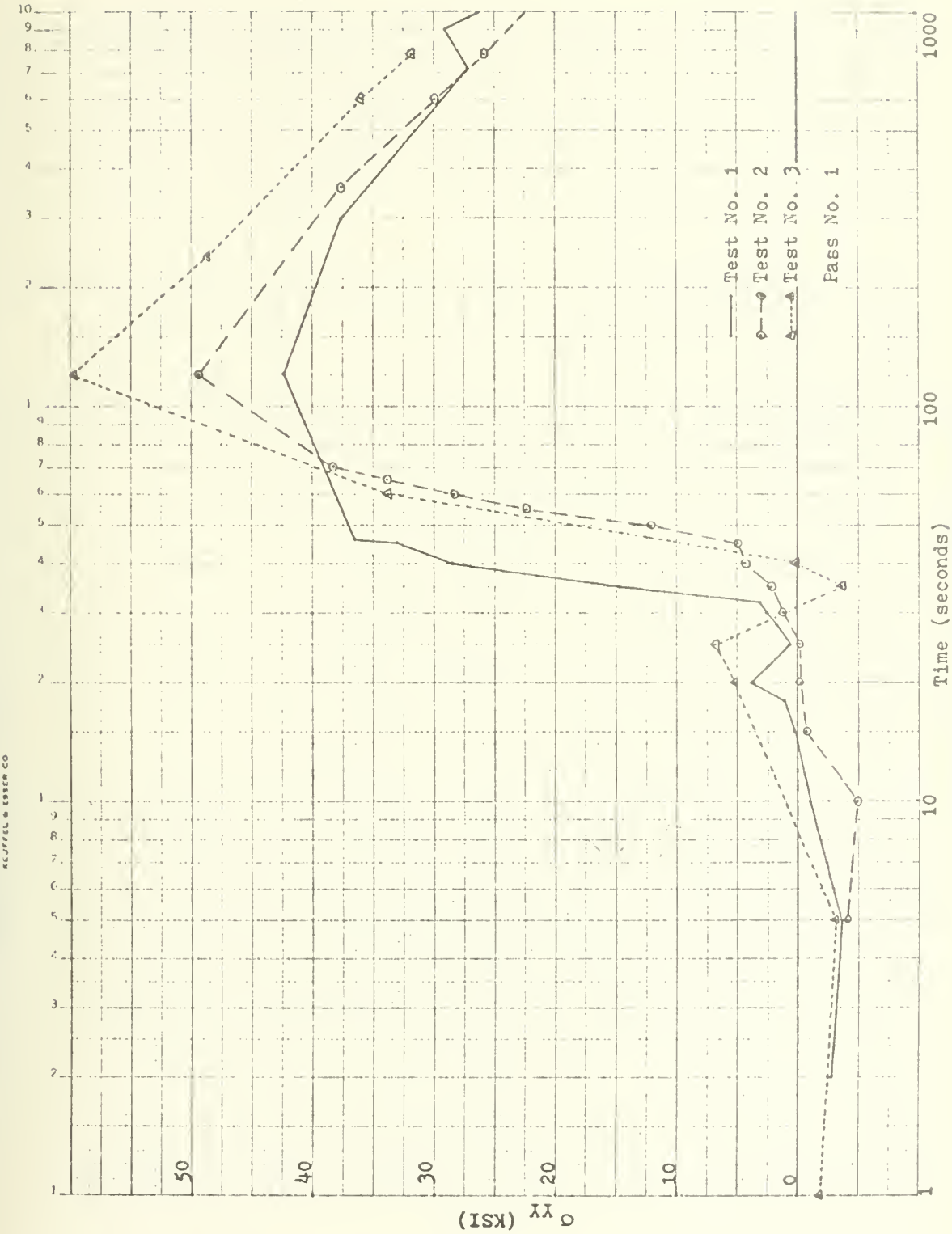

Figure 54. σ_{YY} Distribution

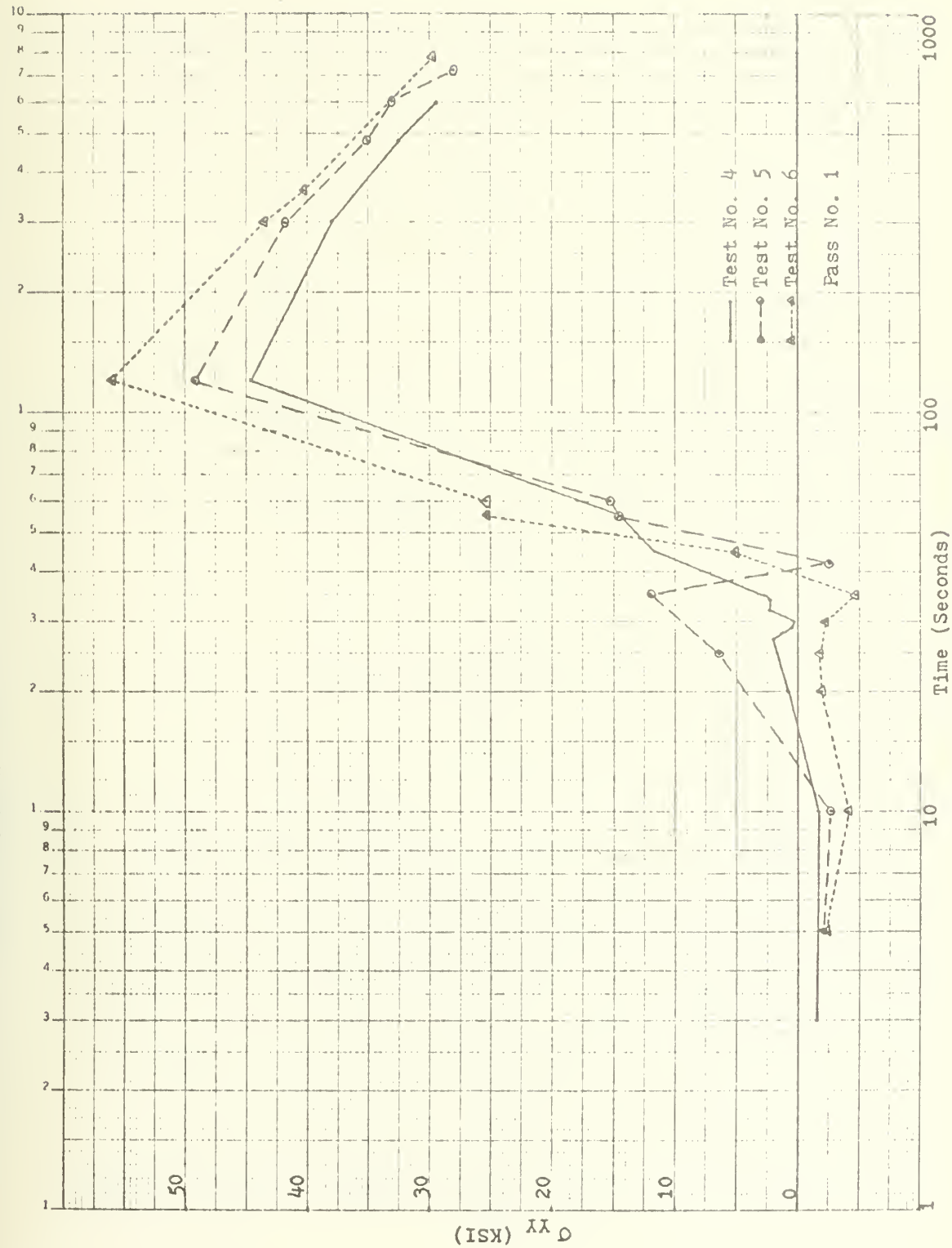

Figure 55. σ_{yy} Distribution

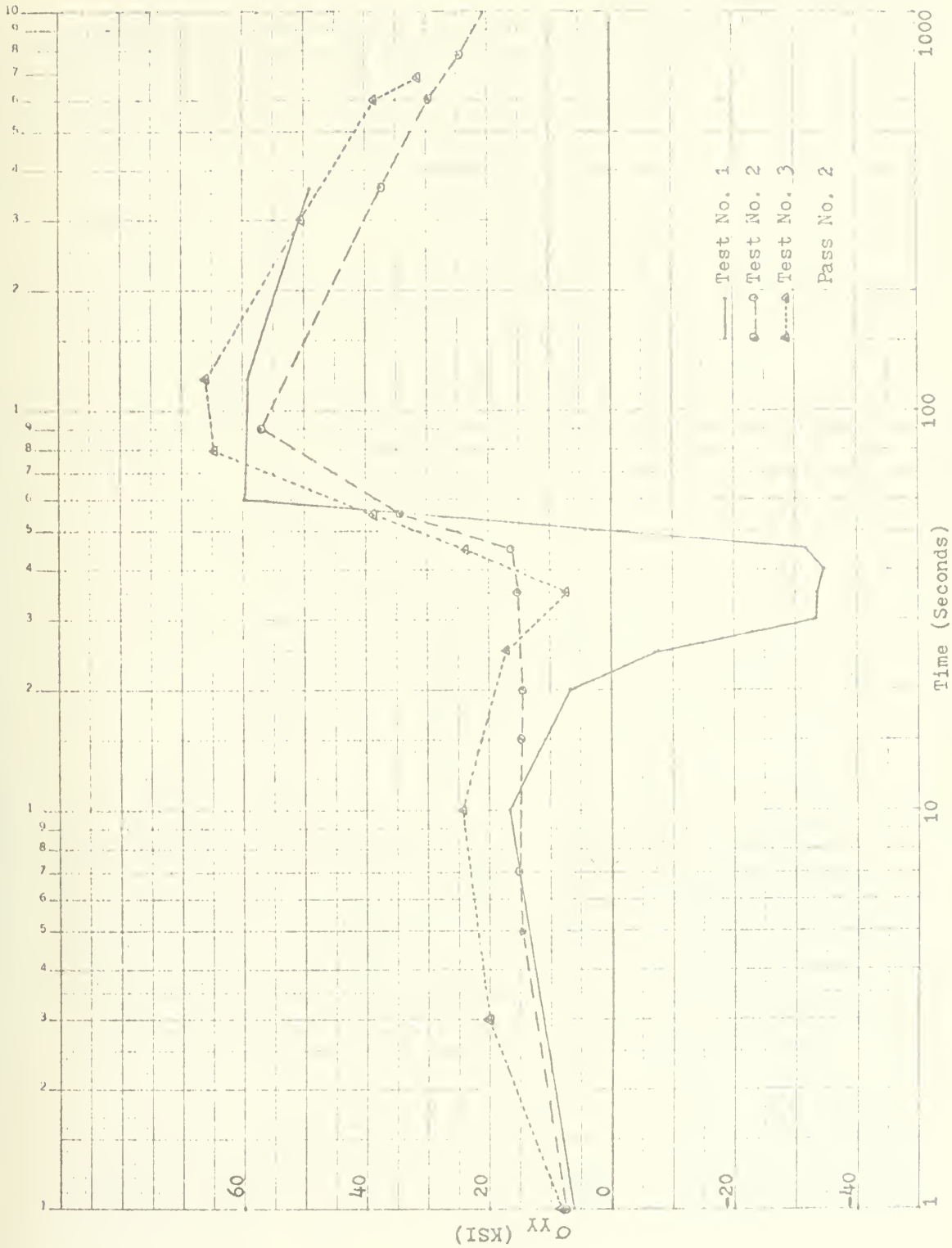

Figure 56. σ_{yy} Distribution

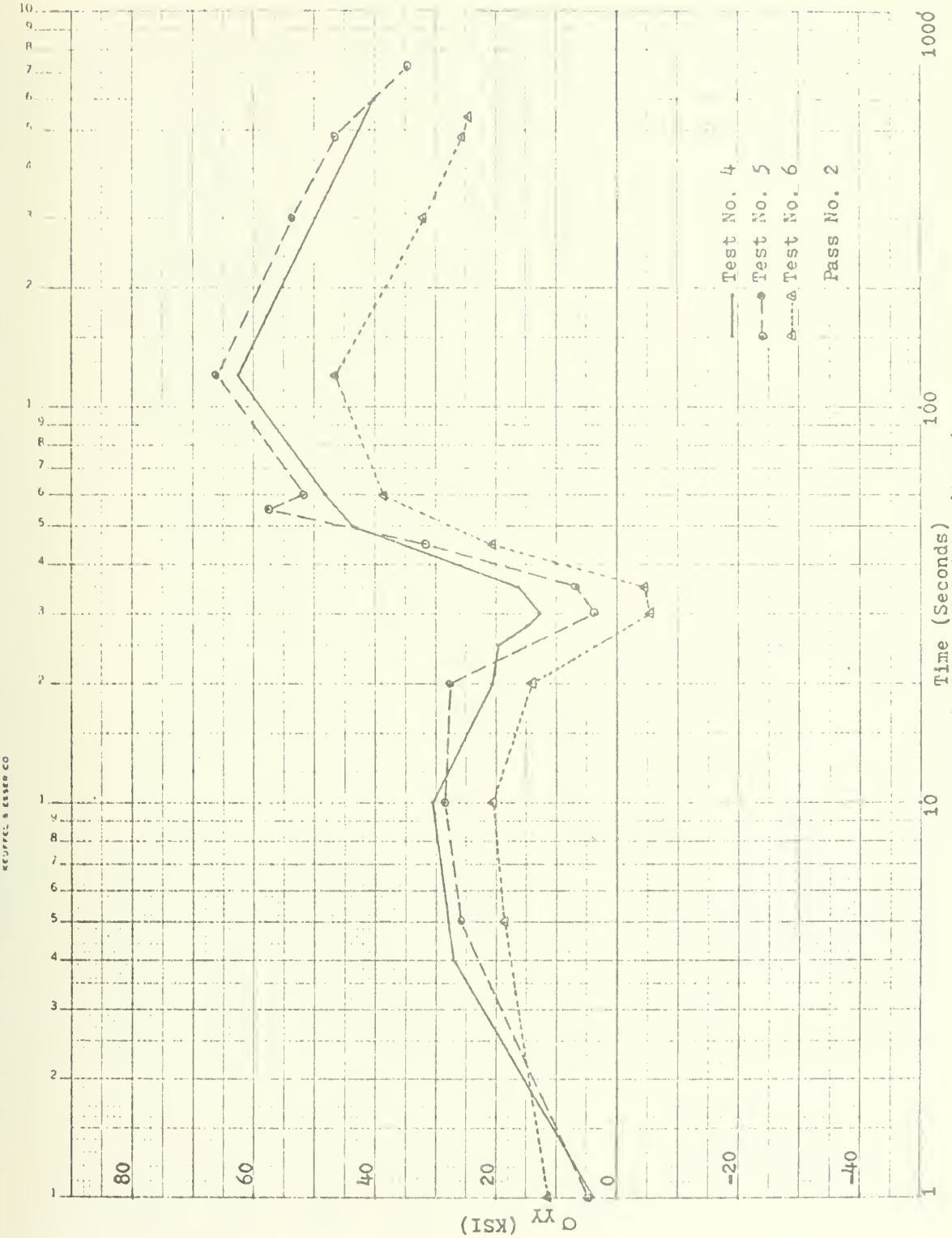

Figure 57. σ_{yy} Distribution

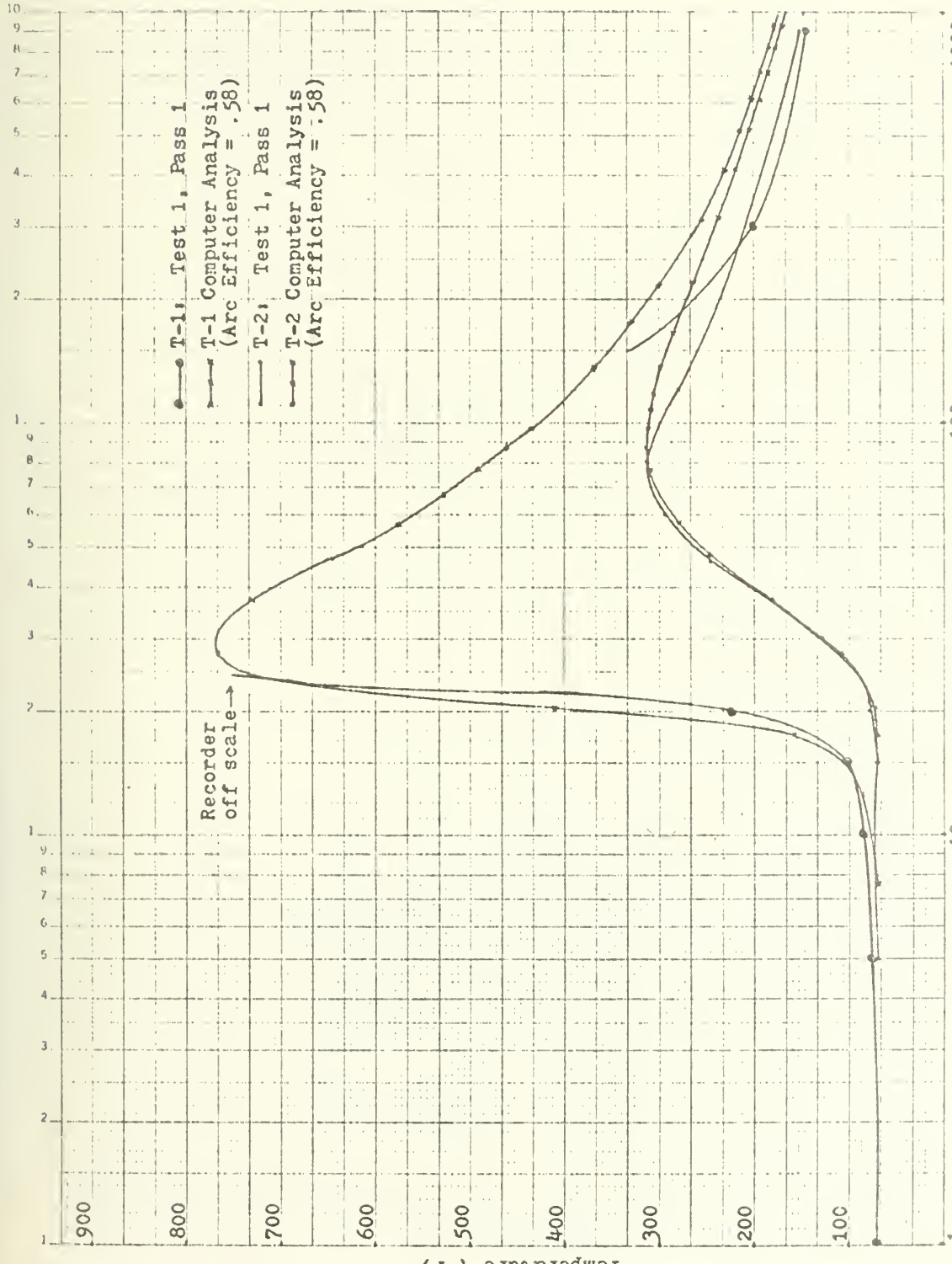

Figure 58. Temperature distribution with one-dimensional computer solution

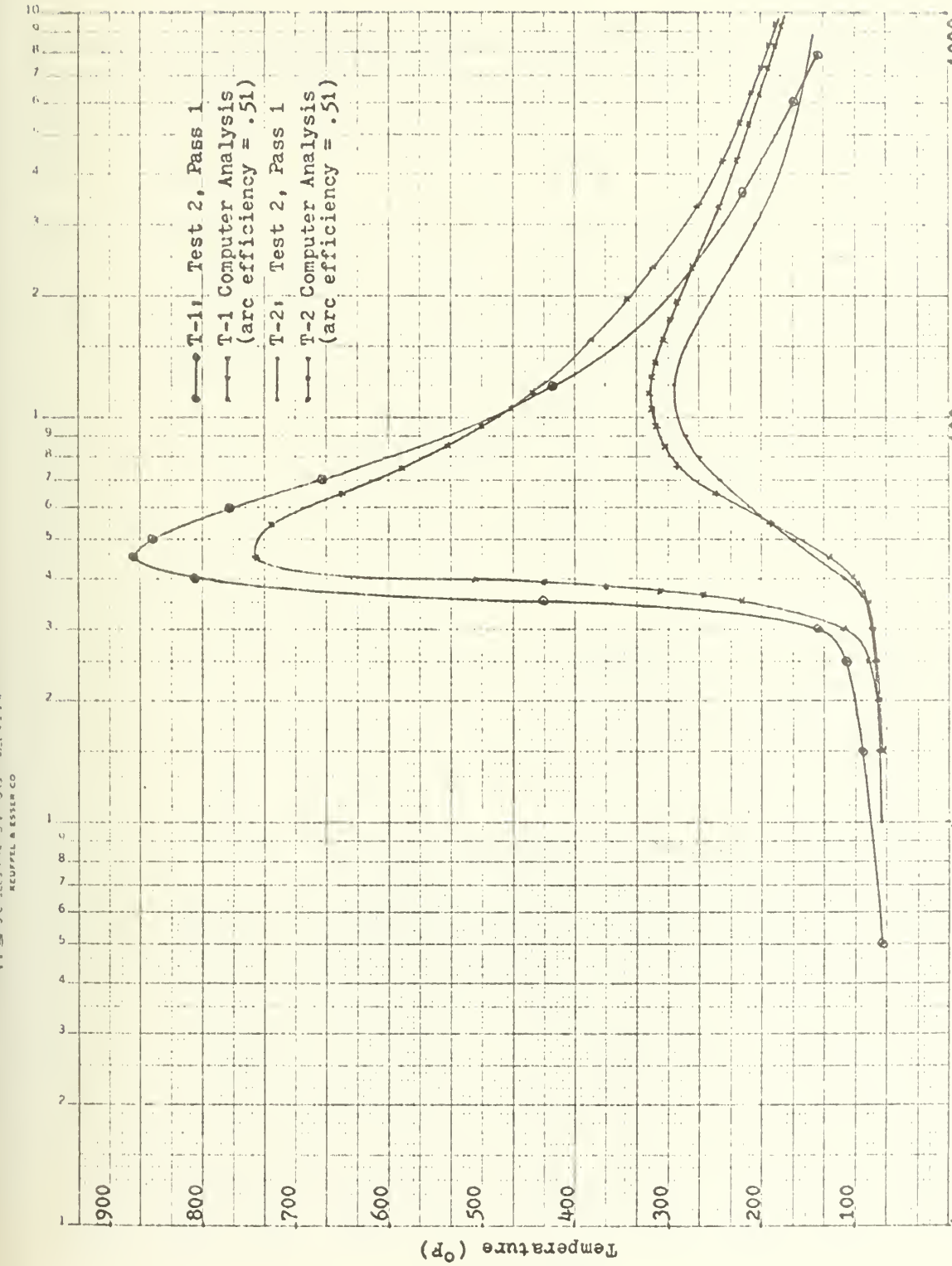

Figure 59. Temperature distribution with one-dimensional computer solution

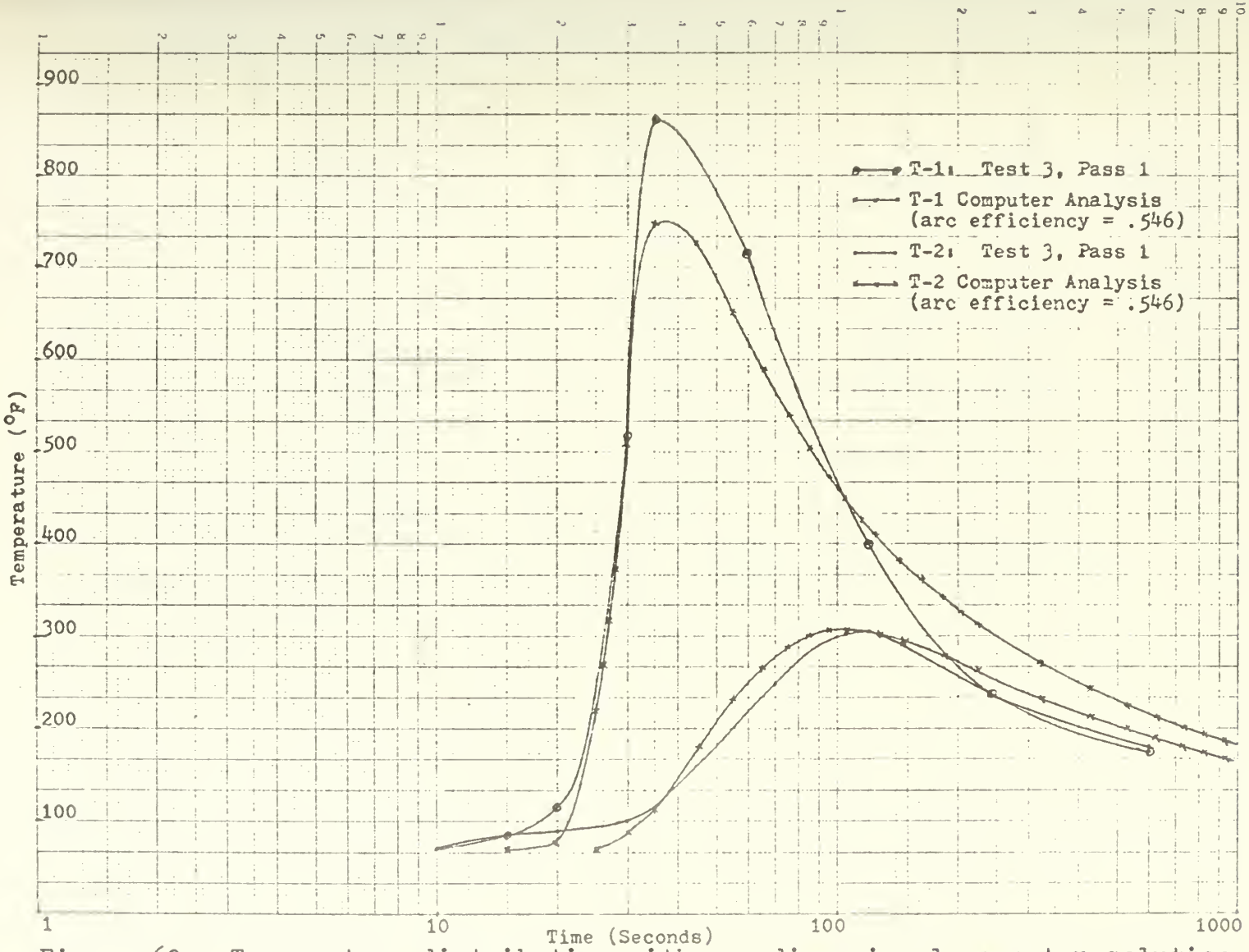

Figure 60. Temperature distribution with one-dimensional computer solution

Table 7. Cracking times and calculated stress intensity factors

Test No.	Time for visual confirmation of crack (seconds)	Time to crack from extensiometer data (seconds)	σ_Y (ksi)	σ_X (ksi)	K (ksi in)
1	960	300	37.6	26.2	138.5
2	600	360	37.5	24.5	134.6
3	535	500	38.5	28.0	144.4
4	300	300	38.0	29.5	146.5
5	450	300	41.5	33.5	162.8
6	334	300	43.5	30.0	159.5

B. Discussion of Results

1. Temperature Distribution

For the first test specimen, the instrumentation scale on the viscorder for the T-1 thermocouple was set too low and temperature data was not recorded for part of the pass. The shape of the temperature distribution with respect to the same test points were approximately the same except for Test 1, Pass 1; but the magnitudes were not. Test No. 4, T-1 and Test No. 6, T-3 were lower by about 30 percent than other T-1 and T-3 readings for Tests 3 through 6. This is difficult to account for since the voltages and amperages were the same for Tests 3 through 6. The author believes that the use of the manual welding process resulted in lower efficiency of welding between tests and thus the lower temperatures. This belief is confirmed by the different weld speeds and by the different weights of weld metal deposited. The temperature distribution does emphasize the fact that repeatable data within approximately 10 percent could be obtained if the welder uses maximum care during the manual welding process. This precision was not stressed in this experiment so that the repeatability could be judged when manual welding was used. The degree of repeatability was confirmed by examining the second pass weld; except for Test 1, where the heat input was very high, the temperature

distribution between tests was within about 20 percent. The efficiency of welding for the computer analysis, shown in Figures 58 through 60, ranged between 50 and 60 percent.

2. Extensiometer Data

The problem of initial measurements, which are a function of initial placement of the holding tabs (discussed by Bryan[16]), was accounted for by (1) carefully placing the holding tabs, and (2) realizing that the maximum transverse shrinkage would be about .01 in 3 inches, or less than a half percent. Therefore, all readings from test to test for the first pass could be assumed at the same displacement at the start of the test. For the second pass, the initial displacement was not the same for all tests because it was then a function of the first pass and the resulting cracking of the first pass weld.

The results of the extensiometer output shows very good repeatability for the first pass; for the second pass the transverse curves were generally the same shape, but not the same magnitude due to different initial displacements. It is the opinion of this author that initial cracking of the weld is indicated by the change in shape at about 300 to 400 seconds after the first pass weld was completed; although visible cracking was sometimes not

observed until about 8 to 10 minutes had passed. Since the second pass was not on the centerline of the through thickness of the plate, the cracking time was more difficult to detect from the extensiometer data due to the possible bending moment. The problem of removing the extensiometer to allow for the weld rod passage (discussed by Bryan[16]) was eliminated by placing the extensiometer below the test plate (figure 22, Chapter III).

3. Strain Results

Figures 42 through 49 are the strains in the X and Y directions for all six tests. There is little correlation between strains from experiment to experiment, a problem that has been present in other butt weld experiments at MIT. This author originally believed that the problem was possibly one of plate movement and unrelated to the welding process during the test. The choice of a high restraint butt weld in this report, besides providing the requirements for cracking, was based on the assumption that plate movement would be eliminated, thereby eliminating the erratic strain results. The erratic strains at their peak values are not the result of plates slipping in their constraints, as other experimenters have proposed.[16] Although the strain gages are small (3/16 inch) their length is enough to allow for as much as 100° temperature difference across the gage itself. This temperature

difference, and the means used in this and other experiments of separating the temperature strain from the total strain, is possibly the cause of the erratic strain indications at peak strains. The peak temperature is at the point of peak strain measured by the strain gages, which does result in maximum temperature differential across the strain gage. In addition, the variance of welding efficiency between and during the tests contributed to the erratic strain behavior.

The stresses in the X and Y directions are illustrated for all six experimental test plates for both passes in Figures 50 through 57. Since the stresses are calculated from the strain readings using Hooke's law, the erratic results for the strains are repeated for the stresses. It is interesting to note that cracking occurred when the stress in the X and Y directions were of the same order of magnitude, indicating that the crack grew from a void or inclusion in the weld.

4. Cracking

The time to crack and the resulting stress intensity factors calculated with Equation 15 of Chapter III, results in values of 134 to 163 ksi$\sqrt{\text{inch}}$, as previously reported.[25] These values are recorded in Table 7 and termed K for stress intensity factor for crack initiation to prevent confusion in assuming that they are critical stress intensity values

for critical crack growth. The use of residual stress values assumes that the stress distribution is a rectangular shape in the X and Y direction. Thermal elastic plastic analysis of a slit-type (Tekken) specimen under a moving welding heat source shows a distribution of stress that is rectangular across the weld slit.[5,26] The probability of detecting cracking is close to 100 percent at the center of the weld bead in a slit-type (Tekken) specimen (as reported by Professor K. Satoh[5]).

In the first pass of all six experiments, cracking was visibly evident at the center of the weld and running along the centerline of the weld. Satoh also concludes that it is quite appropriate to express the mechanical characteristics of weld cracking by the local stresses and strains, including their history during welding.

5. Test Specimen, Instrumentation and Welding Machine

The test specimen has been previously discussed in Chapter III. The possibility of bending strain during the second pass, although mentioned above, was not detected during this experiment. A plane surface was machined in the transverse (Y) direction across the specimens. A metal straight-edge was used during the experiment to reveal that no bending was present during the first or second pass on any test specimen. The degree of constraint resulted in cracking that could be easily detected by

visual examination. Whether or not cracking was completely through the thickness is not known, but the K values in Table 7 are at the point of crack initiation. Although the cracks were on the centerline of the weld; the plate temperatures were in the area of 200°F; therefore, the cracks could be considered the results of cold cracking.

The instrumentation performed without problems except for recording T-1 on the first pass where the scale was set too low. When the arc was initially struck and prior to the forming of any change of strain or temperature at the strain gages, legs A and C of the rosettes reversed their initial positions on the recorder. This small problem, attributed by the author to electrical interaction of the welding machine and the instrumentation, had a minor effect and was not considered important in the temperature compensation system.

The manual welding machine and process presented little difficulty. The continuous variation of the current and voltage during welding was the result of the continuous change of the distance from the weld end to the work piece, and therefore, the varying efficiency of the welding process. The weight of weld metal deposited was recorded as a second check on the welding efficiency and the welding speed.

6. Data Reduction

The experimental strain, temperature and transverse shrinkage data is presented in Appendix A. From this data the reduced data presented in Appendix C was computed using the formulation in Appendix B. Only the mechanical strains and the stress in the X and Y directions were plotted to show correlation between experiments. The other reduced data was presented to achieve one of the objectives of this report--to tabulate experimental and reduced data on HY-130 steel weldments.

C. Summary

Weld cracking can be observed in a high restraint weld of the configuration used in this report. The reason for crack initiation at the center of the weld slit and not the ends is not understood but it does agree with other experimental evidence.

The variance of welding efficiency using manual shield metal arc prevents reasonably duplicating experimental temperatures and strain data.

The use of four rather than two strain gages in the construction of the extensiometer increased the sensitivity to where it could be a valuable tool in welding studies. Mounting the instrument below the plate eliminated any interference problems.

Although the stress intensity values determined in this report are based on an empirical relation, they are based on the concepts of fracture mechanics.

V. RECOMMENDATIONS

1. The physical and mechanical properties of steels and high strength steels is very limited. Research should be undertaken to provide this data.

2. A test specimen and testing procedure should be designed so that finite difference or three-dimensional finite element computer analysis can be performed on the specimen. The material properties as a function of temperature should be incorporated into the computer analysis.

3. More tests similar to the tests in this report should be run using the GMA automatic welding process. Control of the welding parameters is of primary importance in order to achieve better experimental data with a minimum number of tests.

4. Before more experiments are conducted, the accuracy of the present method of correcting for apparent strain should be verified. An experiment could be run where several sizes (grid lengths) of strain gages are used in the same test specimen to determine the optimum size for average strain measurement and smallest error due to apparent strain correction.

5. In this study the apparent strain was determined; in all future experiments the apparent strain should be determined independently for each strain gage. This can be done by placing the test specimen with the gage in place on an area, heating it over the range of temperature for the strain gage and recording the apparent strain prior to welding the specimen.

6. The results of the extensiometer in this study were encouraging. The use of an extensiometer with four gages is recommended, as well as extensiometers of different sizes to allow for measurement much closer to the weld line than is possible with present low-temperature (0-400^{o}F) strain gages. The extensiometer also permits the continued use of the gages, thereby allowing for more tests since the gages are not destroyed from test specimen to test specimen. The cost would be lower and time to prepare the test specimen shorter if extensiometers were used to measure movement in both the transverse and longitudinal directions. The advantage of not having to correct for apparent strain with the extensiometer is evident. The disadvantages of the extensiometer is (1) the need for a highly restrained test specimen arrangement and (2) mounting the extensiometer in a way to avoid interference with the welding machine. It would seem

advantageous to develop testing procedures using an extensiometer of suitable configuration in conjunction with strain gages to obtain the large amounts of transient welding data that is needed.

7. It is recommended that tests in the future be either bead-on-plate or a highly restrained configuration. Bolting or clamping the test plate on a mounting assembly may be closer to simulating an actual weld in production, but it does not provide for accurate experimental data in case of slippage. Test specimens could be either the slit type used in this study or the test plate could be weld-mounted to a heavy test mounting plate to provide for restraint.

8. With the increased size of ships and the increased depth of submersibles, the plate thickness will necessarily be increased to where distortion, although still a problem, may be less a problem than cracking. Increased emphasis should be placed on determining the cause of cracking and the stress-strain levels at which weld cracking occurs. The mechanical aspects of cracking interacting with the metallurgical aspects of the weld need to be determined. Also, the use of fracture mechanics in combination with weld testing and computer finite element analysis of the welding and cracking process is needed.

APPENDIX (A)

Tabulated Experimental Data

1. Time (Seconds)
2. T_1, T_2, T_3 (^{o}F)
3. Strain Gage placed 1.375 inches from center of weld

   (Microinches/inch)

   (- is Compression, + is Tension)

   Legs, A, B, and C
4. Extensiometer

   (Inches/inch)

   (+ is Expansion, - is Contraction)

TEST NO. 1 PASS NO. 1

Time	T_1	T_2	T_3	Strain Gage A	Strain Gage B	Strain Gage C	Extensiometer
0	70	70	70	0	0	0	0
1	70	70	70	-50	0	20	0
2	70	70	70	-80	0	50	0
3	70	70	70	-150	0	125	0
5	72	70	70	-200	-50	175	.00025
10	75	70	70	-200	-75	200	.001
15	80	72	80	-175	-60	300	.0015
16	82	72	80	-150	-60	300	.0015
18	90	72	80	-150	-60	350	.0015
20	100	72	110	-150	-75	400	.001
22	120	72	120	-225	-125	450	.00075
22.6	130	72	130	-250	-150	425	.00075
23	140	72	270	-275	-175	425	.00075
24	180	72	370	-300	-250	400	.00075
25	250	75	470	-375	-325	350	.0005
26	370	78	580	-375	-375	250	.0005

TEST NO. 1 PASS NO. 1

Time	T_1	T_2	T_3	Strain Gage A	Strain Gage B	Strain Gage C	Extensiometer
27	490	80	650	-400	-475	175	.00025
28	588	82	710	-425	-550	75	0
29	660	85	720	-450	-625	-30	0
30	730	90	740	-475	-675	-150	0
31	800	95	750	-500	-760	-275	0
32		100	750	-525	-810	-375	0
33		108	755	-540	-820	-475	0
34		114	758	-565	-870	-590	.00025
35	Off	120	758	-590	-900	-700	.0005
40	Scale	165	718	-800	-1000	-1120	.0019
44.5		201	694	-1040	-1130	-1410	.0035
45		205	678	-1060	-1130	-1430	.0035
46		212	670	-1120	-1190	-1480	.004
50		270	620	-1575	-1530	-1585	.0075
60		290	570	-1590	-1625	-2110	.0058
80	780	310	510	-1630	-1610	-1930	.0052

TEST NO. 1 PASS NO. 1

Time	T_1	T_2	T_3	Strain Gage A	Strain Gage B	Strain Gage C	Extensiometer
100	420	300	440	-1590	-1525	-1910	.00425
120	360	275	390	-1450	-1440	-1720	.0035
300	200	205	222	-850	-620	-900	.001
720	154	155	158	-480	-250	-510	.0009
900	145	145	142	-410	-180	-450	.0009
1200	135	130	130	-325	-100	-350	.002

TEST NO. 1 PASS NO. 2

Time	T_1	T_2	T_3	Strain Gage A	Strain Gage B	Strain Gage C	Extensiometer
0	120	100	130	-175	50	-300	.00225
1	120	115	118	-260	100	-150	.00225
2	120	115	118	-270	110	-90	.00225
3	120	115	118	-330	110	-40	.00225
10	132	118	130	-600	150	380	.00285
20	200	120	170	-1000	-300	660	.0044
25	364	122	302	-1130	-760	210	.0044
30	990	140	490	-1540	-1580	-600	.0045
35	1050	180	662	-1480	-1925	-1520	.0049
40	1210	230	710	-1500	-1950	-2120	.0055
45	1300	275	734	-1520	-1850	-2630	.006
48	1120	295	710	-1620	-1760	-2740	.00635
50	1100	348	690	-1980	-1680	-2680	.0073
55	940	360	675	-2130	-1680	-2560	.0075
60	725	370	650	-2420	-1780	-2480	.00725
70	580	375	610	-2160	-1810	-2410	.00675

TEST NO. 1 PASS NO. 2

Time	T_1	T_2	T_3	Strain Gage A	Strain Gage B	Strain Gage C	Extensiometer
80	500	380	570	-2180	-1970	-2290	.0063
90	440	375	540	-2160	-1950	-2210	.0058
100	400	370	510	-2120	-1835	-2120	.0054
120	345	355	470	-2080	-1800	-2050	.005
300	205	250	210	-1050	-710	-920	.002

TEST NO. 2 PASS NO. 1

Time	T_1	T_2	T_3	Strain Gage A	Strain Gage B	Strain Gage C	Extensiometer
0	70	70	70	0	0	0	0
1	70	70	70	-30	0	30	-.0005
2	70	70	70	-80	0	80	-.00025
3	70	70	70	-160	-40	160	0
5	70	70	70	-320	-80	300	0
10	70	70	70	-200	-120	550	.0007
15	70	70	80	-180	-40	150	.00125
20	90	75	82	-250	-90	220	.001375
25	90	78	93	-240	-100	240	.0014
30	110	78	118	-220	-110	280	.001125
35	142	80	298	-260	-170	300	.00065
40	438	85	510	-370	-410	100	.00025
45	810	115	748	-520	-730	-300	0
46	824	118	763	-550	-790	-400	.0001
47	838	121	776	-580	-840	-490	.000175
48	852	124	789	-620	-890	-565	.00025

TEST NO. 2 PASS NO. 1

Time	T_1	T_2	T_3	Strain Gage A	Strain Gage B	Strain Gage C	Extensiometer
49	865	128	802	-630	-925	-650	.0004
50	878	130	815	-655	-970	-730	.00055
55	854	165	798	-790	-1080	-1080	.001875
60	770	198	765	-970	-1180	-1350	.00345
65	742	222	728	-1160	-1310	-1540	.005
70	670	245	700	-1370	-1450	-1640	.005875
80	610	265	650	-1480	-1500	-1820	.00625
90	560	290	595	-1500	-1560	-2000	.006
100	510	290	545	-1500	-1560	-2020	.00565
120	450	295	485	-1510	-1470	-1880	.0048
300	222	205	174	-800	-625	-940	.002125
600	170	165	158	-490	-310	-620	.001875
780	142	145	135	-340	-160	-450	.0017

TEST NO. 2 PASS NO. 2

Time	T_1	T_2	T_3	Strain Gage A	Strain Gage B	Strain Gage C	Extensiometer
0	130	130	125	-240	-80	-420	.001375
5	130	130	125	-340	0	-200	.001
7	130	130	125	-400	0	-120	.00105
15	130	130	125	-620	-60	210	.0017
20	130	130	136	-770	-250	330	.002
35	1078	155	565	-1080	-520	-625	.002
45	1130	200	739	-1080	-1400	-1440	.0025
50	845	260	725	-1170	-1380	-1640	.00335
55	840	262	722	-1250	-1340	-1760	.00425
60	720	300	680	-1600	-1480	-1860	.0059
70	640	320	610	-1570	-1570	-2080	.0055
80	570	330	565	-1600	-1570	-2100	.00525
90	550	335	528	-1625	-1530	-2050	.005
100	485	335	495	-1620	-1450	-1970	.0045
120	450	330	475	-1575	-1340	-1825	.004
360	214	215	212	-780	-450	-960	.0016

TEST NO. 2 PASS NO. 2

Time	T_1	T_2	T_3	Strain Gage A	Strain Gage B	Strain Gage C	Extensiometer
600	174	175	170	-500	-160	-560	.0013
780	150	150	150	-350	0	-260	.000375
1200	110	120	120	-110	220	-200	.000375

TEST NO. 3 PASS NO. 1

Time	T_1	T_2	T_3	Strain Gage A	Strain Gage B	Strain Gage C	Extensiometer
0	71	71	71	0	0	0	0
2	71	71	71	-50	0	50	0
5	71	71	71	-160	-50	150	0
20	87	83	71	-170	-50	360	.00075
25	111	83	78	-250	-120	460	.0005
35	511	96	699	-680	-800	-50	-.000375
40	863	116	761	-820	-1130	-560	-.0005
50	825	214	712	-1030	-1420	-1340	.001
55	785	238	690	-1150	-1430	-1570	.0025
60	751	253	657	-1300	-1500	-1750	.00375
70	670	277	600	-1530	-1620	-2100	.0051
80	595	290	549	-1550	-1620	-2080	.0049
90	476	300	462	-1550	-1550	-2000	.0045
120	399	307	401	-1500	-1360	-1750	.0038
240	231	239	251	-1000	-800	-1020	.002125
600	171	181	173	-550	-360	-650	.001

TEST NO. 3 PASS NO. 2

Time	T_1	T_2	T_3	Strain Gage A	Strain Gage B	Strain Gage C	Extensiometer
0	151	156	146	-350	-140	-450	.0008
3	151	151	151	-420	-120	-340	.0005
10	151	151	151	-560	-40	-20	.000875
25	187	153	183	-1100	-510	360	.00165
35	1111	171	549	-1240	-1280	-510	.0015
40	1151	215	650	-1180	-1460	-1000	.0016
45	1031	226	656	-1200	-1480	-1390	.0025
50	890	265	633	-1250	-1450	-1570	.00275
55	811	283	621	-1390	-1500	-1770	.00375
60	672	325	590	-1700	-1670	-1940	.0053
70	611	342	549	-1720	-1630	-2080	.0051
80	551	356	521	-1730	-1620	-2100	.0049
90	505	353	491	-1750	-1580	-2030	.00465
120	431	340	421	-1680	-1450	-1820	.00395
300	271	265	271	-1200	-870	-1180	.001875
600	223	221	221	-850	-530	-850	.00125

TEST NO, 4 PASS NO. 1

Time	T_1	T_2	T_3	Strain Gage A	Strain Gage B	Strain Gage C	Extensicmeter
0	72	72	72	0	0	0	0
3	72	72	72	-60	0	60	-.00025
10	72	72	80	-210	-50	200	.001125
20	92	77	220	-180	-70	320	.001375
27	132	77	957	-230	-150	410	.000875
28	152	77	1022	-230	-200	410	.00075
29	172	77	1002	-270	-230	380	.00065
30	200	82	982	-300	-280	350	.000625
32	292	82	937	-320	-350	300	.0005
34	412	84	902	-380	-460	180	.0004
35	472	87	872	-400	-510	110	.000375
40	585	110	784	-450	-680	-180	.00025
45	600	128	704	-560	-770	-480	.00175
50	570	152	656	-700	-920	-770	.003
60	502	212	542	-1050	-1115	-1390	.00525

TEST NO. 4 PASS NO. 1

Time	T_1	T_2	T_3	Strain Gage A	Strain Gage B	Strain Gage C	Extensiometer
70	468	225	499	-1120	-1230	-1540	.005
80	440	242	454	-1220	-1250	-1570	.0045
90	412	249	424	-1260	-1250	-1560	.00405
100	390	256	396	-1270	-1230	-1530	.0039
120	352	258	344	-1240	-1140	-1420	.003375
300	212	210	212	-840	-690	-920	.0027
480	184	184	184	-640	-500	-730	.0023

TEST NO. 4 PASS NO. 2

Time	T_1	T_2	T_3	Strain Gage A	Strain Gage B	Strain Gage C	Extensiometer
0	160	170	168	-540	-400	-625	.002175
4	152	170	164	-600	-330	-500	.001675
10	164	172	168	-740	-255	-220	.0024
20	190	172	222	-1190	-575	-20	.003
25	232	172	632	-1130	-820	120	.00305
28	372	172	740	-1160	-980	-120	.003
30	536	177	790	-1160	-1130	-250	.00305
35	872	184	777	-1110	-1340	-680	.003375
50	720	254	672	-1220	-1450	-1450	.004875
60	608	307	582	-1500	-1670	-1900	.00625
70	552	320	544	-1520	-1680	-2010	.006
80	512	329	514	-1560	-1655	-2025	.0056
90	492	337	492	-1600	-1620	-1990	.00525
120	424	332	409	-1570	-1510	-1830	.0045
300	292	272	272	-1150	-1020	-1270	.00245
600	160	227	224	-780	-780	-950	.00195

TEST NO. 5 PASS NO. 1

Time	T_1	T_2	T_3	Strain Gage A	Strain Gage B	Strain Gage C	Extensiometer
0	72	72	72	0	0	0	0
5	72	72	72	-50	-20	40	0
10	72	72	72	-165	-40	150	.00055
25	72	72	102	-220	0	420	.001625
35	112	77	612	-480	250	520	.00135
42	280	90	1042	-820	-860	50	.001
55	824	167	877	-1020	-1330	-1120	.002375
60	760	214	749	-1150	-1310	-1320	.00355
70	632	255	642	-1480	-1630	-1770	.0049
80	522	244	555	-1630	-1740	-1910	.005
90	440	288	512	-1670	-1700	-1925	.00485
100	370	292	457	-1610	-1630	-1890	.0045
120	280	282	387	-1450	-1350	-1650	.0037
300	212	220	224	-800	-730	-1020	.00105
480	176	190	190	-550	-480	-810	.000625
600	160	176	176	-490	-360	-710	.0005

TEST NO. 5 PASS NO. 2

Time	T_1	T_2	T_3	Strain Gage A	Strain Gage B	Strain Gage C	Extensiometer
0	152	162	162	-410	-330	-620	.000625
5	152	162	162	-490	-240	-470	.0002
10	152	164	164	-600	-180	-290	.0003
20	168	167	182	-920	-300	140	.00125
30	352	169	757	-1250	-1100	-170	.001675
35	732	182	862	-1160	-1410	-700	.002125
45	772	232	712	-1100	-1410	-1410	.00325
55	664	276	632	-1290	-1520	-1730	.00455
60	592	317	572	-1450	-1620	-2000	.0053
70	542	327	527	-1480	-1580	-2090	.005
80	502	338	505	-1500	-1550	-2070	.00465
90	472	349	468	-1520	-1520	-2050	.0043
100	452	340	447	-1520	-1490	-2000	.004
120	400	335	407	-1500	-1400	-1900	.003375
300	200	277	277	-1130	-970	-1370	.00125
480	160	247	244	-940	-760	-1160	.00105

TEST NO. 6 PASS NO. 1

Time	T_1	T_2	T_3	Strain Gage A	Strain Gage B	Strain Gage C	Extensiometer
0	72	72	72	0	0	0	0
5	72	72	72	-130	-30	120	.0001
10	72	72	75	-180	-40	170	.000875
20	72	72	89	-220	-80	370	.00145
25	80	72	337	-280	-100	500	.0012
30	200	72	552	-410	-310	430	.00075
35	480	84	720	-570	-680	80	.000625
40	850	116	764	-650	-940	-350	.00075
45	896	126	742	-700	-1080	-720	.0012
50	860	172	705	-810	-1150	-1020	.002
55	832	190	674	-950	-1230	-1240	.002875
60	760	217	584	-1100	-1260	-1400	.003875
70	682	252	522	-1460	-1400	-1580	.00485
80	603	282	487	-1430	-1450	-1800	.00465
90	552	286	452	-1450	-1440	-1840	.0044
100	502	292	424	-1500	-1390	-1800	.0042

TEST NO. 6 PASS NO. 1

Time	T_1	T_2	T_3	Strain Gage A	Strain Gage B	Strain Gage C	Extensiometer
120	424	297	390	-1525	-1310	-1660	.00375
300	212	218	224	-930	-610	-890	.0025
360	192	202	202	-780	-490	-780	.00225
780	160	142	142	-250	0	-320	.002

TEST NO. 6 PASS NO. 2

Time	T_1	T_2	T_3	Strain Gage A	Strain Gage B	Strain Gage C	Extensiometer
0	160	142	142	-240	0	-320	.00225
5	160	142	142	-350	50	-150	.00125
10	160	142	142	-460	100	50	.001625
20	180	142	187	-800	-200	400	.0025
30	1410	142	642	-1080	-1160	-250	.002875
35	1640	164	732	-1020	-1480	-920	.00325
40	1340	210	706	-930	-1520	-1370	.0036
45	1104	227	702	-1030	-1450	-1580	.00435
50	750	285	625	-1610	-1570	-1820	.0055
60	592	307	552	-1800	-1560	-1850	.0053
70	532	312	510	-1930	-1500	-1810	.0051
80	463	315	473	-2000	-1430	-1760	.00485
90	432	314	442	-2030	-1370	-1690	.0046
120	360	304	372	-2000	-1210	-1500	.0039
300	224	234	242	-1500	-660	-950	.0022
480	200	204	208	-1250	-440	-750	.0018
540	184	197	197	-1180	-380	-700	.00175

APPENDIX (B)

REDUCTION OF DATA

This appendix includes the coordinate system, the nomenclature with definitions, and the equations used to calibrate the reduced data (Appendix C) from the experimental data (Appendix A).

Coordinate System

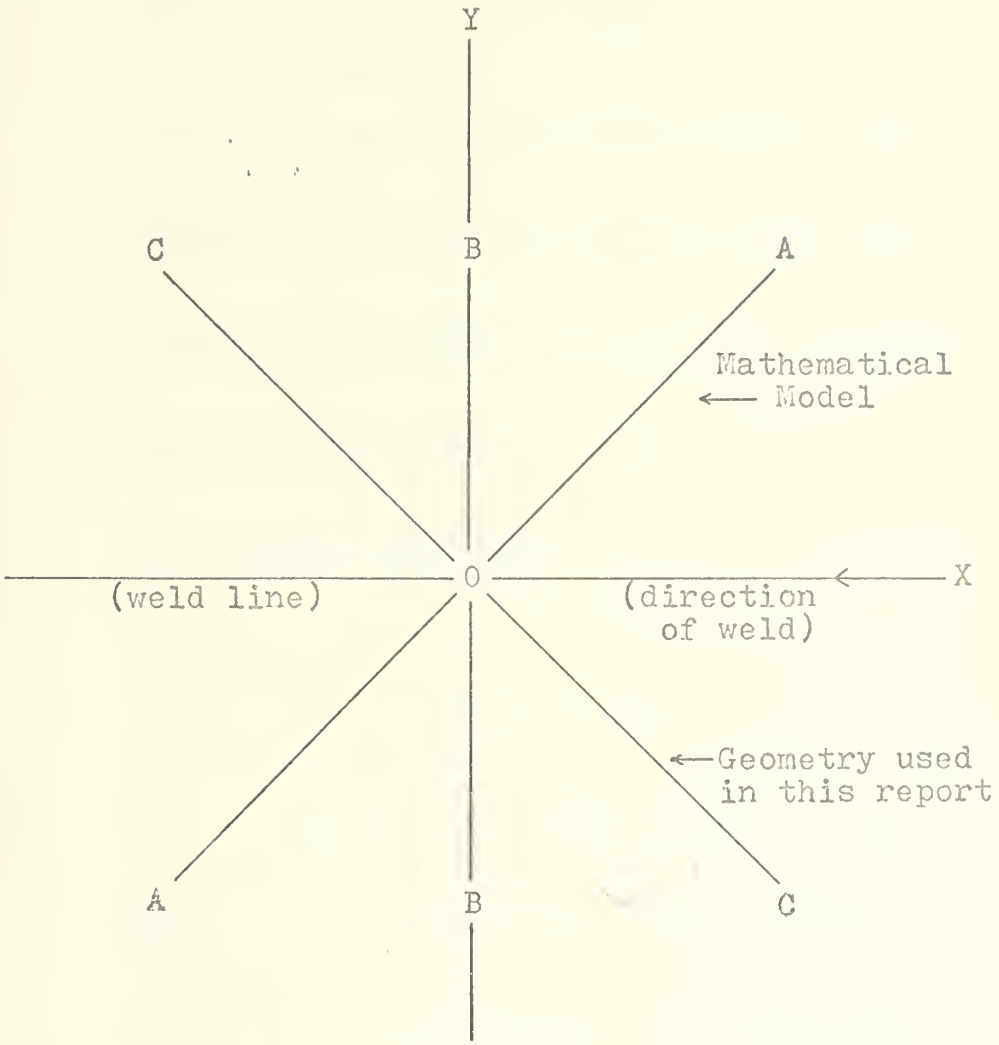

Nomenclature	Definition
0X, 0Y	Rectangular axes shown in coordinate system
01, 02	Principal axes of strain or stress
T-2	Temperature at strain gage (degrees)
ϵ_A	Mechanical strain of A leg of strain gage (microinches/inch)
ϵ_B	Mechanical strain of B leg of strain gage (microinches/inch)
ϵ_C	Mechanical strain of C leg of strain gage (microinches/inch)
ϵ_X	Linear strain component referred to 0X axis (microinches/inch)
ϵ_Y	Linear strain component referred to 0Y axis (microinches/inch)
γ_{XY}	Shear strain component referred to 0X and 0Y axis (microinches/inch)
ϵ_{p1}	Linear strain component referred to 01 axis (microstrain/inch)
ϵ_{p2}	Linear strain component referred to 02 axis (microstrain/inch)
$\phi 1$, $\phi 2$	Angles of reference from positive 0X axis counterclockwise being positive (degrees)
ϕ_X	Angle of reference from 0X axis to 01 axis (degrees)
σ_{XX}	Stress component referred to 0X axis (ksi)
σ_{YY}	Stress component referred to 0Y axis (ksi)
τ_{XY}	Shear stress component referred to 0X and 0Y axis (ksi)
σ_{ys}	Yield stress of material at point of strain measurement at temperature of point (ksi)

Nomenclature	Definition
I	Invariant indicating the residual stress state from Reference 7
I/σ_{ys}	Parameter to determine plasticity condition

Equations

(From References 7 and 27)

$$\begin{bmatrix} \epsilon_X \\ \epsilon_Y \\ \gamma_{XY} \end{bmatrix} = \begin{bmatrix} +1 & -1 & +1 \\ 0 & +1 & 0 \\ 1 & 0 & -1 \end{bmatrix} \begin{bmatrix} \epsilon_A \\ \epsilon_B \\ \epsilon_C \end{bmatrix} \qquad \text{Equation B-1}$$

$$\epsilon_1 = \left(\frac{\epsilon_X + \epsilon_Y}{2}\right) + \frac{1}{2}\sqrt{(\epsilon_X - \epsilon_Y)^2 + \gamma^2_{XY}} \qquad \text{Equation B-2}$$

$$\epsilon_2 = \left(\frac{\epsilon_X + \epsilon_Y}{2}\right) - \frac{1}{2}\sqrt{(\epsilon_X - \epsilon_Y)^2 + \gamma^2_{XY}} \qquad \text{Equation B-3}$$

$$\phi_X = \frac{1}{2}\text{Tan}^{-1}\left(\frac{\gamma_{XY}}{\epsilon_X - \epsilon_Y}\right) \qquad \text{Equation B-4}$$

But ϕ, referred to OA axis, therefore:

$$\Phi_X = \phi_1 + 45^\circ \qquad \text{Equation B-5}$$

$$\sigma_{XX} = \frac{E}{(1 - \nu 2)} (\epsilon_X + \nu \epsilon_Y) \qquad \text{Equation B-6}$$

$$\sigma_{YY} = \frac{E}{(1 - \nu^2)} (\epsilon_Y = \nu \epsilon_Y) \qquad \text{Equation B-7}$$

$$\sigma_1 = \frac{E}{(1 - \nu^2)} (\epsilon_1 + \nu \epsilon_2) \qquad \text{Equation B-8}$$

$$\sigma_2 = \frac{E}{(1 - \nu 2)} (\epsilon_2 + \nu \epsilon_1) \qquad \text{Equation B-9}$$

$$\gamma_{XY} = \epsilon_A - \epsilon_C \qquad \text{Equation B-10}$$

$$\tau_{XY} = \frac{E}{2(1 + \nu)} \quad XY \qquad \text{Equation B-11}$$

E = Modulus

ν = Poisson's ratio

$$I = (\sigma_X^2 - \sigma_X\sigma_Y + \sigma_Y^2 + 3\tau_{XY}^2)^{\frac{1}{2}} \qquad \text{Equation B-12}$$

If plastic condition exists in material, then

$$\frac{I}{\sigma} \geq 1.0 \qquad \text{Equation B-13}$$

The above equations were solved from the experimental data by using the computer program developed in Reference 16, with slight modifications for material and geometry, to obtain the reduced data in Appendix C.

TEST NO. 1 PASS NO. 1

Time	0	2	5	10	15	18	20	22	25
T-2	70	70	70	75	75	75	80	80	90
ϵ_A	-49.69	-129.69	-249.69	-218.63	-193.63	-168.63	-137.58	-212.58	-300.46
ϵ_B	-49.69	-49.69	-99.69	-93.63	-78.63	-78.63	-62.58	-112.58	-250.46
ϵ_C	-49.69	-29.69	125.31	181.37	281.37	331.37	412.42	462.42	424.54
ϵ_X	-49.69	-109.69	-24.69	56.37	166.37	241.37	337.42	362.42	374.54
ϵ_Y	-49.69	-49.69	-99.69	-93.63	-78.63	-78.63	-62.58	-112.58	-250.46
γ_{XY}	0	-100.00	-375.00	-400.00	-475.00	-500.00	-550.00	-675.00	-725.00
ϵ_{p1}	-49.69	-21.38	129.03	194.97	311.10	378.18	477.46	537.61	540.64
ϵ_{p2}	-49.69	-108.00	-253.40	-232.23	-223.36	-215.45	-202.61	-287.77	-416.57
ϕ_X	90.00	60.48	39.35	34.72	31.36	28.69	26.99	27.43	24.62
σ_{XX}	-2.13	-4.11	-1.80	2.24	6.01	8.48	13.11	13.44	15.08
σ_{YY}	-2.13	-2.72	-3.53	-1.22	0.36	1.10	3.89	2.49	0.69
τ_{XY}	0	-1.15	-4.33	-4.61	-5.48	-5.76	-6.34	-7.78	-8.34
σ_{ys}	142.92	142.92	142.92	142.72	142.72	142.72	142.53	142.53	142.13
I	2.129	3.104	1.906	2.145	4.202	6.819	10.81	11.40	13.87
I/σ_{ys}	.01490	.02172	.01333	.01503	.02944	.04778	.07580	.07998	.09758

TEST NO. 1 PASS NO. 1

Time	28	30	32	35	40	44.5	46	120	300
T-2	108	120	132	165	207	231	243	275	205
ϵ_A	-238.66	-214.13	-189.59	-49.62	1.25	-89.68	-95.15	-226.39	-61.18
ϵ_B	-363.66	-414.13	-474.59	-359.62	-198.75	-179.68	-165.15	-216.39	168.82
ϵ_C	261.34	110.87	-39.59	-159.62	-318.75	-459.68	-455.15	-496.39	-111.18
ϵ_X	386.34	310.87	245.41	150.38	-118.75	-369.68	-385.15	-506.39	-341.18
ϵ_Y	-363.66	-414.13	-474.59	-359.62	-198.75	-179.68	-165.15	-216.39	168.82
γ_{XY}	-500.00	-325.00	-150.00	110.00	320.00	370.00	360.00	270.00	50.00
ϵ_{p1}	462.03	345.63	253.14	156.24	6.17	6.72	-64.20	-163.28	170.05
ϵ_{p2}	-439.36	-448.88	-482.32	-365.49	-323.68	-482.65	-486.10	-559.51	-342.40
ϕ_X	16.85	12.07	5.88	6.09	37.98	58.59	60.71	68.52	87.20
σ_{XX}	19.05	19.22	19.63	26.34	30.26	28.71	31.55	35.72	26.10
σ_{YY}	1.83	2.59	3.14	14.70	28.45	33.01	36.52	42.24	37.67
τ_{XY}	-5.74	-3.73	-1.78	1.25	3.63	4.19	4.07	3.04	0.57
σ_{ys}	141.42	140.95	140.47	139.17	137.51	136.57	136.09	134.83	137.59
I	17.73	17.75	18.12	22.94	29.58	31.29	34.49	39.50	33.45
I/σ_{ys}	.1254	.1259	.1290	.1648	.2151	.2291	.2534	.2930	.2431

TEST NO. 1 PASS NO. 1				TEST NO. 1 PASS NO. 2					
Time	720	900	1200	0	10	20	25	30	35
T-2	155	145	130	115	119	122	125	140	180
ϵ_A	-1.74	6.15	-2.02	-54.82	-170.34	-551.71	-663.07	-1010.96	-764.62
ϵ_B	228.26	236.15	222.98	279.82	354.66	-76.71	-518.07	-1275.96	-1434.62
ϵ_C	-31.74	411.65	-27.02	-70.18	934.66	1233.29	801.93	54.04	-679.62
ϵ_X	-261.74	181.65	-252.02	-295.18	409.66	758.29	656.93	319.040	-9.62
ϵ_Y	228.26	236.15	222.98	279.82	354.66	-76.71	-518.07	-1275.96	-1434.62
γ_{XY}	30.00	-405.50	25.00	125.00	-1105.00	-1785.00	-1465.00	-1065.00	-85.00
ϵ_{p1}	228.72	413.48	223.31	286.53	935.34	1326.12	1008.42	480.48	-8.36
ϵ_{p2}	-262.19	4.33	-252.34	-301.90	-171.02	-644.53	-869.57	-1437.40	-1435.89
ϕ_X	88.25	48.83	88.49	83.87	43.58	32.47	25.73	16.87	1.71
σ_{XX}	16.01	27.93	9.68	-6.92	17.96	25.93	19.06	3.20	-1.11
σ_{YY}	27.20	29.17	20.56	6.27	16.70	6.79	-7.87	-33.31	-33.61
τ_{XY}	0.34	-4.64	0.29	1.43	-12.67	-20.46	-16.79	-12.19	-0.97
σ_{ys}	139.57	139.96	140.55	141.14	140.99	140.87	140.75	140.36	139.17
I	23.70	28.33	17.84	11.62	16.24	21.93	22.91	34.49	33.02
I/σ_{ys}	.1698	.2024	.1269	.08231	.1152	.1557	.1628	.2458	.2373

TEST NO. 1 PASS NO. 2						TEST NO. 2 PASS NO. 1			
Time	40	45	60	120	360	0	5	10	15
T-2	230	275	370	355	250	70	70	70	75
ϵ_A	-722.51	-674.19	-431.32	-184.50	193.33	-49.69	-369.69	-599.69	-198.63
ϵ_B	-1397.51	-1229.19	-36.33	-129.50	308.33	-49.69	-129.69	-169.69	-58.63
ϵ_C	-1207.51	-1659.19	-366.33	-29.50	448.33	-49.69	250.31	500.31	131.37
ϵ_X	-542.51	-1104.19	-761.33	-84.50	333.33	-49.69	10.31	70.31	-8.63
ϵ_Y	-1397.51	-1229.19	-36.33	-129.50	308.33	-49.69	-129.69	-169.69	-58.63
γ_{XY}	495.00	985.00	-65.00	-155.00	-255.00	0	-620.00	-1100.00	-330.00
ϵ_{p1}	-476.04	-670.24	-34.87	-26.30	448.94	-49.69	258.12	513.25	133.25
ϵ_{p2}	-1463.99	-1663.14	-762.78	-187.70	182.72	-49.69	-377.49	-612.63	-200.52
ϕ_X	15.03	41.38	87.44	36.91	2.20	90.00	38.64	38.85	40.69
σ_{XX}	-15.42	-29.07	43.45	60.03	49.57	-2.13	-0.94	0.64	0.44
σ_{YY}	-34.89	-31.91	59.58	59.03	49.01	-2.13	-4.17	-4.90	-0.71
τ_{XY}	5.64	11.20	0.72	1.73	-2.88	0	-7.15	-12.69	-3.80
σ_{ys}	138.78	138.34	131.08	131.67	125.82	142.92	142.92	142.92	142.92
I	30.56	31.13	53.35	59.49	49.20	2.129	2.663	3.247	3.225
I/σ_{ys}	.2202	.2250	.4070	.4518	.3623	1.490	.01863	.02272	.02259

TEST NO. 2 PASS NO. 1

Time	20	25	30	35	40	45	50	55	60
T-2	78	78	80	85	105	130	165	198	222
ϵ_A	-250.00	-240.00	-207.58	-216.52	-202.30	-177.02	-114.62	-44.65	-75.59
ϵ_B	-90.00	-100.00	-97.58	-126.52	-242.30	-407.02	-429.62	-334.65	-285.59
ϵ_C	220.00	240.00	292.42	343.48	267.70	22.98	-189.62	-334.65	-455.59
ϵ_X	60.00	100.00	182.42	253.48	307.70	252.98	125.38	-44.65	-245.59
ϵ_Y	-90.00	-100.00	-97.58	-126.52	-242.30	-407.02	-429.62	-334.65	-285.59
γ_{XY}	-470.00	-480.00	-500.00	-560.00	-470.00	-200.00	75.00	290.00	380.00
ϵ_{p1}	231.68	260.00	328.96	401.86	394.44	267.80	127.90	15.41	-74.54
ϵ_{p2}	-261.68	-260.00	-244.11	-274.90	-329.04	-421.83	-432.15	-394.72	-456.64
ϕ_X	36.15	33.69	30.38	27.92	20.26	8.43	3.85	22.50	42.00
σ_{XX}	3.18	4.40	7.66	11.02	16.88	20.02	24.84	28.96	29.30
σ_{YY}	-0.28	-0.21	1.21	2.27	4.25	4.90	12.18	22.37	28.39
τ_{XY}	-5.42	-5.53	-5.76	-6.45	-5.40	-2.29	0.86	3.29	4.30
σ_{ys}	142.61	142.61	142.53	142.33	141.54	140.55	139.17	137.87	136.92
I	2.276	1.930	5.795	9.066	14.67	17.88	21.57	26.48	29.08
I/σ_{ys}	.01596	.01353	.04066	.06370	.1036	.1272	.1550	.1921	.2124

TEST NO. 2 PASS NO. 1								TEST NO. 2 PASS NO. 2	
Time	65	70	120	360	600	780	1080	0	5
T-2	245	265	295	205	165	145	130	130	130
ϵ_A	-122.73	-208.50	-222.17	-11.18	50.38	76.15	82.98	82.98	222.98
ϵ_B	-272.73	-288.50	-122.17	163.82	230.38	256.15	242.98	322.18	323.78
ϵ_C	-502.73	-478.50	-532.17	-151.18	-79.62	-33.85	-77.02	-77.02	522.98
ϵ_X	-352.73	-398.50	-632.17	-326.18	-259.62	-213.85	-237.02	-316.22	422.18
ϵ_Y	-272.73	-288.50	-122.17	163.82	230.38	256.15	242.98	322.18	323.78
γ_{XY}	380.00	270.00	310.00	140.00	130.00	110.00	160.00	160.00	-300.00
ϵ_{p1}	-118.56	-197.73	-78.76	173.63	238.85	262.50	255.97	332.05	530.85
ϵ_{p2}	-507.89	-489.28	-675.58	-335.98	-268.10	-220.20	-250.00	-326.09	215.12
Φ_X	50.94	56.08	74.35	82.03	82.57	83.41	80.78	82.96	35.92
σ_{XX}	32.09	35.82	37.96	26.53	18.74	15.21	10.36	-7.18	16.99
σ_{YY}	33.90	38.29	49.40	37.66	29.92	25.95	21.36	7.44	14.74
τ_{XY}	4.29	3.04	3.48	1.59	1.48	1.26	1.83	1.83	-3.44
σ_{ys}	136.01	135.22	134.04	137.59	139.17	139.96	140.55	140.55	140.55
I	33.23	37.24	44.91	33.58	26.27	22.67	18.65	12.88	15.66
I/σ_{ys}	.2443	.2754	.3350	.2441	.1888	.1620	.1327	.09163	.1114

TEST NO. 2 PASS NO. 2

Time	7	15	20	35	45	55	90	360	600
T-2	130	130	138	175	230	270	335	215	175
ϵ_A	162.98	-57.02	-157.33	-237.51	104.10	182.55	151.28	310.94	342.49
ϵ_B	323.78	263.78	133.47	83.29	-455.10	-146.65	67.08	401.74	443.29
ϵ_C	602.98	932.98	1102.67	377.49	-95.90	-167.45	-53.72	290.94	442.49
ϵ_X	442.18	612.18	811.87	56.69	463.30	161.75	30.48	200.14	341.69
ϵ_Y	323.78	263.78	133.47	83.29	-455.10	-146.65	67.08	401.74	443.29
γ_{XY}	-440.00	-990.00	-1260.00	-615.00	200.00	350.00	205.00	20.00	-100.00
ϵ_{p1}	610.81	962.74	1188.19	377.78	474.07	240.80	152.90	402.23	463.77
ϵ_{p2}	155.16	-86.77	-242.84	-237.80	-465.86	-225.69	-55.34	199.64	321.21
ϕ_X	37.47	35.31	30.85	46.24	6.14	24.31	50.06	87.17	67.73
σ_{XX}	17.65	22.62	29.97	14.60	37.15	41.07	56.33	32.97	27.39
σ_{YY}	14.94	14.64	14.44	15.20	16.37	34.13	57.15	34.54	29.70
τ_{XY}	-5.04	-11.34	-14.42	-7.00	2.26	3.94	2.29	0.23	-1.14
σ_{ys}	140.55	140.55	140.24	138.78	136.61	135.03	132.46	137.20	138.78
I	15.99	19.00	25.11	14.19	32.36	38.23	56.81	35.49	28.56
I/σ_{ys}	.1138	.1352	.1791	.1022	.2369	.2832	.4289	.2587	.2058

TEST NO. 2 PASS NO. 2			TEST NO. 3 PASS NO. 1						
Time	780	1260	0	5	20	25	35	40	60
T-2	150	120	71	71	83	89	116	150	260
ϵ_A	337. 21	390.87	-43.48	-203.48	-138.94	-181.68	-443.97	-372.79	-169.56
ϵ_B	448.01	481.67	-43.48	-93.48	-18.94	-51.68	-563.97	-682.79	-369.56
ϵ_C	587.21	460.87	-43.48	106.52	391.06	528.32	186.03	-112.79	-619.56
ϵ_X	476.41	370.07	-43.48	-3.48	271.06	388.32	306.03	197.21	-419.56
ϵ_Y	448.01	481.67	-43.48	-93.48	-18.94	-51.68	-563.97	-682.79	-369.56
γ_{XY}	-250.00	-70.00	0	-310.00	-530.00	-710.00	-630.00	-260.00	450.00
ϵ_{p1}	588.01	491.74	-43.48	112.92	428.13	593.62	408.10	216.01	-168.18
ϵ_{p2}	336.40	360.00	-43.48	-209.88	-176.02	-246.97	-666.05	-701.59	-620.94
ϕ_X	41.76	73.95	90.00	36.91	30.66	28.82	17.95	8.23	48.17
σ_{XX}	25.24	14.21	-1.86	-1.04	11.87	17.30	16.28	20.49	32.76
σ_{YY}	24.59	16.77	-1.86	-3.11	5.19	6.94	-3.68	0.38	33.88
τ_{XY}	-2.86	-0.80	0	-3.58	-6.10	-8.17	-7.23	-2.97	5.07
σ_{ys}	139.76	140.95	142.88	142.88	142.41	142.17	141.11	139.76	135.42
I	24.75	15.57	1.863	1.783	9.38	14.24	17.80	20.08	33.56
I/σ_{ys}	.1771	.1105	.01304	.01248	.06586	.1002	.1261	.1437	.2478

TEST NO. 3 PASS NO. 1					TEST NO. 3 PASS NO. 2				
Time	120	240	600	780	0	3	10	25	35
T-2	307	239	181	156	151	151	152	162	195
ϵ_A	-77.63	0	89.76	134.48	103.42	383.42	249.63	-228.26	-163.29
ϵ_B	62.37	200.00	279.76	344.48	313.42	473.42	559.63	151.74	-413.29
ϵ_C	-327.63	-20.00	-10.24	34.48	3.42	563.42	889.63	1331.74	666.71
ϵ_X	-467.63	-220.00	-200.24	-175.52	-206.58	473.42	579.63	951.74	916.71
ϵ_Y	62.37	200.00	279.76	344.48	313.42	473.42	559.63	151.74	-413.29
γ_{XY}	250.00	20.00	100.00	100.00	100.00	-180.00	-640.00	-1560.00	-830.00
ϵ_{p1}	90.37	200.24	284.91	349.24	318.18	563.42	889.79	1428.33	1035.58
ϵ_{p2}	-495.64	-220.23	-205.40	-180.29	-211.34	383.42	249.47	-324.84	-532.16
Φ_X	77.37	88.64	84.12	84.56	84.56	135.00	44.11	31.43	15.98
σ_{XX}	47.97	39.10	25.13	19.97	-3.67	20.09	24.66	35.43	37.46
σ_{YY}	59.85	48.59	36.06	31.84	8.21	20.09	24.20	17.18	7.24
τ_{XY}	2.80	0.23	1.14	1.14	1.14	-2.06	-7.31	-17.80	-9.43
σ_{ys}	133.57	136.25	138.54	139.53	139.72	139.72	139.68	139.29	137.99
I	54.96	44.62	32.08	27.93	10.70	19.93	23.98	29.81	34.00
I/σ_{ys}	.4115	.3275	.2316	.2002	.07655	.1427	.1717	.2140	.2464

TEST NO. 3 PASS NO. 2								TEST NO. 4 PASS NO. 1	
Time	45	55	80	120	300	600	780	0	3
T-2	250	290	356	346	271	221	180	72	72
ϵ_A	218.33	276.78	346.72	334.60	348.76	388.20	483.54	-37.27	-97.27
ϵ_B	-271.67	-43.22	246.72	354.60	468.76	498.20	613.54	-37.27	-37.27
ϵ_C	128.33	-3.22	76.72	294.60	468.76	488.20	503.54	-37.27	22.73
ϵ_X	618.33	316.78	176.72	274.60	348.76	378.20	373.54	-37.27	-37.27
ϵ_Y	-271.67	-43.22	246.72	354.60	468.76	498.20	613.54	-37.27	-37.27
γ_{XY}	90.00	280.00	270.00	40.00	-120.00	-100.00	-20.00	0	-120.00
ϵ_{p1}	620.60	364.81	351.18	359.32	493.62	516.31	613.96	-37.27	22.73
ϵ_{p2}	-273.94	-91.26	72.25	269.88	323.91	360.10	373.13	-37.27	-97.27
ϕ_X	2.89	18.94	52.27	76.72	67.50	70.10	87.62	90.00	135.00
σ_{XX}	43.74	46.92	62.92	64.38	47.81	35.75	25.86	-1.60	-1.60
σ_{YY}	23.66	38.83	64.48	66.17	50.51	38.46	31.32	-1.60	-1.60
τ_{XY}	1.02	3.14	3.01	0.45	-1.35	-1.13	-0.23	0	-1.38
σ_{ys}	135.82	134.24	131.63	132.03	134.99	136.96	138.58	142.84	142.84
I	37.97	43.55	63.780	65.30	49.17	37.13	28.97	1.596	1.266
I/σ_{ys}	.2795	.3244	.4846	.4946	.3643	.2711	.2090	.01118	.008865

TEST NO. 4 PASS NO. 1

Time	10	20	27	28	29	30	32	34	35
T-2	74	77	82	83	84	87	95	103	108
ϵ_A	-234.84	-186.21	-205.15	-198.94	-232.73	-244.10	-214.41	-224.72	-213.66
ϵ_B	-74.84	-76.21	-125.15	-168.94	-192.73	-224.10	-244.41	-304.72	-323.66
ϵ_C	175.16	313.79	434.85	441.06	417.27	405.90	405.59	325.28	296.34
ϵ_X	15.16	203.79	354.85	411.06	377.27	385.90	435.59	415.28	406.34
ϵ_Y	-74.84	-76.21	-125.15	-168.94	-192.73	-224.10	-244.41	-304.72	-323.66
γ_{XY}	-410.00	-500.00	-640.00	-640.00	-650.00	-650.00	-620.00	-560.00	-510.00
ϵ_{p1}	180.04	350.32	514.85	552.91	524.53	526.60	555.70	511.35	486.59
ϵ_{p2}	-239.72	-222.74	-285.15	-310.80	-329.99	-364.80	-364.52	-400.79	-403.91
ϕ_X	38.81	30.38	26.57	23.91	24.38	23.41	21.18	18.94	17.47
σ_{XX}	0.28	7.27	13.06	14.74	13.65	14.41	17.93	18.74	19.58
σ_{YY}	-1.79	0.81	2.00	1.38	0.52	0.36	2.29	2.21	2.82
τ_{XY}	-4.73	5.76	-7.37	-7.37	-7.49	-7.48	-7.13	-6.43	-5.86
σ_{ys}	142.76	142.64	142.45	142.41	142.37	142.25	141.93	141.62	141.42
I	3.222	5.502	11.24	13.29	12.53	13.42	16.26	17.20	17.85
I/σ_{ys}	.02257	.03857	.07890	.09334	.08803	.09433	.1145	.1215	.1262

TEST NO. 4 PASS NO. 1							TEST NO. 4 PASS NO. 2		
Time	45	55	120	300	480	600	0	4	10
T-2	150	180	258	210	184	170	170	171	172
ϵ_A	-112.79	-186.46	-121.98	-20.12	18.39	31.43	31.43	517.64	383.85
ϵ_B	-322.79	-366.46	-21.98	129.88	158.39	171.43	171.43	647.64	728.85
ϵ_C	-32.79	-391.46	-301.98	-100.12	-71.61	-53.57	-53.57	702.64	988.85
ϵ_X	177.21	-211.46	-401.98	-250.12	-211.61	-193.57	-193.57	572.64	643.85
ϵ_Y	-322.79	-366.46	-1.98	129.88	158.39	171.43	171.43	647.64	728.85
γ_{XY}	-80.00	205.00	180.00	80.00	90.00	85.00	85.00	-185.00	-605.00
ϵ_{p1}	180.39	-160.46	-1.74	134.04	163.78	176.32	176.32	709.96	991.83
ϵ_{p2}	-325.97	-417.46	-422.22	-254.28	-217.01	-198.45	-198.45	510.33	380.88
ϕ_X	4.55	26.45	77.33	84.06	83.16	83.45	83.45	56.03	49.00
σ_{XX}	23.10	17.94	35.89	29.48	24.12	21.13	-4.63	25.24	28.61
σ_{YY}	11.63	14.41	44.46	38.10	32.53	29.44	3.69	26.95	30.55
τ_{XY}	-0.91	2.33	2.03	0.91	1.02	0.97	0.97	-2.11	6.89
σ_{ys}	139.76	138.58	135.50	137.39	138.42	138.97	138.97	138.93	138.89
I	19.94	16.67	40.93	34.65	29.30	26.35	7.419	26.01	29.28
I/σ_{ys}	.1427	.1203	.3021	.2522	.2117	.1896	.05338	.1872	.2108

TEST NO. 4 PASS NO. 2

Time	20	25	28	30	35	50	60	120	600
T-2	172	177	179	184	207	280	311	322	277
ϵ_A	-66.15	24.91	7.33	38.39	231.25	574.66	487.21	547.65	685.47
ϵ_B	408.85	104.91	47.33	-71.61	-138.75	204.66	177.21	467.65	545.47
ϵ_C	1188.85	1359.91	1132.33	1033.39	746.25	429.66	172.21	372.65	600.47
ϵ_X	713.85	1189.91	1092.33	1143.39	1116.25	799.66	482.21	452.65	740.47
ϵ_Y	408.85	194.91	47.33	-71.61	-138.75	204.66	177.21	407.65	545.47
γ_{XY}	-1255.00	-1335.00	-1125.00	-995.00	-515.00	145.00	315.00	175.00	85.00
ϵ_{p1}	1207.12	1524.91	1337.56	1321.10	1167.03	808.37	548.94	547.97	749.33
ϵ_{p2}	-84.41	-140.09	-197.90	-249.33	-189.53	195.96	110.48	372.33	536.61
ϕ_X	38.17	26.65	23.56	19.66	11.16	6.85	22.96	47.45	11.78
σ_{XX}	27.77	42.48	38.40	40.21	44.73	57.15	54.98	62.44	44.49
σ_{YY}	20.82	19.82	14.60	12.56	16.25	43.77	48.15	62.77	40.07
τ_{XY}	-14.30	-15.20	-12.91	-11.32	-5.84	1.63	3.53	1.96	0.96
σ_{ys}	138.89	138.70	138.62	138.42	137.51	134.63	133.41	132.58	136.72
I	24.15	36.20	32.99	35.15	38.99	51.82	52.00	62.65	42.49
I/σ_{ys}	.1739	.2610	.2380	.2539	.2835	.3849	.3898	.4726	.3108

TEST NO. 5 PASS NO. 1

Time	0	5	10	25	35	42	55	60	120
T-2	72	72	72	74	86	122	200	207	284
ϵ_A	-37.27	-87.27	202.27	-244.84	-430.31	-546.71	-262.23	-348.75	-170.49
ϵ_B	-37.27	-57.27	-77.27	-24.84	299.69	-586.71	-572.23	-518.75	-70.49
ϵ_C	-37.27	2.73	112.73	395.16	569.69	323.29	-362.23	-518.75	-370.49
ϵ_X	-37.27	-27.27	-12.27	175.16	-160.31	363.29	-52.23	-348.75	-470.49
ϵ_Y	-37.27	-57.27	-77.27	-24.84	299.69	-586.71	-572.23	-518.75	-70.49
γ_{XY}	0	-90.00	-315.00	-640.00	-1000.00	-870.00	100.00	170.00	200.00
ϵ_{p1}	-37.27	5.17	116.05	410.42	600.05	532.38	-47.47	-313.55	-46.88
ϵ_{p2}	-37.27	-89.70	-205.58	-260.10	-480.67	-755.79	-577.00	-553.96	-484.10
ϕ_X	90.00	35.78	39.17	36.32	57.35	21.24	5.44	22.50	76.72
σ_{XX}	-1.60	-1.46	-1.17	6.05	1.35	19.25	26.42	19.18	40.18
σ_{YY}	-1.60	-2.16	-2.67	1.44	11.94	-2.53	14.61	15.32	49.17
τ_{XY}	0	-1.04	-3.63	-7.38	-11.51	-9.97	1.14	1.93	2.25
σ_{ys}	142.84	142.84	142.84	142.76	142.29	140.87	137.79	137.51	134.47
I	15.96	.7233	2.353	2.796	9.684	19.89	22.99	17.74	45.42
I/σ_{ys}	.01118	.005064	.01647	.01959	.06806	.1412	.1669	.1290	.3378

TEST NO. 5 PASS NO. 1					TEST NO. 5 PASS NO. 2				
Time	300	480	600	720	0	5	10	20	30
T-2	220	188	176	162	162	164	165	167	167
ϵ_A	81.99	133.23	118.70	111.74	111.74	454.16	350.38	42.80	-287.20
ϵ_B	151.99	203.23	248.70	191.74	191.74	624.16	690.38	582.80	-217.20
ϵ_C	-138.01	-126.77	-101.30	-98.26	-98.26	684.16	870.38	1312.80	1002.80
ϵ_X	-208.01	-196.77	-231.30	-178.26	-178.26	514.16	530.38	772.80	932.80
ϵ_Y	151.99	203.23	248.70	191.74	191.74	624.16	690.38	582.80	-217.20
γ_{XY}	220.00	260.00	220.00	210.00	210.00	-230.00	-520.00	-1270.00	-1290.00
ϵ_{p1}	182.94	241.77	272.71	219.46	219.46	696.64	882.41	1319.86	1221.89
ϵ_{p2}	-238.96	-235.30	-255.31	-205.98	-205.98	441.69	368.35	35.73	-506.29
ϕ_X	74.29	73.49	77.69	75.21	75.21	57.78	53.55	40.75	24.14
σ_{XX}	33.72	26.09	22.24	19.71	-3.95	23.39	24.83	32.20	29.60
σ_{YY}	41.87	35.19	33.17	28.15	4.51	25.90	28.48	27.87	3.37
τ_{XY}	2.49	2.96	2.51	2.40	2.40	-2.62	-5.93	-14.48	-14.71
σ_{ys}	137.00	138.26	138.74	139.29	139.29	139.21	139.17	139.09	139.09
I	38.55	31.78	29.41	25.16	7.792	24.58	26.51	29.54	27.26
I/σ_{ys}	.2814	.2298	.2120	.1807	.05594	.1766	.1905	.2124	.1960

TEST NO. 5 PASS NO. 2 TEST NO. 6 PASS NO. 1

Time	35	45	55	60	120	300	480	720	0
T-2	195	254	317	318	335	277	247	205	72
ϵ_A	-23.29	403.17	604.48	450.69	506.28	516.03	519.69	448.82	-37.27
ϵ_B	-353.29	13.17	294.48	200.69	526.28	596.03	619.69	638.82	-37.27
ϵ_C	646.71	303.17	374.48	110.69	316.28	486.03	509.69	448.82	-37.27
ϵ_X	976.71	693.17	684.48	360.69	296.28	406.03	409.69	258.82	-37.27
ϵ_Y	-353.29	13.17	294.48	200.69	526.28	596.03	619.69	638.82	-37.27
γ_{XY}	-670.00	100.00	230.00	340.00	190.00	30.00	10.00	0	0
ϵ_{p1}	1056.33	686.83	715.86	468.57	560.44	597.21	619.81	638.82	-37.27
ϵ_{p2}	-432.90	9.52	263.09	92.81	262.12	404.85	409.58	258.82	-37.27
ϕ_X	13.37	4.18	15.26	32.40	70.22	85.51	88.64	90.00	90.00
σ_{XX}	37.07	47.08	66.27	55.29	60.90	49.59	41.95	26.09	-1.60
σ_{YY}	6.85	31.74	57.54	51.70	66.04	53.86	46.69	34.71	-1.60
τ_{XY}	-7.61	1.13	2.57	3.80	2.12	0.34	0.11	0	0
σ_{ys}	137.99	135.66	133.17	133.13	132.46	134.75	135.93	137.59	142.84
I	33.83	41.63	62.43	53.69	63.68	51.86	44.51	31.30	1.596
I/σ_{ys}	.2452	.3069	.4688	.4033	.4807	.3849	.3274	.2275	.01118

TEST NO. 6 PASS NO. 1

Time	5	10	20	25	30	35	45	55	60
T-2	72	72	72	72	84	105	158	217	224
ϵ_A	-167.27	-217.27	-257.27	-317.27	-372.73	-402.30	-203.10	-86.64	-193.16
ϵ_B	-67.27	-77.27	-117.27	-137.27	-272.73	-512.30	-583.10	-366.64	-353.16
ϵ_C	82.73	-20.18	332.73	462.73	467.27	247.70	-223.10	-376.64	-493.16
ϵ_X	-17.27	-160.18	192.73	282.73	367.27	357.70	156.90	-96.64	-333.16
ϵ_Y	-67.27	-77.27	-117.27	-137.27	-272.73	-512.30	-583.10	-366.64	-353.16
γ_{XY}	-250.00	-197.09	590.00	-780.00	-840.00	-650.00	20.00	290.00	300.00
ϵ_{p1}	85.21	-11.81	370.98	515.68	575.28	465.70	157.03	-33.53	-192.83
ϵ_{p2}	-169.74	-225.63	-295.51	-370.21	-480.75	-620.30	-583.24	-429.76	-493.50
Φ_X	39.35	56.41	31.14	30.85	26.35	18.38	0.77	23.52	43.09
σ_{XX}	-1.23	-6.04	5.19	7.96	12.53	15.34	22.00	31.49	25.83
σ_{YY}	-2.39	-4.13	-1.96	-1.73	-2.21	-4.64	5.11	25.37	25.38
τ_{XY}	-2.88	-2.27	-6.80	-9.00	-9.67	-7.47	-.23	3.29	3.40
σ_{ys}	142.84	142.84	142.84	142.84	142.37	141.54	139.45	137.12	136.84
I	2.091	4.668	4.533	7.288	12.67	17.49	19.96	29.09	25.80
I/σ_{ys}	.01464	.03268	.03173	.05102	.08902	.1256	.1431	.2121	.1886

TEST NO. 6 PASS NO. 1					TEST NO. 6 PASS NO. 2				
Time	120	300	360	780	0	5	10	20	30
T-2	297	218	202	142	142	142	142	142	164
ϵ_A	-164.75	-60.43	-9.81	147.52	147.52	297.52	187.52	-152.48	-295.84
ϵ_B	50.25	259.57	280.19	397.52	397.52	447.52	497.52	197.52	-625.84
ϵ_C	-299.74	-20.43	-9.81	77.52	77.52	567.52	767.52	1117.52	604.16
ϵ_X	-514.75	-340.43	-299.81	-172.48	-172.48	417.52	457.52	767.52	934.16
ϵ_Y	50.25	259.57	280.19	397.52	397.52	447.52	497.52	197.52	-625.84
γ_{XY}	135.00	-40.00	0	70.00	70.00	-270.00	-580.00	-1270.00	-900.00
ϵ_{p1}	58.21	260.24	280.19	399.66	399.66	568.35	768.21	1178.54	1054.66
ϵ_{p2}	-522.70	-341.10	-299.81	-174.62	-174.62	296.69	186.83	-213.51	-746.33
ϕ_X	83.28	88.090	90.00	86.50	86.50	48.17	46.97	32.91	14.99
σ_{XX}	43.41	29.94	27.21	16.63	-1.74	18.03	19.83	27.01	30.17
σ_{YY}	56.09	43.54	40.38	29.67	11.30	18.71	20.74	13.98	-5.41
τ_{XY}	1.51	-0.45	0	0.80	0.80	-3.09	-6.63	-14.52	-10.26
σ_{ys}	133.96	137.08	137.71	140.08	140.08	140.08	140.08	140.08	139.21
I	50.99	38.56	35.67	25.80	12.36	18.13	19.80	22.45	32.74
I/σ_{ys}	.3806	.2813	.2590	18.42	.08822	.1294	.1414	.1603	.2352

TEST NO. 6 PASS NO. 2

Time	35	45	60	120	300	480	540
T-2	190	250	307	304	234	204	197
ϵ_A	-74.34	288.33	-127.63	-346.27	-281.05	-217.39	-190.87
ϵ_B	-784.34	-401.67	-137.63	193.73	308.95	342.61	359.13
ϵ_C	95.66	-191.67	-107.63	223.73	338.96	352.61	359.13
ϵ_X	805.66	498.33	-97.63	-316.27	-251.05	-207.39	-190.87
ϵ_Y	-784.34	-401.67	-137.63	193.73	308.95	342.61	359.13
γ_{XY}	-170.00	480.00	-20.00	-570.00	-620.00	-570.00	-550.00
ϵ_{p1}	810.19	558.33	-95.27	321.16	446.68	463.66	473.04
ϵ_{p2}	-788.87	-461.67	-139.99	-443.69	-388.78	-328.43	-304.77
Φ_X	3.05	14.04	13.28	65.91	66.04	66.99	67.50
σ_{XX}	31.30	40.98	39.64	35.01	19.40	13.11	11.94
σ_{YY}	-4.86	20.67	38.74	46.44	32.06	25.59	24.43
τ_{XY}	-1.93	5.42	-0.22	-6.39	-7.01	-6.47	-6.25
σ_{ys}	138.18	135.82	133.57	133.68	136.45	137.63	137.91
I	33.90	35.72	39.19	41.68	27.59	21.73	20.71
I/σ_{ys}	.2453	.2630	.2934	.3118	.2022	.1579	.1502

REFERENCES

1. Masubuchi, K., and N. T. Ich. "Computer Analysis of Degree of Constraint of Practical Butt Joints," Welding Research Supplement, April 1970, pp. 166S-176S.

2. Masubuchi, K. "The State-of-the-Act in Predicting Stresses, Strains, and Distortions Produced by Welding," Report to Naval Ship Research and Development Center, Department of the Navy Purchase Order N00167-74-M-1544, Jan. 10, 1974.

3. Satoh, K. "An Analytical Approach to the Problem of Restraint Intensity in Slit Weld," Transactions of JWRI, Vol. I, No. 1, 1972.

4. Masubuchi, K. "Control of Distortion and Shrinkage in Welding," Welding Research Council Bulletin, No. 149, April 1970.

5. Ueda, Y. and Y. Kusachi. "Theoretical Analysis of Local Stress and Strains in RRC Test Specimens at Crack Initiation," Welding Research Institute, Osaka University IIW Document X-662-72, May 1972.

6. Wessel, E. T. and R. R. Hovan. "Effect of Long Time Exposures at 400 to 1000°F on the Strength and Toughness of a Ni-Cr-Mo-V High Strength, Weldable Steel," Symposium on Heat-treated Steels for Elevated Temperature Service, 21st Annual Petroleum-Mechanical Engineering Conference, New Orleans, Louisiana, Sept. 19-20, 1966.

7. Masubuchi, K. "Analytical Investigation of Residual Stresses and Distortions Due to Welding," The Welding Journal 39, (12), Research Supplement, 525-S to 537-S, 1961.

8. Wilson, M. and D. J. H. Corderoy. "The Transient Stress Distribution in Welding," Welding Research Abroad, Vol. XIV, No.2, Feb. 1968.

9. Sato, K., K. Seo, H. Nakajima, and M. Toyosada. "Restraint Intensity of Weld Joints in Structural Elements," Transactions of JWRI, Vol. 2, No. 1, 1973.

10. Satoh, K., Y. Ueda, and H. Kihara. "Recent Trend of Researches on Restraint Stress and Strains for Weld Cracking," Transactions of JWRI, Vol I, No. 1, 1972.

11. Osgood, Carl. "A Basic Course in Fracture Mechanics," Penton Publishing Co., 1971.

12. Kobayashi, A., Ed. Experimental Techniques in Fracture Mechanics. The Iowa State University Press, Ames, Iowa, 1973.

13. Irwin, G. R. and J. Kies. "Fracturing and Fracture Dynamics," Welding Journal Research Supplement, February 1952.

14. Orowan, E. "Fundamentals of Brittle Behavior of Metals," Fatigue and Fracture of Metals, John Wiley and Sons, 1952, pp. 139-167.

15. Klein, K. "Investigation of Welding Thermal Strains in Marine Steels," M. S. Thesis, MIT, May 1971.

16. Bryan, J. "Analysis of Two Dimensional Thermal Strains and Metal Movement During Welding," M. S. Thesis, MIT, May 1973.

17. Hibbitt, H. D. "A Numerical Thermo-Mechanical Model for the Welding and Subsequent Loading of a Fabricated Structure," PhD Thesis, Brown University, June 1972.

18. Willner, A. R. and Soline, M. L. "Materials Survey for the Rescue and Search Vehicles of the Deep-Submergence Systems Project," David Taylor Model Basin Report 1987, U. S. Navy, March 1965.

19. Manganello, S. J., B. Mravic and L. F. Porter. "Development of a Low-Manganese HY-150 Steel-I," United Stetes Steel Technical Report, Pennsylvania, January 1968.

20. Rathbone, A. M. "Welding Characteristics of Four Promising 130 to 150 KSI Yield-Strength Submarine-Hull Steels-II," United States Steel Technical Report, Pennsylvania, September 1963.

21. Aerospace Structural Metals Handbook, AFML-TR-68-115, Air Force Materials Laboratory, Air Force Systems Command, Wright-Patterson Air Force Base, Ohio, 1970.

22. Masubuchi, K. "Residual Stresses in Weldments of High-Strength Steel" MIT Report No. 71-2, January 1971.

23. Eldridge, E. A. and H. W. Deem. "Report on Physical Properties of Metals and Alloys from Cryogenic to Elevated Temperatures," ASTM Special Technical Publication No. 296.

24. Tall, L. "Residual Stresses in Welded Plates - A Theoretical Study," Welding Journal 43 (1), 1964.

25. "Effects of Welding Position and Process on the K_{ISCC} of HY-130T Weld Metals," Technical Report Applied Research Laboratory, January 1, 1968.

26. Satoh, K., Y. Ueda, and H. Kihara. "Recent Trend of Researches on Restrain Stress and Strains for Weld Cracking," Transactions of JWRI, Vol. I, No. 1, 1972.

27. Murray, W. M. "Stress and Strain Relations," Lecture Series, MIT.

153104

Thesis
S3485 Schrodt
Fracture of high restraint welds in high strength quenched and tempered steel.